Summer 2013

Population pharmacokinetics and pharmacodynamics of pyronaridine

Janthima Methaneethorn
University of Iowa

POPULATION PHARMACOKINETICS AND PHARMACODYNAMICS OF PYRONARIDINE

by

Janthima Methaneethorn

A thesis submitted in partial fulfillment
of the requirements for the Doctor of
Philosophy degree in Pharmacy
in the Graduate College of
The University of Iowa

August 2013

Thesis Supervisor: Professor Lawrence L. Fleckenstein

Graduate College
The University of Iowa
Iowa City, Iowa

CERTIFICATE OF APPROVAL

_____

PH.D. THESIS

_____

This is to certify that the Ph.D. thesis of

Janthima Methaneethorn

has been approved by the Examining Committee
for the thesis requirement for the Doctor of Philosophy
degree in Pharmacy at the August 2013 graduation.

Thesis Committee: _____
Lawrence L. Fleckenstein, Thesis Supervisor

_____
Maureen D. Donovan

_____
Daryl J. Murry

_____
Erika J. Ernst

_____
Kai Wang

To my dad, my mom, and my sister.
For their unconditional love, care, support, and encouragement.

It is not the fruits of scientific research that elevate man and enrich his nature, but the urge to understand, the intellectual work, creative or receptive.

Albert Einstein
Ideas and Opinions, 1954

ACKNOWLEDGMENTS

This thesis would not have been possible without the help and support of all the wonderful people in my life, to only some of whom it is possible to give particular mention here.

Above all, I would like to thank my advisor Professor Larry Fleckenstein for his guidance, mentoring, and encouragement throughout my Ph.D. program. Without his devotion and mentorship, I would never have accomplished this big part of my life.

I am also grateful to the committee members: Dr. DJ Murry, Dr. Erika Ernst, Dr. Maureen Donovan, and Dr. Kai Wang who have provided ideas and helpful advices.

I would also like to thank all my former and current colleagues: Dr. Thitima Wattanavijitkul and Dr. Denise Morris for your advice, encouragement and support. Carrie Morris, thank you for all your help and suggestions. Amal Suleiman Ayyoub, thank you for your great friendship. Rowan Ejielat, Xiaofeng Wang, Supreet Agarwal, Tatian Kirresh, Maha Alkeilani, and Nattawut Leelakanok, thank you for being good friends and sharing all moments together. Paul Imming, Mark Schmidt and Grace Kim, thank you for being good lab colleagues.

My Thai friends in Iowa City and in Thailand: thank you for their generosity, moral support, and friendship.

Finally, I would like to thank my father, Thammanoon Methaneethorn, my mother, Phensri Methaneethorn, thank you so much for your unconditional love, and support. Words cannot express my appreciation. I would not have come this far without you. I also want to thank my sister, Jutima Methaneethorn, thank you for all your supports and advice in all aspects.

ABSTRACT

Pyronaridine/Artesunate (PA) 3:1 fixed dose combination is a novel artemisinin-based combination therapy (ACT) in development for the treatment of acute uncomplicated *Plasmodium falciparum* or *Plasmodium vivax* malaria. An understanding of both pharmacokinetics and pharmacodynamics of pyronaridine is of importance in order to achieve optimal therapeutic outcome.

In this thesis, population pharmacokinetic models for pyronaridine in healthy subjects, and adult and pediatric malaria patients were developed. Pyronaridine pharmacokinetics in both adult and pediatric populations were best described by a two compartment model with first order absorption and elimination from the central compartment. A presence of malaria infection and body weight were the significant covariates that explained pyronaridine pharmacokinetic variability in the adult population. For the pediatric population, age was the only significant covariate that explained pyronaridine pharmacokinetic variability.

Monte Carlo simulations were also performed to address differences in pyronaridine exposures among these populations and to explore the exposures of pyronaridine among recommended dosage regimens for pediatric and adult malaria patients. Healthy adults had a higher exposure to pyronaridine as compared to adult malaria patients. For the pediatric population, younger children had a higher exposure to pyronaridine as compared to older children. The overall range of pyronaridine exposures among dosing groups for adult and pediatric malaria patients were relatively similar.

The cut-off values of pyronaridine pharmacokinetic parameters associated with successful treatment outcome were also determined by means of receiver operating characteristic (ROC) curve. These cut-off values can be used to optimize the outcome of malaria treatment. Additionally, Cox proportional hazard model was conducted to determine the relationship between several covariates and time to the occurrence of

re-infection or recrudescence. The models showed that as the levels of predicted pyronaridine concentrations on day 7 increased, the risks of acquiring re-infection or recrudescence decreased.

Finally, pharmacokinetic drug-drug interaction of pyronaridine and ritonavir was assessed based on the overlap pathway for metabolism of both drugs and the high rates of HIV and malaria co-infection. There was an effect of ritonavir on pyronaridine pharmacokinetics. However, the results were not considered clinically relevant. An increase in ritonavir exposure was observed in the presence of fixed dose PA.

TABLE OF CONTENTS

LIST OF TABLES

LIST OF FIGURES

CHAPTER 1

INTRODUCTION

Malaria

Malaria causes substantial mortality and morbidity in the world population. According to the World Malaria Report 2011 (1), approximately 200 million cases of malaria occurred worldwide, most cases were in Africa. Nearly a half million malaria deaths were estimated the same year, the majority of them occurred in children under 5 years of age. Malaria also has a serious impact on socio-economic status in malaria endemic countries. Economic growth reduces approximately 1.3% per person per year in countries with intensive malaria. Additionally, it has been estimated that an increase in 0.3% economic growth in these countries is associated with 10% reduction in malaria (2). Neuro-cognitive impairment resulting from malaria may affect future education and employment of children.

Malaria is caused by parasites genus *Plasmodium* that are transmitted from one human to another by infected female *Anopheles* mosquitoes. Five *Plasmodium* species that have been shown to infect humans include *P. falciparum, P, vivax, P. ovale, P. malariae, and P.knowlesi.* The last species was recently confirmed in areas of Southeast Asia. While infections by *P. vivax* are more widespread, *P. falciparum* is the most deadly species that affects more red blood cells than other types. Infections by the other three species are less common. Transmissions can also occur from a mother to her unborn baby or by blood transfusions.

The life cycle of *Plasmodium* parasite involves two hosts, humans and female *Anopheles* mosquitoes, and undergoes three distinct stages: liver stage, blood stage, and mosquito stage (Figure 1.1) (3). Liver stage begins when an infected mosquito takes a blood meal from a human and transfers sporozoites into the human host. Sporozoites, then, migrate to the liver and infect hepatocytes where they start their asexual

reproduction producing thousands of merozoites. Liver stage is asymptomatic and takes about 1 week. However, *P. vivax and P. ovale* can produce dormant liver stage (hypnozoites) and cause relapses by invading red blood cells several weeks or months later. Blood stage starts when released merozoites from hepatocytes infect erythrocytes and undergo asexual reproduction. Merozoites, then, develop into trophozoites (immature ring stage). The nucleus of trophozoites divides asexually to produce mature schizonts containing several mononucleated merozoites. Erythrocytes rupture and release merozoites which invade new erythrocytes. Pathology associated with malaria occurs at this stage due to synchronous lysis of infected erythrocytes. The cycle of fevers and chills are different depending on Plasmodium species. Fevers spike every 72 hours in malaria caused by *P. malariae*, while *P. vivax* and *P. ovalae* exhibit 48 hour cycles. Continuous fever and more severe morbidity are often observed in *P. falciparum* infection. This increase in virulence is attributed to relatively high parasitemias and sequestration during infection. Some trophozoites develop into gametocytes (sexual form). In a mosquito, gametocytes that are taken up during blood meal form female and male gametes. These gametes fuse to form zygotes which develop into ookinetes and oocysts in the gut wall of the mosquito. Repeated mitotic divisions take place within the oocysts producing a large number of sporozoites. Oocysts, then, rupture and release sporozoites which migrate to the mosquito's salivary gland. The cycle starts again when the infected mosquito takes another blood meal from a human.

There are two main strategies involving malaria management: malaria prevention and treatment of malaria (discussed next section) (4). Malaria prevention includes vector control (e.g. indoor residual spraying, and insecticide-treated bed-nets), drug prophylaxis, particularly in vulnerable groups and use of vaccine. Insecticide-treated bed-nets have proved to reduce the incidence of malaria. However, a need of regular re-treatment has limited their sustained use (5). Rapid reduction of transmission by indoor residual spraying makes it suitable for the area where malaria is unstable (5). Despite its useful

impact, indoor residual spraying is not fully used to its potential due to environmental issues and costs. Moreover, pyrethroids, environmental friendly insecticides used in insecticide-treated bed-nets and indoor residual spraying, are more expensive and have developed resistance (5). Antimalarial drugs for prophylaxis are used in travelers visiting areas where malaria is endemic. Vaccines for malaria are still under development.

Treatment of malaria

Malaria can be classified as uncomplicated and complicated or severe malaria based on clinical manifestation. Severe malaria is a medical emergency and can produce 100% mortality if not treated promptly. The main objective of treatment of severe malaria is to prevent death while prevention of disabilities and prevention of recrudescence are secondary objectives. The mortality from severe malaria falls to 15-20% with the effective antimalarial treatment and supportive care. Parenteral treatment with quinine, quinidine, or artemisinin derivatives is essential and recommended in the treatment of severe malaria (6).

Clinical manifestation of uncomplicated malaria varies depending on immunity of the person infected. Generally, it presents with fever (sometimes periodic), headache, chills and sweats. Nausea, vomiting, watery diarrhea, anemia, and jaundice may also occur. Treatment of uncomplicated malaria has shifted from monotherapy to combination therapy of drugs with different mechanisms of action due to an increase in antimalarial drug resistance (7-11). Among the combination therapies available, the World Health Organization (WHO) malaria program has recommended artemisinin-based combination therapies (ACTs) as a first line treatment for uncomplicated malaria (6). The rationale for this combination is to rapidly reduce parasite biomass by artemisinin or its derivatives and to completely eliminate the residual parasites by the partner drugs (7,12). Artemisinins are antimalarial drugs of choice for a combination therapy because of their high parasite reduction rate. Following administration of artemisinins, the numbers of

parasites reduce by 10^4 fold per asexual cycle leaving less than 0.0001% of parasites to be eliminated by a partner drug (9). Artemisinins are also active against gametocytes, therefore, can reduce rate of malaria transmission (9,12,13). The partner drug of artemisinins should have the following properties: 1) long half-life, 2) no pharmacological interaction, and 3) different mechanism of action (14,15).

The current ACTs recommended by WHO for the treatment of uncomplicated malaria include artemether-lumefantrine (AL), artesunate-amodiaquine (AS-AQ), artesunate-mefloquine (AS-MQ), artesunate-sulfadoxine-pyrimethamine (AS-SP), and dihydroartemisinin-piperaquine (DHA-PPQ) (6). AL has proved to be effective and been widely used for treatment of uncomplicated P. falciparum malaria throughout the world (16). However, the difficulty in AL administration that has to be administered twice a day for 3 days with fatty food to ensure adequate bioavailability is an obstacle (17). MQ can be associated with neuropsychiatric disorders including psychosis and convulsion (18). The widespread use of SP is likely to worsen antimalarial drug resistance (6). Similarly, the availability of AQ monotherapy may result in the worsening of drug resistance (6). DHA-PPQ is relatively inexpensive, effective and well tolerate. However, the relatively long half-life of PPQ (2-3 weeks) (19,20) compared to other partner drugs may result in the selection of resistance parasites by sub-therapeutic concentrations (8).

Pyronaridine

Pyronaridine is a blood schizonticide antimalarial agent that is effective against uncomplicated *P. falciparum* and *P. vivax* malaria as well as chloroquine-resistant strains of falciparum malaria both *in vitro* and *in vivo* (21-24). Clinical efficacy against *P. ovale* and *P. malariae* were also observed in 22 Cameroonian patients (25). Based on its activity *in vitro* and *in vivo*, pyronaridine is a promising partner drug for ACTs for the treatment of uncomplicated malaria. Pyronaridine/artesunate (PA) or Pyramax is a new fixed dose (3:1 ratio) ACT developed for three days treatment of uncomplicated

falciparum and vivax malaria. PA Phase II and III clinical trials have demonstrated high efficacy in falciparum malaria with >95% cure rates at day 28 (corrected for re-infection). In Asian patients, PA efficacy was 98.1%, equivalent to that of AL (26). In Asian and African patients, PA was non-inferior to AS-MQ and efficacy was >95% (27). Against *P. vivax*, PA had similar efficacy to chloroquine, but with faster parasite clearance ($P<0.001$) and fever clearance ($P=0.002$) (28). Finally, PA granule formulation has been shown to be efficacious and non-inferior to AL (29).

Physicochemical properties

Pyronaridine, a benzonaphthyridine derivative, was originally synthesized from 2-aminopyridine at the Institute of Parasitic Disease, Chinese Academy of Preventive Medicine in 1970 (21,22,30,31). The chemical structure of pyronaridine is shown in Figure 1.2. Its chemical name is 2-methoxy-7-chloro-10[3', 5'-bis (pyrrolidinyl-1-methyl) 4'-hydroxyphenl] amino-benzo[*b*]-1, 5-naphthyridine. Two forms of pyronaridine are available: pyronaridne free base and pyronaridne tetraphosphate. The salt form contains 57% free base and appears as a yellow or orange yellow crystalline powder, odorless, with a bitter taste and is slightly hygroscopic. It is sparingly soluble in water (1.46%w/v), and very slightly soluble in methanol, ethanol, and chloroform (30). Pyronaridine base, a more lipophilic form, is very slightly soluble in water (0.02%w/v), while it is sparingly soluble in chloroform (1.34%w/v) (30). The ionization constant (pKa) values of pyronaridine obtained from titration were 7.08, 7.39, 9.88, and 10.25 (30). All pyronaridine dosages used in clinical trials were pyronaridine tetraphosphate. Fifty seven percent of pyronaridine tetraphosphate is converted to pyronaridine free base.

Mechanism of action

Like chloroquine and other chloroquine related compounds, pyronaridine exerts its antimalarial activity by targeting β-haematin formation and interfering with the glutathione-dependent heme detoxification during blood stages of parasites (31-34).

Figure 1.3 shows a schematic representation of hemoglobin ingestion and catabolism in the malarial parasite (35). In erythrocytes, hemoglobin is digested from cytoplasm via cytosome and transported to food vacuole of parasites. In the food vacuole, hemoglobin is digested by several enzymes to break down protein to peptides which then are hydrolyzed to amino acids in parasite cytosol. This process releases heme containing Fe^{2+} which is then oxidized to hematin containing Fe^{3+} that is toxic to parasites. Hematin is detoxified by incorporating into microcrystalline hemozoin, a malaria pigment. Chloroquine and chloroquine related compounds, including pyronaridine, are believed to exert their mechanism of action by forming a complex with hematin, inhibiting the incorporation of hematin into hemozoin. Therefore, the toxic compound is accumulating in parasites resulting in the death of parasites.

Pharmacokinetics

Published data on the pharmacokinetics of pyronaridine in human are limited. Phase I-III clinical trials have shown that pyronaridine peak concentrations are generally reached between 2 and 8 hours post-dose following administration of Pyramax tablet to healthy and malaria infected subjects. A linear and dose proportional relationship between C_{max} and $AUC_{0-\infty}$ of pyronaridine tetraphosphate over the 6-15 mg/kg dose range has been observed following 3 day dose administration of pyronaridine tetraphosphate. Pyronaridine pharmacokinetics following single intravenous and oral administration have been investigated in rat and dog. The oral bioavailability of pyronaridine in rat and dog was calculated to be 42% and 35%, respectively (31). Based on data obtained *in vitro,* pyronaridine is highly bound to human serum proteins (92-95%). Pyronaridine distribution was estimated to be 1.5 fold higher in whole blood than in plasma. Metabolism is the major pathway for pyronaridine elimination. *In vitro* studies indicate the CYP450 isoforms are potentially responsible for PYR metabolism and have shown that PYR could be metabolized by CYP2D6, CYP1A2 and CYP3A4. Additionally,

inhibitory effects of pyronaridine investigated using pooled human liver microsomes and isozyme-specific probe substrates indicated that pyronaridine had a strong, moderate, and weak inhibitory effect on CYP2D6, CYP1A2, and CYP3A4, respectively. No inhibitory effect was observed on CYP2C9 and CYP2C19 with the maximum tested concentration of 50 µM. Nine and eleven metabolites were obtained following *in vitro* incubation with rat and human liver microsomes, respectively (36). A mass balance study in 6 healthy subjects has shown that thirteen metabolites (M1-M13) were identified by LC/MS in human blood, urine, and feces samples (unpublished data). Some of these metabolites had been found in human liver microsomes incubation. Figure 1.4 shows proposed metabolic pathways of pyronaridine in human blood, urine, and feces. Finally, pyronaridine has been shown to act as both substrate and inhibitor of P-glycoprotein (Pgp), suggesting an interaction with drugs transported by this pump (37-39).

Population pharmacokinetics

According to the USFDA, population pharmacokinetics can be defined as "the study of sources and correlates of variability in drug concentrations among individuals who are the target patient population receiving clinically relevant doses of a drug of interest" (40). Several factors can alter dose-concentration relationships such as patient demographic, pathophysiologic, therapeutic and environmental factors. Population pharmacokinetics is a tool to identify the measurable factors and the extent that they produce clinically significant changes in the dose-concentration relationship so that appropriate dosage regimens can be applied to individuals (41). Population pharmacokinetics also plays an important role in drug development by designing dosing guidelines for drug labeling, implementing important aspects of drug clinical pharmacology to regulatory bodies and selecting competing dosing regimens based on outcomes of clinical trials (42).

Traditionally, pharmacokinetic studies are conducted in a group of homogeneous subjects which reflect artificial conditions and do not represent real situations in which the drug will be used (42,43). Additionally, intensive sampling approach used to collect plasma drug concentrations is an obstacle to the conduct of pharmacokinetic studies in special population e.g. pediatrics, pregnant women or elderly. In contrast, population pharmacokinetics allows data from both sparse and intensive sampling approaches as well as unbalanced observations from heterogeneous group of subjects to be used which enables pharmacokinetic studies to be conducted in target patient populations.

Population pharmacokinetics can be conducted by several approaches: Naïve average data approach, Naïve pooled data analysis, two-stage approach, Bayesian estimation, and nonlinear mixed-effects modeling approaches. While Naïve pooled analysis estimates mean pharmacokinetic parameters from all individuals as if there were no kinetic differences between subjects, Naïve average approach estimates population parameters after computing the average value of the data for each sampling time (44). Both methods could lead to biased estimates if variations between subjects are large. Alternatively, the two-stage approach first estimates pharmacokinetic parameters for each individual separately, and then, in the second stage, population estimates are obtained across individuals. This approach relies on the individual parameter estimates which may result in erroneous population estimates if individual estimates are biased (45). Additionally, inter-individual variability may be overestimated since it includes variability from non-biological origins such as intra-individual variability and measurement errors (46). The Bayesian approach uses prior distribution of the parameter estimates and actual data to obtain the posterior distribution of parameters and to estimate individual parameters (44). This method is challenging since the results depend on uncertainties in prior distribution. Nonlinear mixed-effects modeling, a one-stage approach, estimates population parameters and variability simultaneously using data from all individuals. Studies have shown that the nonlinear mixed-effect modeling approach

produces accurate and precise estimates of both population mean kinetics and variability (45-47). Therefore, it is probably the most commonly used method for population pharmacokinetic analysis.

Nonlinear mixed-effects modeling

The term "mixed-effects" is obtained since it allows both "fixed" and "random" effects to be modeled simultaneously. The fixed effects refer to population estimates of pharmacokinetic parameters or effects of covariates on those parameters; whereas random effects refer to variability unexplained by fixed effects, inter-individual and residual variability. Residual variability includes measurement errors, model misspecification error, intra-individual variability (random variation in patient's parameters over time), and inter-occasion variability (variation in patient's parameters from one period to another period) (42).

A relationship between fixed and random effects for a one-compartment model of a single intravenous bolus administration can be described as follows:

$$C_{ij} = \frac{D_i}{V_i} e^{-\left(\frac{CLi}{Vi}\right)t} + \varepsilon_{ij}$$

$$\varepsilon_{ij} \sim N(0, \sigma^2)$$

where C_{ij} is the j^{th} drug concentration of i^{th} subject, D_i is the given dose. Fixed effect in this equation includes V_i (volume of distribution), and CL_i.(clearance). Random effect includes ε_{ij} (residual variability) which is assumed to be normally distributed with a mean of zero and variance of σ^2.

Another component of random effects is inter-individual variability which explains variability in pharmacokinetic parameters among subjects. A relationship between inter-individual variability and fixed effect (e.g. clearance) can be written as a function of creatinine clearance (CRCL) as follows:

$$CL_i = \theta_1 + \theta_2 * CRCL + \eta_i$$

$$\eta_{ij} \sim N(0, \omega^2)$$

where CL_i is the clearance of individual i. θ_1 and θ_2 are the parameters describing the linear relationship between CL_i and CRCL. η_i is the inter-individual variability that accounts for the deviation in CL_i from the population mean clearance and is assumed to be normally distributed with a mean of zero and variance of ω^2.

A Nonlinear mixed-effect model is comprised of three sub-models known as the structural or base model, the statistical model or model of variability, and the covariate model. While the structural model generally expresses the overall trend of the data and gives estimates of pharmacokinetic parameters in the absence of covariates, the covariate model describes the relationship between covariates and parameters obtained from the structural model. Several types of structural models: absorption model, disposition model, or semi-mechanistic model, can be developed depending on types of available data. Different types of covariate models will be discussed later in this thesis.

Determination of the structural or base model is the first step of population pharmacokinetic model development. The combination of several criteria, likelihood ratio test (LRT), Akaike information criterion (AIC), precision of parameter estimates, and graphical examination, are used for selecting the optimal base model as well as an adequate statistical model (48). The influences of covariates are explored after identifying the best structural model. Then, the final model needs to be evaluated in a consistent manner with the intended purpose (49).

Several software packages are available for nonlinear mixed-effect modeling such as NONMEM, SAS, S-plus, and Pharsight WinNonmix. NONMEM was selected in this research.

Thesis outlines and research objectives

A knowledge of pyronaridine pharmacokinetics and pharmacodynamics is of importance to achieve optimal therapeutic outcomes in the treatment of malaria with fixed dose PA. Up to now, published data on the pharmacokinetics and pharmacodynamics of pyronaridine are limited. The overall objective of this work is to determine pharmacokinetic and pharmacodynamic properties of pyronaridine as well as potential drug-drug interaction with other drugs metabolized by CYP2D6. In particular, the specific aims in Chapter 2 were to develop a population pharmacokinetic model for pyronaridine in healthy subjects and adult malaria patients and to determine the potential covariates that affect pyronaridine pharmacokinetic variability in this population. In Chapter 3, population pharmacokinetic model for pyronarine in pediatric malaria patients was developed. Monte Carlo simulation was also conducted in both Chapter 2 and Chapter 3 in order to address any differences in pyronaridine exposures between healthy adults, adult malaria patients and pediatric malaria patients and to explore the exposures of pyronaridine among recommended dosing groups of recommended dosage regimen for pediatric and adult malaria patients. The cut-off values of pyronaridne pharmacokinetic parameters associated with successful treatment outcome and the relationships between survival time and several covariates that affect the treatment outcome of PA are presented in Chapter 4. Chapter 5 focuses on the drug interactions between PA and the protease inhibitor, ritonavir, in healthy volunteers. The last chapter summarizes the findings in this thesis.

Figure 1.1 Life cycle of the malaria parasite (50)

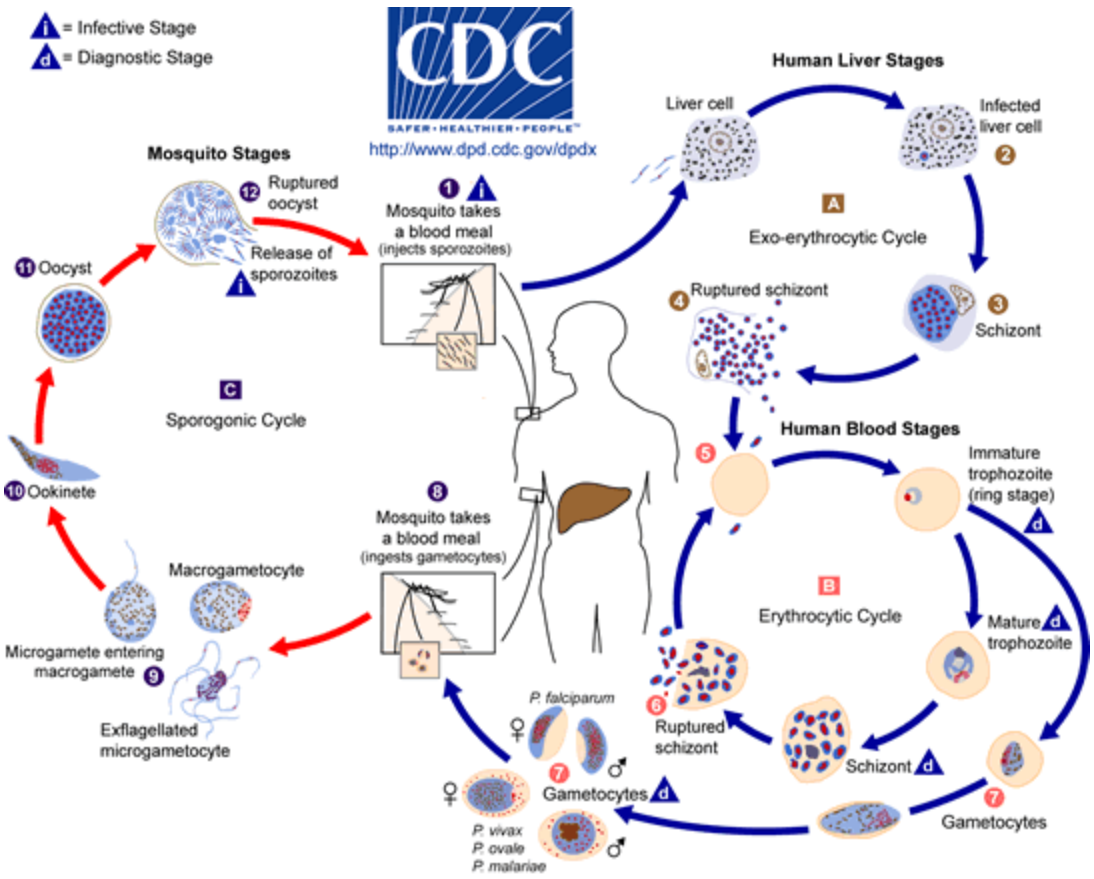

Figure 1.2 Chemical structure of pyronaridine tetraphosphate

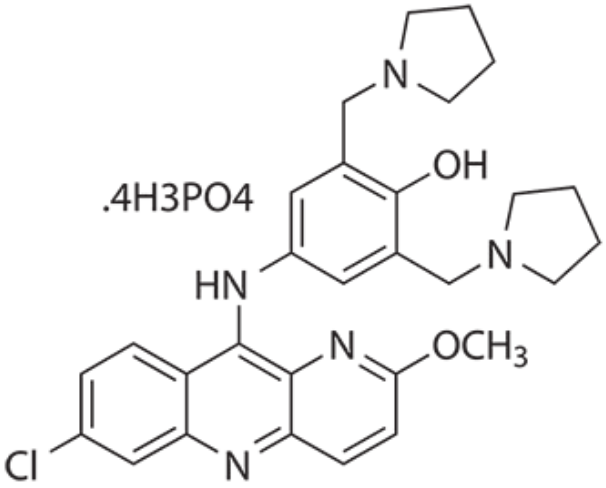

Figure 1.3 Schematic representation of hemoglobin ingestion and catabolism in the malaria parasite (35)

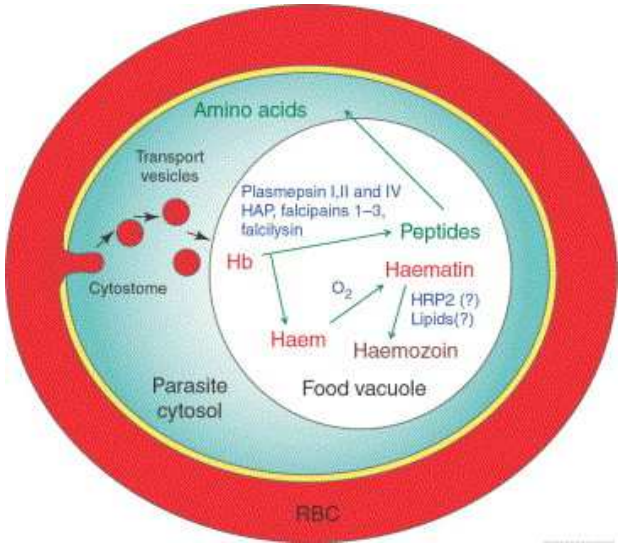

Figure 1.4 Proposed metabolic pathways of pyronaridine in human blood, urine, and feces

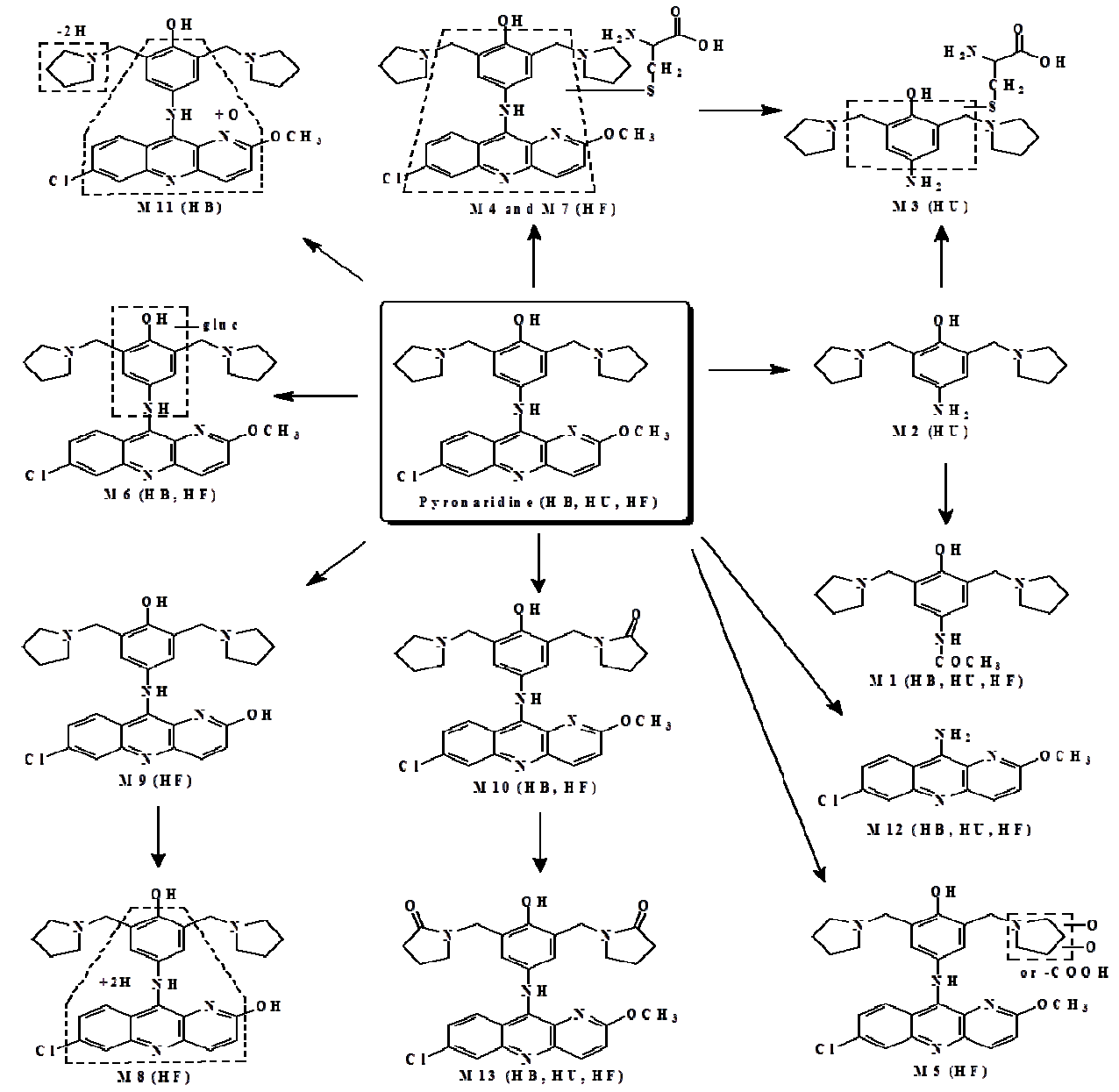

CHAPTER 2

POPULATION PHARMACOKINETICS OF PYRONARIDINE IN HEALTHY SUBJECTS AND ADULT MALARIA PATIENTS

Introduction

Pyronaridine is a blood schizonticidal antimalarial agent that targets hematin in the food vacuole of malaria parasites (33,34). It is considered a promising ACT partner drug as shown by its efficacy against antimalarial-resistance strains in vivo and in vitro (51-53). In humans, pyronaridine has shown efficacy against *P. falciparum*, *P. vivax*, *P. ovale*, and *P. malaria* (23-25).

Pyronaridine-artesunate (PA) 3:1 fixed dose combination (Pyramax®) is a new ACT developed for the treatment of uncomplicated *P. falciparum* and blood stage *P. vivax* malaria. The drug has two formulations: a tablet (180 mg pyronaridine: 60 mg artesunate) for adults and granules (60 mg pyronaridine: 20 mg artesunate) for pediatrics. The efficacy of this fixed dose formulation has been confirmed in several clinical trials. A comparative efficacy study with artemether-lumefantrine has shown that efficacy of pyronaridine-artesunate was non-inferior to that of artemether-lumefantrine with 99.7% and 98.1% cure rates in Africans and Asians, respectively (26). The non-inferiority of pyronaridine-artesunate versus mefloquine-artesunate was also confirmed with the cure rates of 99.2% (27). Additionally, pyronaridine-artesunate has shown similar efficacy to that of chloroquine against *P. vivax* malaria, but with shorter parasite clearance time ($p<0.001$) and fever clearance time ($p<0.05$) (28).

Pharmacokinetics of pyronaridine following intramuscular and oral administration has been studied in 10 Chinese malaria patients (54). A two compartment model adequately described pyronaridine pharmacokinetics. Central and peripheral volumes of distribution of pyronaridine were estimated to be 11.1 and 71.5 L/kg, respectively,

suggesting extensive distribution of the drug to peripheral tissues. The elimination half-life was approximately 60 hours.

To date, there is no published data on population pharmacokinetics of pyronaridine incorporating a large data set from both healthy and malaria subjects. Therefore, the objectives of this work were: to develop a population pharmacokinetic model of pyronaridine for healthy subjects and adult malaria patients, to evaluate influences of covariates on pyronaridine pharmacokinetic parameters, and to conduct Monte Carlo simulations to address differences in exposure between healthy subjects and adult malaria patients and to explore the exposure of pyronaridine among recommended dosing groups for adult malaria patients.

Theoretical

Nonlinear mixed-effects modeling using NONMEM

NONMEM estimates parameters by searching for parameters that minimize the objective function, called the extended least squares objective function (OFV_{ELS}), described as follows:

$$OFV_{ELS} = \Sigma_i^n \Sigma_j^n \left[\left\{ \frac{(y_{obsij} - y_{predij})^2}{Var_{ij}} \right\} + \ln(Var_{ij}) \right] \qquad 2.1$$

Where Y_{obsij} is the observed value of the j^{th} observation for the i^{th} individual, Y_{predij} is the predicted value of the j^{th} observation for the i^{th} individual, and Var_{ij} is the variance of the j^{th} observation for the i^{th} individual. Under an assumption that residuals (□) are independently normally distributed with mean of zero and variance of σ^2, extended least square estimation of θ is proportional to minus two times log of the likelihood of the data.

Several approximation methods are used to optimize parameter estimates in NONMEM: first-order method (FO), first-order conditional method (FOCE) with or

without interaction, Laplacian method, and hybrid method. The details of these methods can be found elsewhere (55,56).

Structural and statistical model development

Visual inspection of concentration time profiles from intensive sampling or information from previous studies can be used as a guide for determination of a structural model, the first step in population pharmacokinetic model development. Generally, a statistical model (model of variability) is determined together with structural model in order to estimate the fixed effects in a model precisely. Several common types of statistical models are given below:

Types of inter-individual variance model

1. Additive (constant variance) model

$$P_i = P_{pop} + \eta_i \qquad 2.2$$

2. Proportional (constant coefficient of variation) model

$$P_i = P_{pop} * (1 + \eta_i) \qquad 2.3$$

3. Exponential (log normal distribution) model

$$P_i = P_{pop} * \exp(\eta_i) \text{ or } \ln(P_i) = \ln(P_{pop}) + \eta_i \qquad 2.4$$

where P_i is the estimated parameter value for individual i and P_{pop} is the population estimate for the parameter. η_i is the deviation of P_i from P_{pop} and is assumed to be independent and symmetrically distributed with zero mean and variance ω^2.

Types of residual variance model

1. Additive (constant variance) model

$$Y_{ij} = F_{ij} + \varepsilon_{1ij} \quad 2.5$$

2. Proportional (constant coefficient of variation) model

$$Y_{ij} = F_{ij} * (1 + \varepsilon_{1ij}) \quad 2.6$$

3. Combination additive and proportional model

$$Y_{ij} = F_{ij} * (1 + \varepsilon_{1ij}) + \varepsilon_{2ij} \quad 2.7$$

4. Exponential model

$$Y_{ij} = F_{ij} * \exp(\varepsilon_{1ij}) \text{ or } \ln(Y_{ij}) = \ln(F_{ij}) + \varepsilon_{1ij} \quad 2.8$$

where Y_{ij} and F_{ij} are the j^{th} observed and model predicted concentrations for i^{th} individual, respectively. ε_{ij} is the residual random error for individual i and observation j and is assumed to be independently normally distributed with mean of zero and variance of σ^2.

Covariate modeling

The next step of population pharmacokinetic model development is to determine influences of covariates on pharmacokinetic parameters that account for variability among individuals. Several approaches to screen potential influential covariates have been proposed. Two approaches were used in this analysis: Generalized Additive Model

(GAM) and graphical analysis using the plots between individual empirical Bayes estimates of pharmacokinetic parameters and covariates. The shape of each relationship can also be obtained from these plots (57).

Briefly, the GAM procedure is performed using a stepwise addition or deletion method by regressing empirical Bayes estimates of pharmacokinetic parameters on each covariates in any functions (linear, spline, etc.). In each step, the model is selected by the greatest decrease in the Akaike information criterion (AIC) after addition or deletion of one term. The final model obtained from GAM is the model with a minimum AIC value. A general equation for GAM is given by (58):

$$p_{kl} = \alpha_{k0} + \Sigma_{l=1}^{n} g_{kl}(X_{li}) \qquad 2.9$$

where $g_{kl}(X_{li})$ is any arbitrary univariate function with $\Sigma_{l=1}^{n} g_{kl}(X_{li}) = 0$, α is the intercept. The potential covariates identified are then included in the structural model in various functions depending on GAM and graphical analysis. Normally, all continuous covariates are centered at median so that the parameter estimates obtained reflect the average of the population. Common types of covariate models are given below:

<u>Continuous covariate model</u>

1. Linear function

$$\mathrm{P} = \theta_1 + \theta_2 * (\mathrm{COV} - \mathrm{COV}_{\mathrm{median}}) \qquad 2.10$$

2. Linear proportional function

$$\mathrm{P} = \theta_1 * (1 + \theta_2 * (\mathrm{COV} - \mathrm{COV}_{\mathrm{median}})) \qquad 2.11$$

3. Power function

$$P = \theta_1 * (COV/COV_{median})^{\theta_2} \quad 2.12$$

4. Exponential function

$$P = \theta_1 * \exp(\theta_2 * (COV - COV_{median})) \quad 2.13$$

where P represents the pharmacokinetic parameter estimate of the population, COV is the continuous covariate tested, θ_1 is the parameter estimate of an individual with COV equal to COV_{median}, and θ_2 represents a factor describing the effect of covariate.

Categorical covariate model

1. Linear additive function

$$P = \theta_1 + \theta_2 * COV \quad 2.14$$

2. Linear proportional function

$$P = \theta_1 * (1 + \theta_2 * COV) \quad 2.15$$

3. Power function

$$P = \theta_1 * \theta_2^{COV} \quad 2.16$$

4. Exponential function

$$P = \theta_1 * \exp(\theta_2 * COV) \qquad 2.17$$

where P represents a pharmacokinetic parameter estimate of the population, COV is the categorical covariate tested, θ_1 is the parameter estimate of an individual with COV coded as 0, and θ_2 is the additional change in the parameter corresponded to categorical covariate being tested.

Covariate model selection is based on statistical significance, physiologic plausibility, and clinical relevance. Statistical significance is normally tested using stepwise forward addition and stepwise backward elimination. A clinical significance can be evaluated from the percentage change in the affected parameter, the reduction in inter-individual and residual variability as well as an improvement in the precision of parameter estimates.

Model evaluation

Model evaluation should be applied to the final model according to the purpose of the developed model: descriptive or predictive (49). The model to be used for descriptive purpose should be assessed for its goodness of fit, reliability and stability. While validation is essential for a model developed for predictive purposes. There are two types of model validation: internal and external. Statistical techniques used for internal validation include cross validation, data splitting, bootstrap analysis, posterior or visual predictive check. Whereas, external validation can be performed using normalized prediction distribution error (NPDE), prediction discrepancies (PD), and standardize prediction error (SPE) (59). Model evaluation techniques used in the analysis are discussed below.

Diagnostic plots

Commonly used diagnostic plots for model evaluation include the plots between observed versus population predicted concentration (PRED), observed versus individual predicted concentration (IPRED), conditional weighted residual (CWRES) versus PRED and CWRES versus time. The plots between observed concentrations versus PRED and IPRED should be explained for any bias of model prediction. Ideally, the concentrations should be uniformly distributed along the line of identity without any trends. Similarly, there should be a balance scattered of CWRES along the zero line.

Bootstrap analysis

Bootstrap datasets are generated by resampling with replacement of the observations from the original dataset. The final model is repeatedly fitted to the bootstrap datasets to obtain means and 95% confidence intervals of the parameter estimates. These values are then compared with those obtained from the final model.

Visual predictive check

Visual predictive check is used to assess predictive ability of the final model. It is performed by simulating drug concentrations at each sampling time point. Then 5^{th} and 95^{th} percentiles of the simulated concentration (90% prediction interval) are plotted with the observed concentrations. The final model is considered to be predictive if the majority of the observed concentrations lie within the 90% prediction interval.

Condition number

A condition number is used to evaluate the stability of the model. It is the ratio of the largest eigenvalue to the smallest eigenvalue generated by NONMEM with PRINT=E command in $COVARIANCE record. A condition number of greater than 1000 indicates that the model is unstable.

Materials and Methods

Study designs and blood sampling

Pooled data from three Phase I studies, one Phase II study and three Phase III studies were used for the population pharmacokinetic analysis. The design for population pharmacokinetic studies and the bio-analysis was conducted by Clinical Pharmacokinetic Laboratory, College of Pharmacy, the University of Iowa. Study designs, dosage regimen, and blood sampling of each clinical study were summarized as follows:

Phase I (SP-C-001-03, SP-C-009-07, and SP-C-010-10)

SP-C-001-03 was divided into 4 parts. **Part 1** was conducted to evaluate the pharmacokinetics, safety and tolerability of PA using a single oral ascending dose. Subjects were randomized in a 7:2 ratio to receive PA:placebo at following doses: PA 6:2 mg/kg, PA 9:3 mg/kg, PA 12:4 mg/kg, and PA 15:5 mg/kg. The aim of **Part 2** was to evaluate the potential drug interaction between pyronaridine and artesunate of a single oral dose of PA. It was conducted as a two-cohort parallel, two-period randomized crossover design. Five subjects received pyronaridine tetraphosphate 12 mg/kg alone (cohort 1) or artesunate 4 mg/kg alone (cohort 2) followed by PA 12:4 mg/kg after a 21 day washout period, the reverse order of these treatments was assigned to an additional five subjects for each cohort. **Part 3** was a study of food effects on the pharmacokinetics of PA. Twenty subjects were randomized into two arms. In period 1, subjects were administered PA 12:4 mg/kg after an overnight fast (arm 1) or 30 minutes after consumption of a high fat meal (arm 2). In period 2, the same subjects received these treatments in reverse order. The two periods were separated by 21-day washout interval. **Part 4** was identical to part 1, except subjects were administered PA ascending dose for 3 days and were randomized in a 6:2 ratio to PA: placebo. Eight subjects received PA or placebo at each dose level. For part 1-3, blood samples were collected at pre-dose and at 0.33, 0.67, 1, 1.33, 1.67, 2, 2.5, 3, 4, 5, 8, 12, 24 hours and 2, 3, 5, 7, and 10 days post-

dose. For part 4, blood samples were collected immediately before each dose and at 0.33, 0.67, 1, 1.33, 1.67, 2, 2.5, 3, 4, 5, 8, 12, 24 hours and 2, 3, 5, 7, and 10 days after the third dose.

SP-C-009-07 was a two-way crossover study to evaluate the bioequivalence of a single dose combination of PA (180:60 mg) to-be-marketed tablet to the clinical trial reference tablet. After an overnight fast, subjects were administered four PA reference tablets followed by four PA to-be-marketed tablets in sequence 1. The order of formulation administration was reversed in sequence 2. Two treatment periods were separated by a 43 day washout interval. Blood samples were collected at pre-dose and at 0.5, 1, 1.5, 2.5, 4, 6, 8, 12, 24, 48, 72, hours and at 5, 7, 14, 21, 28, 35, and 42 days post-dose for each period.

SP-C-010-10 was conducted to determine any drug interaction between PA (180:60 mg) and the protease inhibitor ritonavir in healthy adult volunteers. Thirty four subjects were randomized into two arms. Subjects in arm A received both ritonavir and PA. A single dose of ritonavir 100 mg was given on day 1 and q 12 hours on days 2-17. PA was given once daily on days 8-10. Subjects in arm B received PA alone once daily on days 1-3. In both arms, PA was administered according to body weight: < 65 kg received three tablets, and ≥ 65 kg received four tablets. For Arm A, blood samples were collected at pre-dose, and at 0.5, 1, 1.5, 2, 3, 4, 6, 8, 12 hours and 4, 5, 6, 8, 15, 22, 29 and 36 days after the third dose. For Arm B, blood samples were drawn at pre-dose on days 8, 9 and 10, and at 0.5, 1, 1.5, 2, 3, 4, 6, 8, 12, 18, 24 hours and 11, 12, 13, 15, 22, 29, 36, and 43 days after the third dose.

Phase II (SP-C-002-05)

SP-C-002-05 was conducted to assess safety, tolerability and efficacy of the 3 day regimen of PA in adult patients with acute uncomplicated *P. falciparum* malaria. Patients were randomized to one of 3 treatment groups: Group A: PA 6:2 mg/kg, Group B: PA 9:3

mg/kg, and Group C: PA 12:4 mg/kg. Blood samples were collected immediately before each dose, and at 0.5, 1, 1.5, 2, 2.5, 4, 8, 16, 24 hours and 3, 5, 12, 19 days after the third dose.

Phase III (SP-C-004-06, SP-C-005-06, and SP-C-006-06)

SP-C-004-06 and SP-C-005-06 were comparative, randomized studies to assess the efficacy and safety of PA (180:60 mg) with that of mefloquine (250 mg) plus artesunate (100 mg) and with that of artemether-lumefantrine (20:120 mg) (Coartem®), respectively in children and adult patients with uncomplicated *P. falciparum* malaria.

SP-C-006-06 was a comparative, randomized double blind, double dummy study to assess the safety and efficacy of PA (180:60 mg) with that of chloroquine (155 mg) in patients with acute *P. vivax* malaria.

For all studies in phase III, PA was given according to body weight: 20 - ≤ 25 kg received one tablet, 26 - < 45 kg received two tablets, ≥ 45 - < 65 kg received three tablets, and ≥ 65 - 90 kg received four tablets. One or two blood samples were collected at two different time points (between Day 0 and Day 3, and between Day 4 and Day 42). All subjects provided written informed consent for their participation in the trial. All studies were approved by the local Ethics Committee.

Sample analysis

Blood samples were collected into sterile glass tubes containing EDTA as the anticoagulant (Lavender–top Vacutainer® EDTA tubes) and then were transferred into two approximately equal volume aliquots in screw cap Nalgene cryovials. All samples were stored at or below -80°C until analysis. For SP-C-001-03, pyronaridine concentrations were determined using a validated high performance liquid chromatography (HPLC) with UV detection as described by Chen et al (60). The coefficient of variation for intra-day and inter-day precision ranged from 3.0% to 5.9% and 5.0% to 10.0%, respectively. For all other studies, except SP-C-001-03, pyronaridine

concentrations were determined by a validated liquid chromatography-mass spectrometric method (LC/MS) as described by Naik et al (61). The coefficient of variation for intra-day and inter-day precision ranged from 2.2% to 11.1% and 7.8% to 15.9%, respectively. The lower limit of quantification (LLOQ) for both HPLC and LC/MS methods was 5.7 ng/mL.

Population pharmacokinetic analysis

Nonlinear mixed-effect modeling was conducted to obtain estimates of population pharmacokinetic parameters, inter-individual variability (IIV) and residual variability (RV). NONMEM software version VII level 2.0 (ICON Development Solutions, 2009) was used. NONMEM output was processed using PDx-Pop version 4.0 (ICON Development Solutions, 2007) and Xpose version 4.3.0 (Uppsala University, Uppsala, Sweden, 2010). Graphical plots were produced using TIBCO Spotfire S+ version 8.1 (TIBCO Software Inc., 2008) and R 2.10.1 (The R Foundation for Statistical Computing, 2010). All pyronaridine concentrations were transformed into their natural-logarithms and the dose of pyronaridine tetraphosphate (PP) was converted to pyronaridine base by multiplying by the factor of 0.57 prior to modeling.

Structural model development

Two- and three- compartment models with first-order absorption and elimination from the central compartment were evaluated as the kinetic models for orally administered pyronaridine based on concentration time profiles. Inter-individual and residual variability were modeled with an exponential error model (Eq. 2.4 and Eq. 2.8, respectively).

Covariate model building

The influences of 5 continuous covariates (body weight, lean body weight (LBW), body mass index (BMI), age, and creatinine clearance (CRCL)), and 5

categorical covariates (malaria infection, aspartate aminotransferase (AST), alanine aminotransferase (ALT), gender, and ritonavir administration) on pharmacokinetic parameters were evaluated after the optimal base model was identified. Generalized additive models (GAM), plots of the individual Bayes parameter estimates versus covariates, as well as physiologic plausibility were applied to select potential covariates. Then these covariates were tested for statistical significance using stepwise forward addition and stepwise backward elimination. The significance levels of 0.05 and 0.001 which correspond to the difference in OFV of 3.84 and 10.83 were used as statistical criteria for stepwise forward addition and stepwise backward elimination, respectively.

Continuous covariates (code) included in the dataset were:

1. Total body weight in kilograms (WT)
2. Lean body weight in kilograms (LBW)
3. Body mass index (BMI) in meter^2, calculated as:

   BMI (kg/m^2) = weight (kg) / height^2 (m^2)
4. Age in years (AGE); the cut-off age of greater than or equal to 16 years was used to separate adult and pediatric subjects based on General Considerations for Pediatric Pharmacokinetic Studies for Drugs and Biological Products (62)
5. Creatinine clearance (CRCL) was estimated using the Cockcroft and Gault equation with SCr given as mg/dL:

   Males:

   CRCL (mL/min/1.73 m^2) = [(140 – age)*IBW/ (72*Scr)]

   IBW= 0.9*(height in cm above 152 cm) + 50 kg

   If WT<IBW or height<152 cm, WT was substituted for IBW

Females:

CRCL (mL/min/1.73 m^2) = [(140 – age)*IBW/ (72*Scr)]*0.85

IBW = 0.9*(height in cm above 152 cm) + 45.5 kg

If WT<IBW or height<152 cm, WT was substituted for IBW

All creatinine clearance estimates were adjusted for body surface area (BSA). BSA was computed using the Haycock formula:

BSA (m^2) = ($Wt^{0.5378}$)*($Ht^{0.3964}$)*0.024265

Categorical covariates (code) included in the dataset were:

1. Infection status (INFEC), coded as 0 if subjects did not have malaria infection and 1 if subjects had malaria infection.
2. Baseline aspartate aminotransferases (AST), coded as 0 if baseline AST level was ≤ 1.5 x upper limit of normal range (ULN) and 1 if baseline AST level was > 1.5 x ULN. (ULN for AST was defined as 19 U/L for SP-C-003-05 and 41 U/L for all Phase III studies and SP-C-002-05. For Phase I study SP-C-001-03, ULN for AST was 40 U/L. For SP-C-009-07, the ULN for AST was 34 U/L).
3. Baseline alanine aminotransferases (ALT), coded as 0 if baseline ALT level was ≤ 1.5 x upper limit of normal range (ULN) and 1 if baseline ALT level was > 1.5 x ULN. (ULN for ALT was defined as 23 U/L for SP-C-003-05 and 45 U/L for all Phase III studies and SP-C-002-05. For SP-C-001-03, the ULN for ALT was 40 U/L. For SP-C-009-07, the ULN for ALT was 55 U/L).
4. Gender (SEX), coded as 0 for female and 1 for male.
5. Ritonavir administration (RTV), coded as 0 if subjects did not receive ritonavir and 1 if subjects received ritonavir.

All continuous covariates were centered with the median values and were evaluated with a linear function (Eq. 2.10), a power function (Eq. 2.12) and an exponential function (Eq. 2.13), depending on GAM and graphical exploration of the relationships between covariates and pharmacokinetic parameters. The influences of categorical covariates on the parameter were modeled with an additive relationship (Eq. 2.14). The importance of covariates as predictors was determined by a statistically significant improvement in the MOFV, improvement in the precision of the parameter estimate (relative standard error), percentage change in affected covariates and reduction in IIV and RV.

Model evaluation

Model goodness-of-fit was assessed using diagnostic plots of observed pyronaridine concentrations versus PRED and versus IPRED, CWRES versus PRED and versus time. Precision of the parameter estimates was assessed using a nonparametric bootstrap approach. One thousand bootstrap runs were generated using Perl-Speaks-NONMEM version 3.1.0. Predictive ability of the final model was evaluated using visual predictive check (VPC) by simulating one thousand pyronaridine observations at each sampling time point. The observed pyronaridine concentrations were then plotted with the 5^{th}, 50^{th}, and 95^{th} percentiles of the simulated observations to obtain the population median concentrations and 90% prediction interval. The percentage of observed pyronaridine concentrations above and below the 90% prediction interval was calculated. Model stability was assessed by a condition number with the criteria of less than 1000 as indicative model stability.

Simulations

One thousand simulations were conducted to address any differences in exposures between healthy subjects and adult malaria patients. Parameter estimates obtained from

the final model, the median weight, and the dose of 10 mg/kg pyronaridine tetraphosphate were used for the simulation.

In order to explore the exposure of pyronaridine among recommended dosing groups of current proposed PA tablet labelling (Table 2.6), two extreme weight values (lower and upper limits) in each dosing group were used for the simulations.

Results

Demographic data

A total of 5,127 blood samples were collected to determine pyronaridine level. Of these 297 (5.9%) observations were below LLOQ, one (0.02%) observation was identified as an outlier. Since the number of concentrations below LLOQ was only 5.9%, they were excluded from the analysis (63). In total, 4,756 blood pyronaridine concentrations collected from 476 subjects (166 healthy and 310 adult malaria patients) were available for population pharmacokinetic analysis. The numbers of missing observations, demographic and clinical characteristics of the population in each clinical study are summarized in Table 2.1. The median age and median weight of this population were 26 years and 56 kg, respectively. The number of males and females in this population were 66.8% and 33.2%, respectively.

Population pharmacokinetic model

A two compartment model with first order absorption and elimination from the central compartment best described pyronaridine data. The final base model was parameterized in terms of absorption rate constant (K_a), apparent central volume of distribution (V2/F), apparent peripheral volume of distribution (V3/F), oral clearance (CL/F) and inter-compartmental clearance (Q/F) where F is oral bioavailability. Figure 2.1 shows the distribution of continuous covariates. The correlation matrix of continuous covariates is presented in Figure 2.2. The potential covariate-parameter relationships

obtained from GAM, graphical exploration and physiologic plausibility were malaria infection, age, and body weight on CL/F, V2/F, and V3/F; ALT, AST, CRCL, and ritonavir administration on CL/F; LBW on CL/F and V2/F and BMI on V3/F. A summary of forward addition and backward elimination steps is presented in Table 2.2. Only malaria infection and body weight were retained in the final model. Malaria infection was found to be a significant covariate on CL/F, V2/F, and V3/F and body weight was found to be a significant covariate on CL/F and V2/F. After the inclusion of statistically significant covariates, the population parameter estimates of CL/F, V2/F, V3/F, Q/F and K_a were 501 L/day, 741 L, 5,370 L, 1,150 L/day and 16.3 day^{-1}, respectively. The corresponding %CV of IIV estimates for CL/F, V2/F, V3/F, and K_a were 35.1 %, 62.4%, 31.2%, and 64.3%, respectively. The IIV on Q/F was fixed to zero since the estimate could not be obtained with good precision. The derived mean $t_{1/2\beta}$ of pyronaridine in healthy adult subjects and adult malaria patients was estimated to be 10.7 and 25.2 days, respectively (Table 2.4). The derived $AUC_{0-\infty}$ values and pyronaridine concentrations on day 7 following 3 dose administrations are summarized in Table 2.4. The parameter estimates obtained from the final model are summarized in Table 2.3. The relationships between significant covariates and pharmacokinetic parameters were described as follows:

$$CL/F\ (L/day) = [(501 + 582(\text{malaria infection}))*(\text{body weight}/56)^{0.874}]*\exp(\eta)$$

$$V2/F\ (L) = [(741 + 9{,}070(\text{malaria infection}))*(\text{body weight}/56)^{1.25}]*\exp(\eta)$$

$$V3/F\ (L) = [5{,}370+10{,}800(\text{malaria infection})]*\exp(\eta)$$

Model evaluation

Figure 2.3-2.4 shows goodness-of-fit plots of pyronaridine. The individual plots for selected subjects are presented in Figures 2.5-2.6. The final model was repeatedly fitted to 1,000 bootstrap data sets. 92.6% of the bootstrap runs successfully converged. The mean parameter estimates and 95% confidence intervals obtained from bootstrap are

summarized in Table 2.3. The bootstrap estimates were reasonably close to those obtained from the final model with less than 10% difference and the estimates obtained from the final model were contained within the 95% confidence intervals obtained from bootstrap suggesting that the model is reliable. The result of VPC is presented in Figure 2.7. Approximately 2.86% and 3.45% of pyronaridine observations were below and above 90% prediction interval, respectively suggesting that the final model has good predictive ability. Finally, the condition number of the final model was 80.0 indicating that the final model was stable.

Simulations

The simulated pyronaridine concentrations for healthy adults versus adult malaria patients are presented in Figure 2.8. Figure 2.9 shows Ln(AUC) distributions of pyronaridine based on 4 dosing regimens for adult malaria patients. Healthy adults had higher exposures to pyronaridine as compared to adult malaria patients. The overall range of exposures among dosing groups for adult malaria patients were relatively similar.

Discussion

In this study, a population pharmacokinetic model of pyronaridine was developed using pooled data from three Phase I, one Phase II and three Phase III clinical studies. Extensive design was used in Phase I and Phase II studies while sparse design was used in Phase III studies. 476 subjects (166 healthy subjects and 310 adult malaria patients) with a total of 4,756 blood pyronaridine concentrations were included in the analysis. Only 5.9% of the observations were below LLOQ and were excluded from the analysis (63).

Goodness-of-fit plots showed no major bias suggesting that there was no major model misspecification. The under-prediction of low pyronaridine concentrations was

probably due to a proportion of data below the LLOQ. The population pharmacokinetic estimates of pyronaridine yielded relatively large V2/F and V3/F suggesting the extensive distribution of the drug through the body. All parameters were estimated with acceptable precision with relative standard error values of less than 15% on all pharmacokinetic parameters and less than 30% on variability parameters. The variability on Q/F was fixed to zero since it could not be estimated with good precision and the 95% CI of the estimate included zero. The parameter estimates obtained from the final model were close to those generated from 1000 bootstrap runs, indicating the reliability of the model. The VPC results showed that the final population model had predictive ability. Finally, the model was stable as evidenced by the condition number.

Covariates found to have a significant influence on pyronaridine pharmacokinetics were malaria infection on CL/F (additive function), V2/F (additive function) and V3/F (additive function), and body weight on CL/F (power function), and V2/F (power function). Both body weight and LBW were significant on the same parameters (CL/F and V2/F) during step one of stepwise forward addition. However, due to the high degree of collinearity between body weight and LBW (Figure 2.1) and the greater reduction in MOFV after including body weight as compared to LBW, body weight was incorporated into the next step of covariate model building rather than LBW. CL/F and V2/F were approximately 2 times and 14 times higher in adult malaria patients compared to healthy subjects. These findings were consistent with the results from non-compartmental analysis in Phase I and Phase II. The higher V2/F observed in malaria patients might be due to the mechanism of action of pyronaridine that form a complex with hematin to enhance hematin induced red blood cell lysis (34). Age was significant

on V3/F and was included in the full model during stepwise forward addition of the covariate model building (p-value < 0.05). However, it was not significant during stepwise backward elimination with the significant level of 0.001.

The effect of renal function was also evaluated using creatinine clearance computed from baseline serum creatinine (SCr). Creatinine clearance was significant on CL/F during the first 2 rounds of stepwise forward addition. However, there was no significant improvement in MOFV after malaria infection was included in the model. Patients in the modeled dataset had mild, uncomplicated malaria, characterized by lower levels of parasitemia (1,000-100,000 asexual parasite count/µL of blood). In addition, the exclusion criteria for the Phase II – III trials selected patients who were unlikely to be predisposed to more severe illness. Thus, patients with medical histories which included clinically significant disorders affecting essentially any organ system were excluded, as were patients with ALT or AST elevations more than 2.5 or 3 x ULN, SCr values equal to or greater than 1.4 mg/dL, or hemoglobin levels below 8 g/dL. Severely malnourished patients and patients with significant electrolyte disturbances were also excluded. Therefore, while we did not detect a disease effect in the current analysis, such an effect may well be apparent in more severe malaria infection or more extensive involvement of other organ systems.

Ritonavir is an inducer of CYP3A4 and CYP1A2 (64). Additionally, it is both an inhibitor and substrate of CYP3A4, CYP2D6, and P-gp (65,66). *In vitro* studies have shown that pyronaridine could be metabolized by CYP1A2, CYP2D6 and CYP3A4. Therefore, there might be potential drug-drug interactions between pyronaridine and ritonavir. However, in this analysis, ritonavir administration was not found to have

significant effect on pyronaridine pharmacokinetics. This result was consistent with that from drug-drug interaction study (SP-C-010-10) that the 90% confidence intervals for the Arm A/Arm B ratios of geometric means of all computed pharmacokinetic parameters ($AUC_{0\text{-}tau}$, $AUC_{0\text{-}t}$, and $AUC_{0\text{-}\infty}$) with the exception of C_{max}, were contained in the acceptance range of 0.667 -1.50. However, the effect of ritonavir on pyronaridine C_{max} was not considered to have clinical relevance given that the 90% confidence interval for the geometric mean of C_{max} was very close to the acceptance range (67). These results would be expected given that there is no major pathway for metabolizing pyronaridine. Additionally, the cytochrome P450 used to metabolize pyronaridine accounts for an unknow fraction of pyronaridine metabolism.

Monte Carlo simulation was performed to address any differences in exposures between healthy subjects and adult malaria patients. The simulated pyronaridine concentrations are higher in healthy adult subjects as compared to adult malaria patients (Figure 2.6). These results are consistent with those from non-compartmental analysis in Phase I and Phase II studies. The lower simulated pyronaridine concentrations in adult malaria patients may reflect the larger V2/F and higher CL/F as compared to healthy adults (Table 2.5). Additionally, the simulation results comparing pyronaridine exposures among dosing groups of current proposed PA tablet labelling (Figure 2.7) showed that pyronaridine exposures were consistent among different dosing groups.

Conclusions

In summary, data from seven clinical trials of a novel artemisinin-based combination therapy, pyronaridine-artesunate were included in population pharmacokinetic analysis of pyronaridine. A two-compartment model with first order

absorption and elimination from the central compartment best described pharmacokinetics of pyronaridine in healthy subjects and adult malaria patients. The significant covariates in the final model included malaria infection on apparent clearance, apparent central and peripheral volumes of distribution and body weight on apparent clearance and apparent central volume of distribution. The final model was reliable, predictive, and stable as confirmed by criteria of model validation.

Table 2.1 A summary of study data, patient demographics and covariates included in the analysis

Characteristics	Phase I			Phase II	Phase III			All studies
	SP-C-001-03	SP-C-009-07	SP-C-010-10	SP-C-002-05	SP-C-004-06	SP-C-005-06	SP-C-006-06	
Number of subjects [N]	91	42	33	16	213	56	25	476
Number of observations								
Total	2195	1422	625	248	403	105	49	5047
Excluded as LOQ [N(%)]	45 (2.1)	117 (8.2)	7 (1.1)	2 (0.8)	83 (20.6)	27 (25.7)	16 (32.7)	297 (5.9)
Excluded as outliers [N(%)]	0 (0)	1 (0.1)	0 (0)	0 (0)	0 (0)	0 (0)	0 (0)	1 (0.02)
Included in the analysis [N(%)]	2150 (97.9)	1304 (91.7)	618 (98.9)	246 (99.2)	320 (79.4)	78 (74.3)	33 (67.3)	4749 (94.1)
Median age (range) (years)	23 (19-40)	33.5 (20-45)	46 (19-55)	30 (16-60)	26 (16-58)	22.5 (16-55)	30 (17-53)	26 (16-60)
Median weight (range) (kg)	61.7 (50.1-70)	68.8 (55.2-75)	70.3 (54.5-90.1)	53.8 (42-74.5)	51.9 (38.1-72.3)	55.5 (33-80)	52.1 (41.3-67)	56 (33-90.1)
Median BMI (range) (kg/m^2)	21.1 (18.1-23.8)	23.6 (19.4-27.5)	23.9 (19.6-29.4)	20.4 (17-32)	19.9 (14.3-26.9)	22.4 (15.4-35.6)	19.8 (16.6-27.1)	20.8 (14.3-35.6)
Median LBW (range) (kg)	50.2 (37.9-57.4)	52 (41.2-61.6)	54.8 (40.2-67.4)	42.5 (32.2-58.7)	43.2 (29.2-56.5)	42.7 (28.2-57.1)	42.6 (31.7-52.3)	45.1 (28.2-67.4)
Median Creatinine Clearance (range) (mL/min)	95.0 (61.4-127.6)	104.1 (63.4-160.8)	103.7 (68.5-227.6)	69.5 (29.8-99.9)	73.4 (28.5-228.8)	97.3 (51.8-251.7)	77.3 (53.8-115.8)	82.97 (28.46-251.71)

Table 2.1 -continued

Characteristics	**Phase I**			**Phase II**	**Phase III**			**All studies**
	SP-C-001-03	**SP-C-009-07**	**SP-C-010-10**	**SP-C-002-05**	**SP-C-004-06**	**SP-C-005-06**	**SP-C-006-06**	
Gender [N(%)]								
Female	37 (40.7)	18 (42.9)	14 (42.4)	12 (75)	40 (17.8)	32 (57.1)	5 (20)	158 (33.2)
Male	54 (59.3)	24 (57.1)	19 (57.6)	4 (25)	173 (81.2)	24 (42.9)	20 (80)	318 (66.8)
AST>1.5 ULN	0	0	0	1	12	4	2	19
ALT>1.5 ULN	0	0	0	1	6	0	2	9

Table 2.2 A summary of covariate model development

Step	Covariate added to Base model [a]	MOFV	Δ MOFV
0	Base model	-735.61	-
1	INFEC on V2/F	-1195.15	459.54
2	INFEC on V2/F, INFEC ON V3/F	-1389.38	194.23
3	INFEC on V2/F, INFEC ON V3/F, INFEC ON CL/F	-1428.68	39.3
4	INFEC on V2/F, INFEC ON V3/F, INFEC ON CL/F, WT ON V2/F	-1454.85	26.17
5	INFEC on V2/F, INFEC ON V3/F, INFEC ON CL/F, WT ON V2/F, WT ON CL/F	-1469.31	14.46
6	INFEC on V2/F, INFEC ON V3/F, INFEC ON CL/F, WT ON V2/F, WT ON CL/F, AGE ON V3/F (Full Model)	-1474.63	5.32
Step	**Covariate removed from Full model [a]**	**MOFV**	**Δ MOFV**
1	INFEC on V2/F	-1038.46	436.17
	INFEC on V3/F	-1422.8	51.83
	INFEC on CL/F	-1423.69	50.94
	WT on V2/F	-1454.4	20.23
	WT on CL/F	-1462.09	12.54
	AGE on V3/F	-1469.31	5.32

[a] WT = body weight, INFEC = malaria infection

Table 2.3 Final population pharmacokinetic and bootstrap results for pyronaridine

Parameter [a]	Estimate (95%CI)	%RSE [b]	%CV [c]	Bootstrap estimate (95% CI) [d]
PK Parameters				
CL/F (L/day)	501 (447-555)	5.47		503 (460-550)
V2/F (L)	741 (572-910)	11.6		734 (653-818)
V3/F (L)	5,370 (4,940-5,800)	4.04		5,387 (4,964-5,814)
Q/F (L/day)	1,150 (1,100-1,200)	2..21		1,156 (1,075-1,239)
K_a (day^{-1})	16.3 (13.6-19.0)	8.47		16.2 (14.3-18.4)
Malaria infection on CL/F	582 (389-775)	16.9		586 (430-752)
Malaria infection on V2/F	9,070 (8,150-9,990)	5.16		9,016 (7,929-10,213)
Malaria infection on V3/F	10,800 (3,530-18,100)	34.4		10,584 (7,716-13,600)
Body weight on CL/F	0.874 (0.584-1.16)	16.9		0.833 (0.389-1.29)
Body weight on V2/F	1.25 (0.827-1.67)	17.3		1.32 (0.746-1.84)
IIV				
IIV-CL/F	0.123 (0.088-0.158)	14.4	35.1	0.124 (0.084-0.173)
IIV-V2/F	0.390 (0.316-0.464)	9.67	62.4	0.383 (0.261-0.500)
IIV-V3/F	0.0974 (0.0506-0.144)	24.5	31.2	0.095 (0.0539-0.139)
IIV-Q/F	-	-	-	-
IIV-K_a	0.413 (0.197-0.629)	26.6	64.3	0.404 (0.292-0.527)
RV (additive error)				
RV	0.200 (0.196-0.204)	1.03		0.200 (0.173-0.230)

[a] CL/F = apparent clearance, V2/F = apparent central volume of distribution, V3/F = apparent peripheral volume of distribution, Q/F = apparent intercompartmental clearance, K_a = first-order absorption rate constant, F = bioavailability.

[b] %RSE = relative standard error computed by (SE/mean)x100%.

[c] %CV= coefficient of variation computed by $\%CV = \sqrt{\exp(\omega^2) - 1} * 100\%$

[d] 95% CI of bootstrap estimate are the 2.5 and 97.5 percentile of the bootstrap estimates.

Table 2.4 Derived parameters obtained from post-hoc Bayes estimates of the final model

Parameter	Estimate (mean ± SD)
$t_{½\alpha}$ (days) [a]	
Healthy adult subjects (age ≥ 16 years)	0.34 ± 0.17
Adult malaria patients (age ≥ 16 years)	2.60 ± 1.16
$t_{½\beta}$ (days) [a]	
Healthy adult subjects (age ≥ 16 years)	10.68 ± 2.31
Adult malaria patients (age ≥ 16 years)	25.19 ± 3.64
$AUC_{(0-\infty)}$ (mg*day/L) [b]	
Healthy adult subjects (age ≥ 16 years)	2.98 ± 1.10
Adult malaria patients (age ≥ 16 years)	1.10 ± 0.22
Predicted pyronaridine day 7 concentration (ng/mL) [c]	
Healthy adult subjects (age ≥ 16 years)	73.59 ± 27.95
Adult malaria patients (age ≥ 16 years)	31.79 ± 6.38

[a] $t_{½\alpha}$ and $t_{½\beta}$ are the distribution and elimination half-lives, respectively.

[b] Area under the concentration-time curve from 0 to ∞ was computed using a 3 day dose of PA and microparameters obtained from post-hoc Bayes estimates of the final model.

[c] Predicted pyronaridine day 7 concentrations were computed using a 3 day dose of PA an microparameters obtained from post-hoc Bayes estimates of the final model.

Table 2.5 Weight normalized individual empirical Bayes parameter estimates for healthy adults, and adult malaria patients

Parameters	Healthy adults (n=166)	Adult malaria patients (n=310)
	Mean ± SD	**Mean ± SD**
CL/F/WT (L/day/kg)	9.33 ± 3.16	19.89 ± 3.38
V2/F/WT (L/kg)	14.70 ± 9.2	201.36 ± 126.35
V3/F/WT (L/kg)	84.14 ± 17.69	310.46 ± 47.66

Table 2.6 Dosage regimen for adult malaria patients

Weight range (kg)	No. of Tablets	PP dose (mg/kg)
20 - 23 kg	1 (180 mg)	7.8 – 9.0
24 - 44 kg	2 (360 mg)	8.2 – 15.0
45 - 64 kg	3 (540 mg)	8.4 – 12.0
65 - 90 kg	4 (720 mg)	8.0 – 11.1

Figure 2.1 Distribution of continuous covariates in adult population

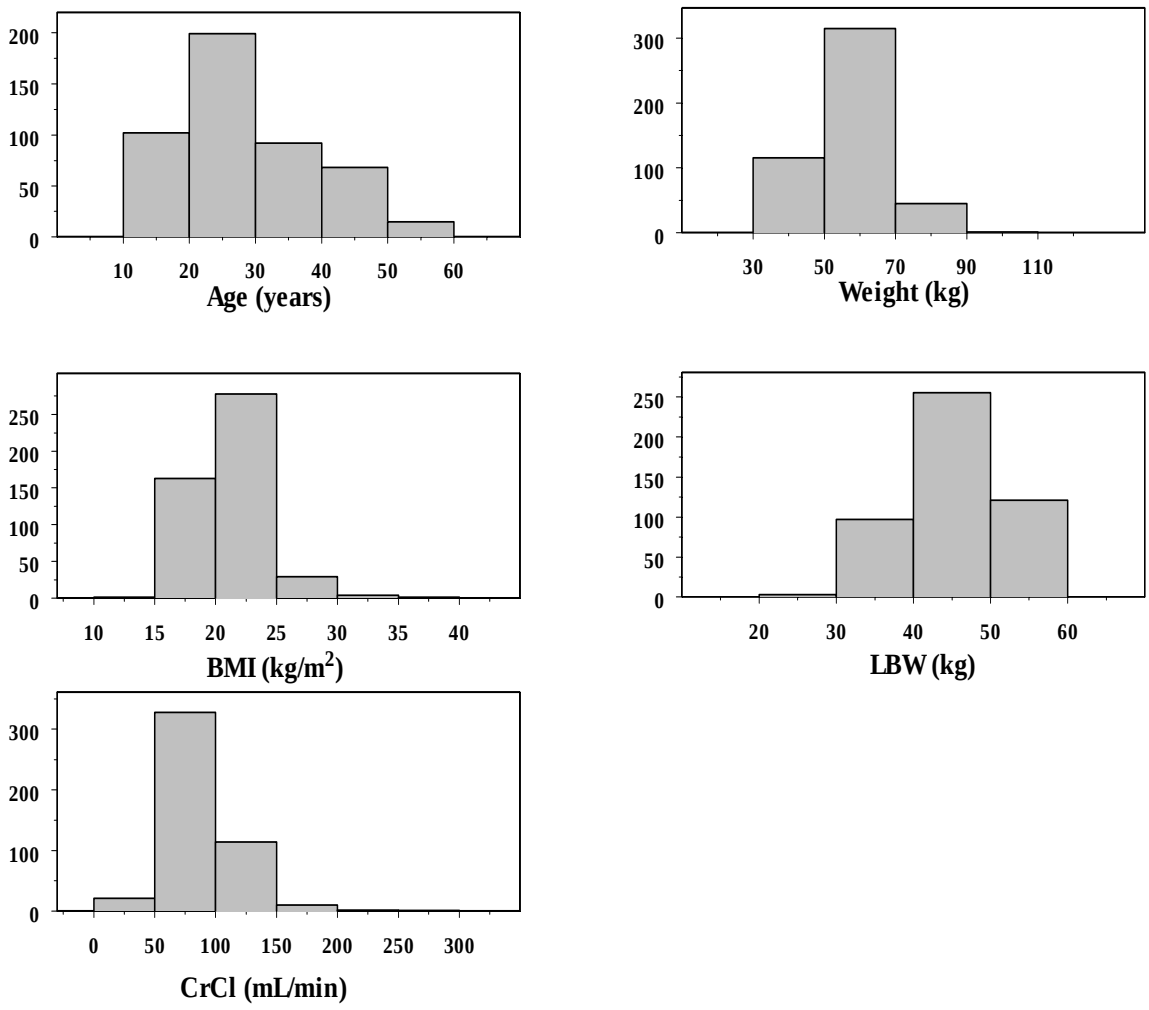

Figure 2.2 Correlation matrix of continuous covariates

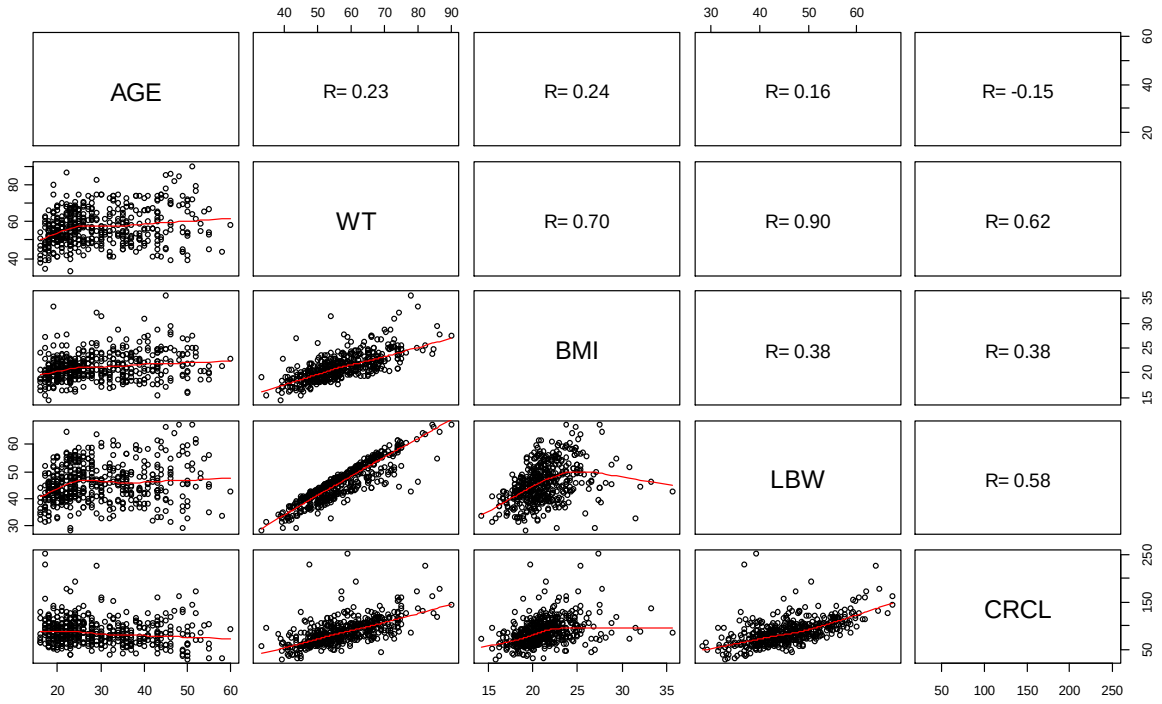

Figure 2.3 Plots of population and individual predicted Ln PYR concentration versus observed Ln PYR concentration for the final model. The solid lines are lines of identity. The broken lines are loess smoothing lines

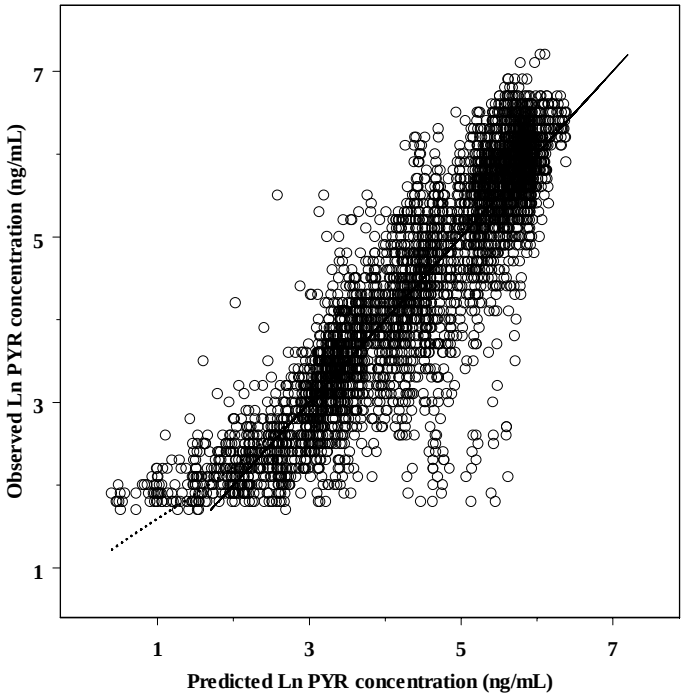

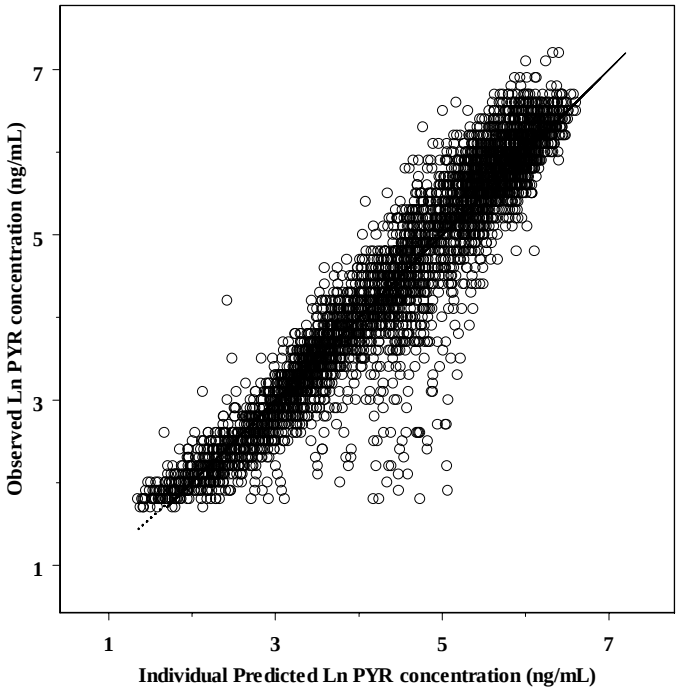

Figure 2.4 Plots of conditional weighted residuals versus population predicted Ln PYR concentration and time after dose of the final model. The broken lines are loess smoothing lines

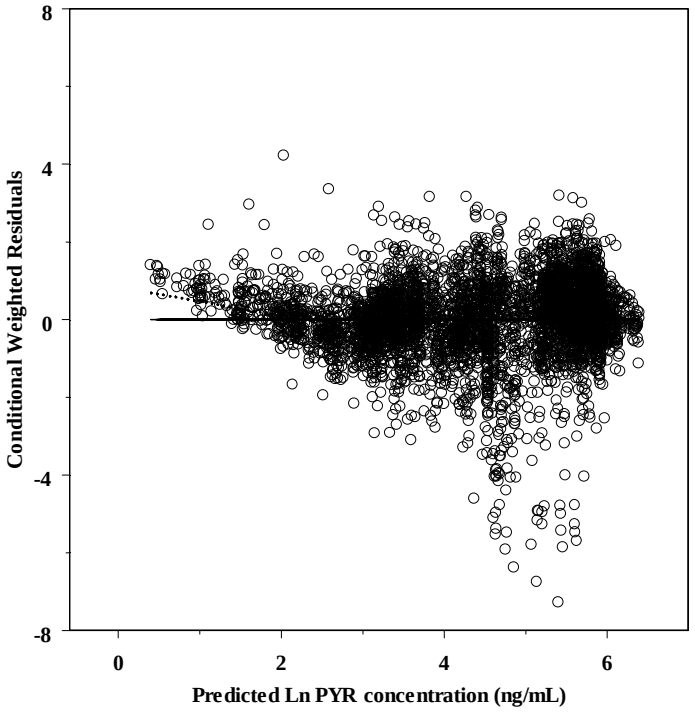

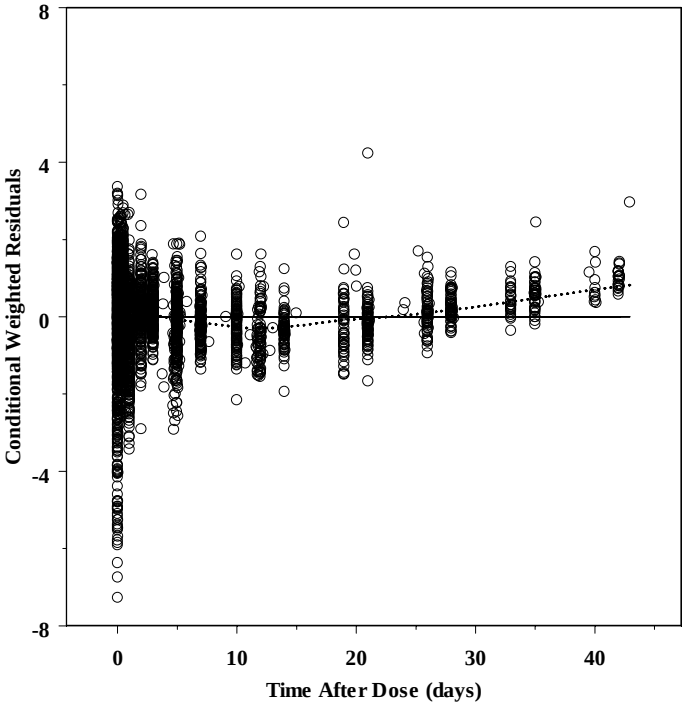

Figure 2.5 Plots of observed (open circles), population predicted (solid lines) and individual predicted (dotted lines) Ln pyronaridine concentrations obtained from intensive sampling versus time form the final model for selected subject

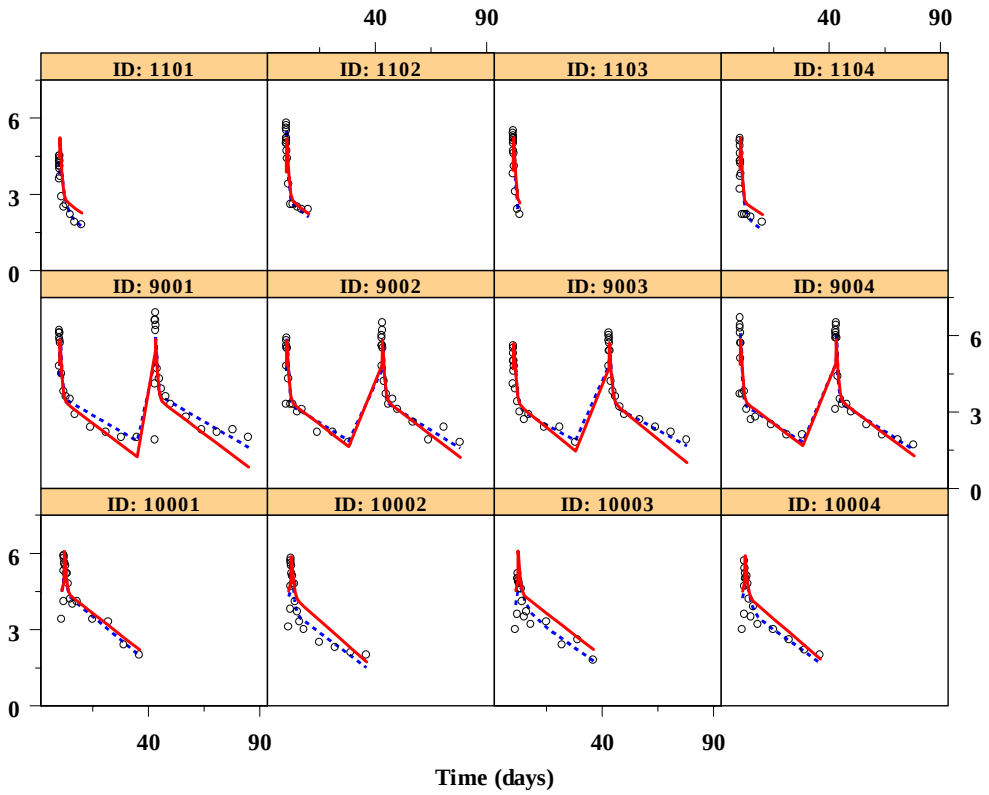

Figure 2.6 Plots of observed (open circles), population predicted (solid lines) and individual predicted (dotted lines) Ln pyronaridine concentrations obtained from sparse sampling versus time form the final model for selected subject

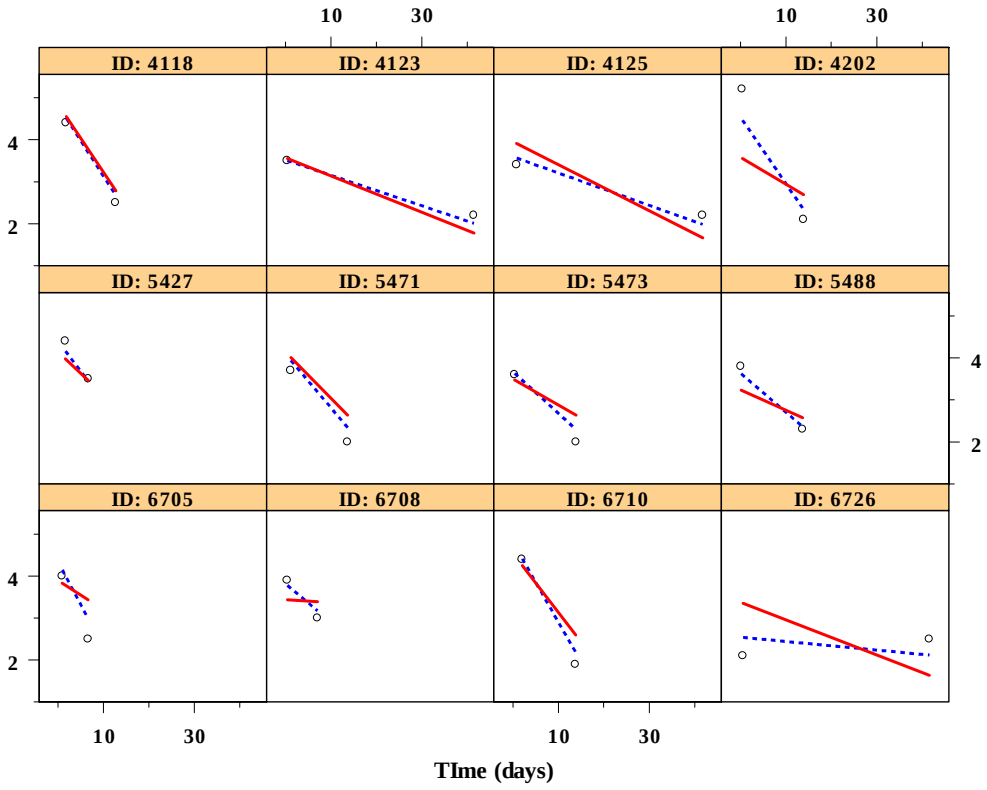

Figure.2.7 Visual Predictive Check of the final model. The open circles represent the observed concentrations, solid lines represent the 5^{th} and 95^{th} percentiles, and the dotted line represents the 50^{th} percentile obtained from the simulations

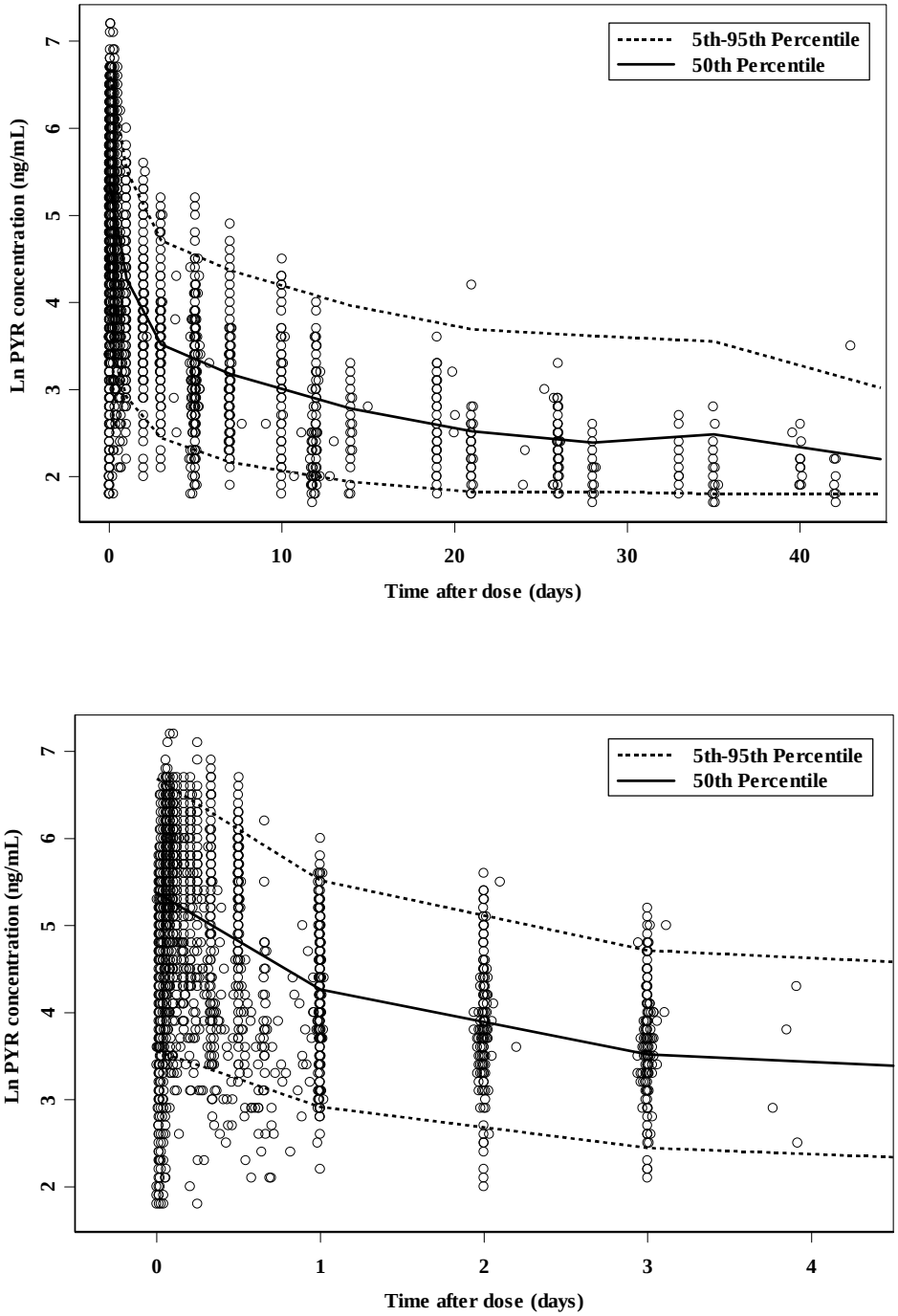

Figure 2.8 Monte Carlo simulations for healthy subjects versus malaria infected adults. The PP dose of 10 mg/kg and the median weight of 56 kg were used for the simulation

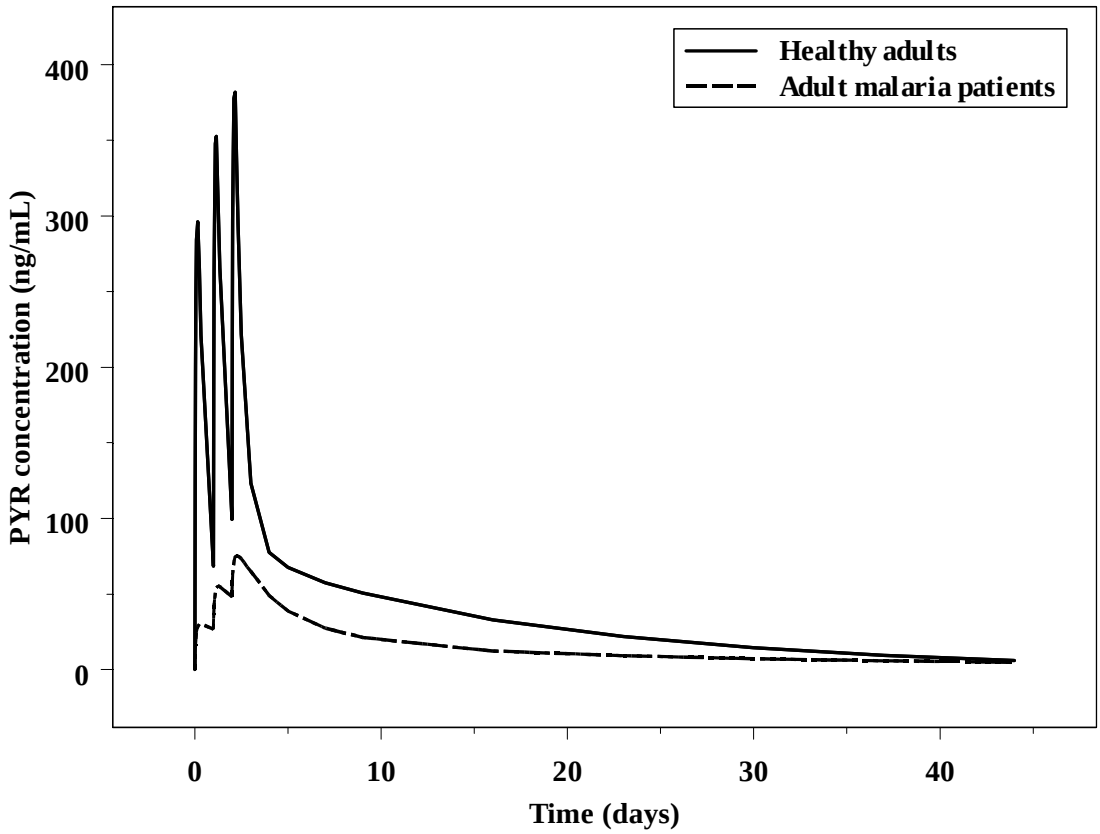

Figure 2.9 Box-plot depicting number of tablets and Ln(AUC) distribution of pyronaridine based on 4 dosing regimens for adult malaria patients; bars represent 25th and 75th percentiles; whiskers represent 10th and 90th percentiles

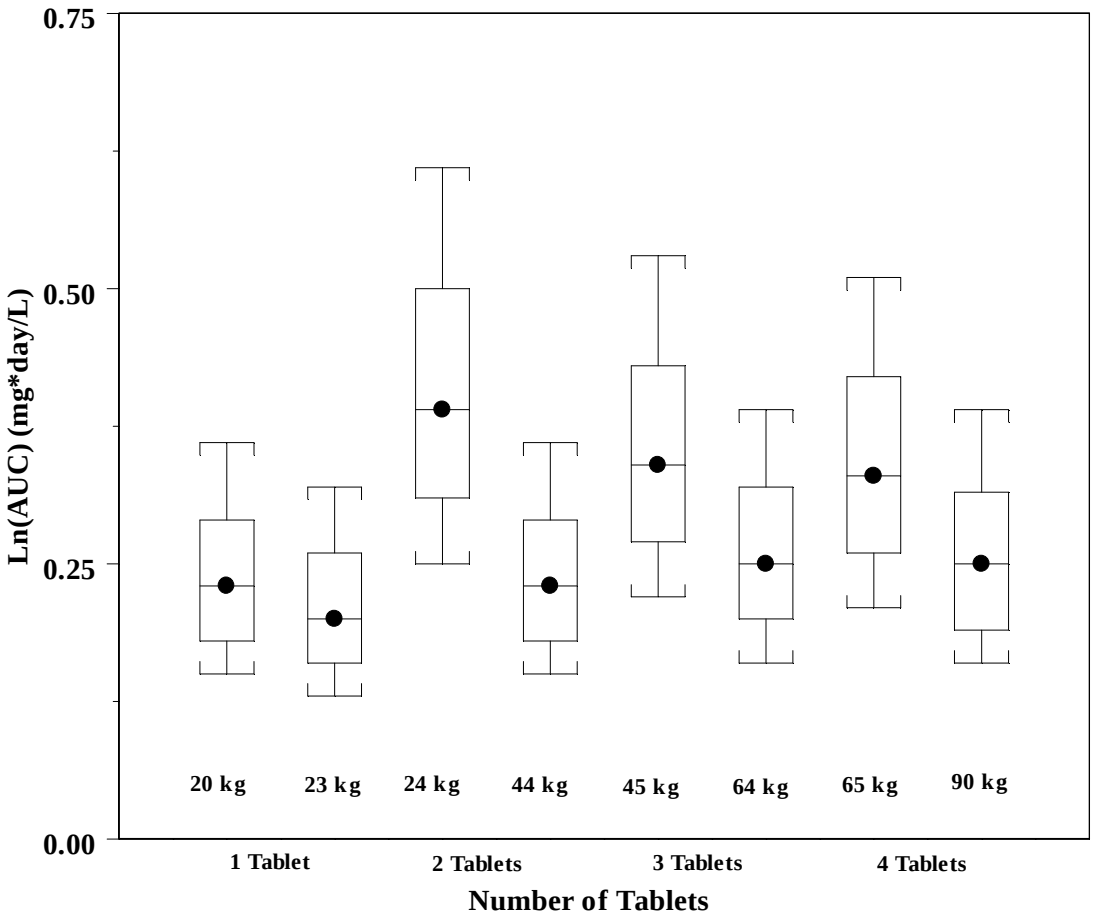

CHAPTER 3

POPULATION PHARMACOKINETICS OF PYRONARIDINE IN PEDIATRIC MALARIA PATIENTS

Introduction

According to WHO, in 2009 there were an estimated 225 million cases of malaria worldwide. The global number of malaria deaths is estimated to be 781,000 in 2009. About 85% of deaths globally were in children under 5 years of age (1). It is widely accepted that children are at increased risk for severe malaria and death between the ages of six months and five years. No doubt that acquired immunity plays a large role in protection from malaria, but age is known to affect malaria burden independently of previous exposure. It is likely that the rates at which various organs affected by malaria develop in children and adults can result in different disease severity. Younger children are more likely to suffer from severe anemia, while older children are more likely to develop cerebral malaria. Children aged between six months and five years are at increased risk for severe malaria and death because of the lower and slower immune responses as well as the smaller erythrocytes to which the malaria parasites attach (68). Moreover, the higher fraction of infected erythrocytes given the same number of parasites has been reported due to the lower level of erythrocytes in children.

Apart from the differences in response to malaria infection, the differences in responses to drugs between children and adults due to developmental changes of various organs have also been reported. All pharmacokinetic processes can be affected by developmental changes in children (69). For oral absorption, the gastric pH is elevated in neonates and slowly decreases to reach adult values at the age of 2 years (70). Moreover, gastric emptying time and intestinal transit time are prolonged in neonates due to the reduced motility and peristalsis (71). Distribution capacity is also affected by developmental changes. The total body water is higher but the fat content is lower in

children resulting in the larger or smaller volume of distribution for hydrophilic or lipophilic drugs, respectively (72). The level of protein binding is low in infants and reaches adult values by 1 year and 3-4 years of age for acidic and basic drugs, respectively (71). Finally, changes in metabolizing enzyme capacity, renal function and liver flow are influenced by physiological changes, depending on age (73).

A population pharmacokinetic model for pyronaridine in healthy subjects and adult malaria patients was successfully developed and presented in Chapter 2. However, children's responses to drugs differ from adults in many aspects, due to several factors including variation of body composition and the differences in organ function caused by developmental changes. These factors may result in the differences in the pharmacokinetics of pyronaridine between pediatric and adult malaria patients. Therefore, the objectives of this study were: to develop a population pharmacokinetic model for pyronaridine in pediatric malaria patients, to evaluate influences of covariates on pyronaridine pharmacokinetics in pediatric malaria patients, and to conduct Monte Carlo simulations to address differences in pyronaridine exposures between selected age ranges and to explore the exposure of pyronaridine among recommended dosing groups for pediatric malaria patients.

Materials and Methods

Study design and blood sampling

The population pharmacokinetic analysis in this chapter was conducted using data from 5 clinical studies, one Phase II study (SP-C-003-05) and four Phase III studies (SP-C-004-06, SP-C-005-06, SP-C-006-06, and SP-C-007-07). Three studies from phase III (SP-C-004-06, SP-C-005-06, and SP-C-006-06) were the same as those used to conduct population pharmacokinetics of pyronaridine in healthy and malaria infected adults. A cut-off age of 16 years was used to separate adult and pediatric patients based on the general considerations for pediatric pharmacokinetic studies for drugs and biological

products (62). The design for population pharmacokinetic analysis was conducted by Clinical Pharmacokinetic Laboratory, College of Pharmacy, the University of Iowa. Study designs, dosage regimen, and blood sampling of each clinical study were summarized as follows:

Phase II (SP-C-003-05)

SP-C-003-05 was aimed to assess safety, tolerability and pharmacokinetics of the 3 day regimen of PA in tablets and granules formulations for the treatment of uncomplicated *P. falciparum* malaria in pediatric patients in Gabon. For PA tablets, patients were sequentially assigned to one of 3 treatment groups similar to those in **SP-C-002-05.** For granule formulations, the PA dose of 9:3 mg/kg was used. Blood samples were collected immediately before each dose and at 0.5, 1, 1.5, 2.5, 4, 8, 12 hours, and at 3, 7, 14 and 21 days after first dose.

Phase III (SP-C-004-06, SP-C-005-06, SP-C-006-06, and SP-C-007-07)

All studies in phase III were comparative, randomized studies to assess efficacy and safety of PA with other antimalarial drugs. **SP-C-004-06** and **SP-C-005-06** were comparative studies to assess the efficacy and safety of PA (180:60 mg) with that of mefloquine (250 mg) plus artesunate (100 mg) and with that of artemether-lumefantrine (20:120 mg) (Coartem®), respectively, in children and adult patients with uncomplicated *P. falciparum* malaria. **SP-C-006-06** was conducted to compare the safety and efficacy of PA (180:60 mg) with that of chloroquine (155 mg) in patients with acute *P. vivax* malaria. **SP-C-007-07** was a comparative, randomized study to assess safety and efficacy of a granule formulation (60:20 mg) (pediatric PYRAMAX®) versus Coartem® crushed tablets in infants and children with acute uncomplicated *P. falciparum* malaria. For SP-C-

004-06, SP-C- 005-06, and SP-C-006-06, PA was given according to body weight: 20 - ≤ 25 kg received one tablet, 26 - < 45 kg received two tablets, ≥ 45 - < 65 kg received three tablets, and ≥ 65 - 90 kg received four tablets. For SP-C-007-07, PA was given as follows: ≥ 5 - < 9 kg received one sachet, 9 - < 17 kg received two sachets, and 17 - < 25 kg received three sachets. For all Phase III studies, one or two blood samples were collected at two different time points (between Day 0 and Day 3, and between Day 4 and Day 42). All subjects provided written informed consent for their participation in the trial. All studies were approved by the local Ethics Committee.

Sample analysis

Blood samples were collected into sterile glass tubes containing EDTA as the anticoagulant (Lavender–top Vacutainer® EDTA tubes) and then were transferred into two approximately equal volume aliquots in screw cap Nalgene cryovials. All samples were stored at or below -80°C until analysis. Pyronaridine concentrations were determined by a validated liquid chromatography-mass spectrometric method (LC/MS) as described by Naik et al (61). The coefficient of variation for intra-day and inter-day precision ranged from 2.2% to 11.1% and 7.8% to 15.9%, respectively. The lower limit of quantification (LLOQ) was 5.7 ng/mL.

Population pharmacokinetic analysis

Nonlinear mixed-effect modeling was conducted to obtain estimates of population pharmacokinetic parameters, inter-individual variability (IIV) and residual variability (RV). NONMEM software version VII level 2.0 (ICON Development Solutions, 2009) was used. NONMEM output was processed using PDx-Pop version 4.0 (ICON Development Solutions, 2007) and Xpose version 4.3.0 (Uppsala University, Uppsala, Sweden, 2010). Graphical plots were produced using TIBCO Spotfire S+ version 8.1 (TIBCO Software Inc., 2008) and R 2.10.1 (The R Foundation for Statistical Computing, 2010). All pyronaridine concentrations were transformed into their natural-logarithms

and the dose of pyronaridine tetraphosphate (PP) was converted to pyronaridine base by multiplying the factor of 0.57 prior to modeling. The theoretical nonlinear mixed-effect model, including structural and statistical model development, covariate modeling and model evaluation, was described in Chapter 2.

Structural model development

Based on concentration time profiles, two- and three- compartment models with first-order absorption and elimination from the central compartment were evaluated as the kinetic models for orally administered pyronaridine. Inter-individual and residual variability were modeled with exponential error models (Eq. 3.1 and Eq. 3.2, respectively).

$$P_i = P_{pop} * \exp(\eta_i) \text{ or } \ln(P_i) = \ln(P_{pop}) + \eta_i \qquad 3.1$$

where P_i is the estimated parameter value for individual i and P_{pop} is the population estimate for the parameter. η_i is the deviation of P_i from P_{pop} and is assumed to be independent and symmetrically distributed with zero mean and variance ω^2.

$$Y_{ij} = F_{ij} * \exp(\varepsilon_{1ij}) \text{ or } \ln(Y_{ij}) = \ln(F_{ij}) + \varepsilon_{1ij} \qquad 3.2$$

where Y_{ij} and F_{ij} are the j^{th} observed and model predicted concentrations for i^{th} individual, respectively. ε_{ij} is the residual random error for individual i and observation j and is assumed to be independently normally distributed with mean of zero and variance of σ^2.

Covariate model building

The influences of 4 continuous covariates (age, creatinine clearance (CRCL), baseline hemoglobin, and baseline parasite count), and 4 categorical covariates (aspartate aminotransferase (AST), alanine aminotransferase (ALT), gender, and formulation) on pharmacokinetic parameters were evaluated after optimal base model was identified. Generalized additive models (GAM), plots of the individual Bayes parameter estimates versus covariates, as well as physiologic plausibility were applied to select potential covariates. Then these covariates were tested for statistical significance using stepwise forward addition and stepwise backward elimination. The significance levels of 0.05 and 0.001, which correspond to the difference in OFV of 3.84 and 10.83, respectively were used as statistical criteria for stepwise forward addition and stepwise backward elimination, respectively.

Continuous covariates (code) included in the dataset were:

1. Age in years (AGE)
2. Creatinine clearance (CRCL) was estimated using the Shull formula:

   $$\text{CRCL (mL/min/1.73 m}^2\text{)} = (3.5*(\text{Age in years}) + 23.6)/\text{SCr (mg/dL)}$$

   CRCL estimates were adjusted for body surface area (BSA). BSA was computed using the Haycock formula:

   $$\text{BSA (m}^2\text{)} = (\text{Wt}^{0.5378})*(\text{Ht}^{0.3964})*0.024265$$
3. Baseline hemoglobin (HGB) (g/dL)
4. Baseline log parasite count (LOGPARA) (per µL)

Categorical covariates (code) included in the dataset were:

1. Baseline aspartate aminotransferases (AST), coded as 0 if baseline AST level was ≤ 1.5 x upper limit of normal range (ULN) and 1 if baseline AST level was > 1.5 x ULN. (ULN for AST was defined as 19 U/L for SP-C-003-05 and 41 U/L for all Phase III studies and SP-C-002-05. For Phase I study SP-C-001-03, ULN for AST was 40 U/L. For SP-C-009-07, the ULN for AST was 34 U/L).
2. Baseline alanine aminotransferases (ALT), coded as 0 if baseline ALT level was ≤ 1.5 x upper limit of normal range (ULN) and 1 if baseline ALT level was > 1.5 x ULN. (ULN for ALT was defined as 23 U/L for SP-C-003-05 and 45 U/L for all Phase III studies and SP-C-002-05. For SP-C-001-03, the ULN for ALT was 40 U/L. For SP-C-009-07, the ULN for ALT was 55 U/L).
3. Gender (SEX), coded as 0 for female and 1 for male.
4. Formulation (FORM), coded as 0 for tablet and 1 for granule.

All continuous covariates were centered with the median values and were evaluated with a linear function (Eq. 3.3), a power function (Eq. 3.4) and an exponential function (Eq. 3.5), depending on GAM and graphical exploration of the relationships between covariates and pharmacokinetic parameters. The influences of categorical covariates on the parameter were modeled with an additive relationship (Eq. 3.6). The importance of covariates as predictors was determined by a statistically significant improvement in the MOFV, improvement in the precision of the parameter estimate (relative standard error), percentage change in affected covariates and reduction in IIV and RV.

$$P = \theta_1 + \theta_2 * (COV - COV_{median}) \quad 3.3$$

$$P = \theta_1 * (COV/COV_{median})^{\theta_2} \quad 3.4$$

$$P = \theta_1 * \exp(\theta_2 * (COV - COV_{median})) \quad 3.5$$

$$P = \theta_3 + \theta_4 * \text{Cat\_COV} \qquad 3.6$$

where P represents pharmacokinetic parameter estimate of the population, COV is the continuous covariate tested, Cat_COV is the categorical covariate tested, θ_1 is the parameter estimate of an individual with COV equal to COV_{median}, θ_2 represents a factor describing the effect of continuous covariate, θ_3 is the parameter estimate of an individual with Cat_COV coded as 0, and θ_4 is the additional change in the parameter corresponded to categorical covariate being tested.

Model evaluation

Model goodness-of-fit was assessed using diagnostic plots of observed pyronaridine concentrations versus PRED and versus IPRED, CWRES versus PRED and versus time. Precision of the parameter estimates was assessed using nonparametric bootstrap approach. One thousand bootstrap runs were generated using Perl-Speaks-NONMEM version 3.1.0. The predictive ability of the final model was evaluated using visual and numerical predictive check by simulating one thousand pyronaridine observations at each sampling time point. The observed pyronaridine concentrations were then plotted with the 5^{th}, 50^{th}, and 95^{th} percentiles of the simulated observations to obtain the population median concentrations and 90% prediction interval. The percent of observed pyronaridine concentrations above and below the 90% prediction interval was calculated. Model stability was assessed by a condition number with the criteria of less than 1000 as indicative of model stability.

Simulations

One thousand simulations were conducted to address differences in exposures between pediatric malaria patients in selected age ranges. Parameter estimates obtained from the final model, the median weight, and the dose of 10 mg/kg pyronaridine tetraphosphate were used for the simulation.

In order to explore the exposure of pyronaridine among recommended dosing groups, two extreme weight values (lower and upper limits) in each dosing group of current PA dosing regimens for pediatric patients (Table3.6) were used for the simulations.

Results

Demographic data

A total of 1,220 blood pyronaridine levels from 332 pediatric malaria patients were obtained from 5 studies in phase II and phase III. Approximately, 13.5% (165 observations) and 0.2% (2 observations) of the samples were below LLOQ and were identified as outliers, respectively. In total, 1,053 blood pyronaridine concentrations were included in the population pharmacokinetic analysis. The observations that were below LLOQ and outliers were excluded from the analysis.

Table 3.1 summarizes number of subjects and observations, demographic, and clinical characteristics of the population in each clinical study. This pediatric population has a median age and median weight of 8 years and 22.1 kg, respectively. The number of males and females in this population was comparable (52.1% and 47.9% for females and males, respectively). Most of the patients received PA as a tablet formulation (70.5%).

Population pharmacokinetic model

Similar to the model developed for healthy and malaria infected adults, the best base model of pyronaridine for pediatric malaria patients was a two compartment model with first order absorption and elimination from the central compartment. Figure 3.1 shows the distribution of continuous covariates. Based on the inspection of collinearity among continuous covariates (Figure 3.2), there was a high correlation between age and the effect of body size (body weight, LBW, and BSA). Since the proposed dosage regimen of a fixed dose combination of pyronaridine-artesunate for pediatric malaria

patients is based on body weight, the effect of body weight was treated as a fixed covariate using an allometric scaling approach with the exponent of 1 and 0.75 on volume parameters and clearance, respectively. According to GAM, graphical exploration and physiologic plausibility, the potential covariate-parameter relationships to be tested using stepwise forward addition and backward elimination were formulation on K_a; age, CRCL, HGB, gender, ALT, and AST on CL/F; and age on V2/F. A summary of forward addition and backward elimination steps is presented in Table 3.2.

In the first step of stepwise forward addition, AST was the most significant predictor on CL/F (with the difference in MOFV from the base model of 22.8). However, the model incorporating the effect of AST resulted in the change in the estimate of CL/F of less than 20% which was not considered to be clinically significant based on pre-specified criteria. Therefore, a model with age, the next most significant predictor, was used as a new base model for the second step of stepwise forward addition. The effect of formulation was found to be significant predictor on K_a with 79.63% change in the estimate of K_a from the base model. During stepwise backward elimination, the effect of K_a was not significant at $\alpha = 0.001$, but was significant at $\alpha = 0.01$.

The population parameter estimates of CL/F, V2/F, V3/F, Q/F and K_a of the final model were 459 L/day, 2,720 L, 2,470 L, 700 L/day and 27 day^{-1}, respectively. The IIV on Q/F and V3/F were fixed to zero as the estimates cannot be obtained with good precision. The percent coefficient of variation of IIV on CL/F, V2/F and K_a were 39%, 95.9%, and 82.5%, respectively. These estimates from the final model are summarized in Table 3.3. The derived mean $t_{1/2\beta}$, $AUC_{(0-\infty)}$, and predicted day 7 concentration of pyronaridine in pediatric malaria patients are presented in Table 3.4. The relationships between significant covariates and pharmacokinetic parameters were described as follows:

$$\text{CL/F (L/day)} = [(459*(\text{body weight}/22.1)^{0.75}*(\text{age}/8)^{0.295}]*\exp(\eta)$$

$$\text{Q/F (L/day)} = [(700*(\text{body weight}/22.1)^{0.75}]*\exp(\eta)$$

$V2/F\ (L) = [2{,}720 * (\text{body weight}/22.1)^{1}] * \exp(\eta)$

$V3/F\ (L) = [2{,}470 * (\text{body weight}/22.1)^{1}] * \exp(\eta)$

For the model with effect of formulation on K_a at the significant level of 0.01, the covariate-parameter relationships were as follows:

$CL/F\ (L/day) = [(458 * (\text{body weight}/22.1)^{0.75} * (\text{age}/8)^{0.293}] * \exp(\eta)$

$Q/F\ (L/day) = [(703 * (\text{body weight}/22.1)^{0.75}] * \exp(\eta)$

$V2/F\ (L) = [2{,}721 * (\text{body weight}/22.1)^{1}] * \exp(\eta)$

$V3/F\ (L) = [2{,}460 * (\text{body weight}/22.1)^{1}] * \exp(\eta)$

$K_a\ (day^{-1}) = [21.5 + 27.0 * \text{formulation}] * \exp(\eta)$

Model evaluation

Figure 3.3 and 3.4 are the goodness-of-fit plots of the final model. The individual plots for selected subjects are presented in Figure 3.5-3.6. Bootstrap results (Table 3.3) showed that 87.3% of the bootstrap runs were successfully converged. All the parameter estimates obtained from the final model were contained within 95% confidence intervals obtained from the bootstrap. Figure 3.7 shows the results of VPC. About 0.66% and 3.89% of pyronaridine observations were above and below the 90% prediction interval obtained from the simulations. The condition number of the final model was 17.9.

Simulations

Figure 3.8 shows the simulated pyronaridine concentration time profiles in each age range. The Ln(AUC) distribution of pyronaridine based on 4 dosing regimens for pediatric malaria patients is presented in Figure 3.9. Simulated concentration time profiles of pyronaridine were highest in pediatric malaria patients age 2 years, followed by 12 years and 16 years, respectively. The overall ranges of pyronaridine exposures among dosing groups for pediatric malaria patients were relatively similar.

Discussion

Population pharmacokinetic model for pediatric malaria patients was developed using a total of 1,053 blood pyronaridine concentrations from 332 pediatric patients participated in one phase II and four phase III clinical trials. Approximately13.5% of the observations was below LLOQ and was excluded from the analysis (63). The data did not support a 3-compartment model as evidenced by the difficulty to converge the model. Additionally, the model that successfully converged yielded correlations of the estimates of greater than 0.95 suggesting that the model may be over-parameterized and unstable. Finally, this 3-compartment model resulted in a condition number of 2466 suggesting ill conditioning of the model. Therefore, a simpler, 2-compartment model with first order absorption and first order elimination from the central compartment was conducted.

Two major aspects affecting differences in pharmacokinetics among infants, children and adolescents are growth and developmental changes which can be accounted for by body size and age (74). Covariate screening showed a high collinearity between age and body size which might contribute to a potential source of errors in estimating individual covariates (75). Body size has been considered the primary factor to describe variability in pharmacokinetics among children as confirmed by the theory explaining the link between mass and function across magnitudes of organs (76). However, body size alone does not take into account developmental changes (77). Therefore, we attempted to treat the effect of body size as a fixed covariate by using an allometric exponent that has a strong theoretical and empirical basis (74). Age was then treated as part of the covariate modeling to account for the developmental changes in children. An allometrically-scaled, two-compartment model with the exponent of body weight of 0.75 on clearance parameters and 1.0 on volume parameters adequately fit pyronaridine data (130.416 reduction in MOFV from the base model). After covariate screening, the potential covariates included in stepwise forward addition/backward elimination were: formulation on K_a; age, CRCL, HGB, gender, ALT, and AST on CL/F; and age on V2/F. AST was

the most statistically significant predictor on CL/F. However, it did not meet the pre-specified criteria of clinical significance (20% changes in parameter estimates for the categorical covariate) and was excluded from the subsequent round. Age was found to be a significant covariate on CL/F in the final model with the exponent of 0.295.

According to the FDA, the pediatric population can be categorized into 4 age ranges: infants and neonates (< 2 years), children (2-12 years), adolescents (12-<16 years), and adults (≥ 16 years) (62). In this data set, there were only six subjects who ages were less than 2 years; none of them were neonates. A comparison of weight normalized clearance and central volume of distribution in each age range is presented in Table 3.5. Figure 3.10 and 3.11 are the plots between weight normalized clearance versus age and weight normalized central volume of distribution versus age, respectively. Inclusion of age in the model is likely to reflect developmental changes in pyronaridine clearance and central volume of distribution. Therefore, the lower weight normalized clearance observed in younger children could be explained by the lower level of enzymes used to metabolize pyronaridine. The higher central volume of distribution in younger ages could be explained by the reduced protein binding as well as the higher level of extracellular fluid volume of total body water. The derived pharmacokinetic parameters show the longer $t_{1/2\beta}$, higher levels of $AUC_{(0-\infty)}$, and higher predicted pyronaridine day 7 concentrations in younger children. This would be expected given the lower weight normalized CL/F observed in younger children.

Some patients (98 subjects) received PA granule formulations; therefore the effect of formulation was tested. Formulation was found to be a significant predictor on K_a with a 79.6% change in the estimate of K_a from the base model. During stepwise backward elimination, the effect of K_a was significant at $\alpha = 0.01$. Figure 3.12 is a box-plot of age versus distribution of pediatric malaria patients receiving different formulations of PA. Most of the subjects receiving the granule formulation were young children. A plot between empirical Bayes estimates of K_a and formulations is presented in Figure 3.13. As

would be expected, a higher K_a is observed for the granule formulation, most likely due to the faster dissolution rate. However, there is a high variability in K_a in both tablet and granule formulations which could be explained by: sparse sampling strategy used for most patients with 1 observation during day 0 to day 3 and the effect of organ development on absorption varies depending on age (71). Gastric pH in infants is higher than that in adults, thus pyronaridine, a basic drug, tends to be absorbed more in infants. However, there are other factors that can also affect the absorption rates of drugs. For example, gastric emptying time is delayed after birth and approaches adult values within 6-8 months. Also intestinal transit time is prolonged in infants and neonates because of reduced motility and peristalsis. All of these developmental changes in absorption could explain the high variability observed in K_a.

Simulation results showed that given the same body weight and the dose of pyronaridine tetraphosphate, the simulated pyronaridine concentrations were higher in younger children as would be expected given the lower apparent clearance. Moreover, the exposures of pyronaridine were consistent across the proposed dosage regimen in PA granule labeling for pediatric malaria patients and were comparable to those of adult malaria patients.

Conclusions

In conclusion, population pharmacokinetics of pyronaridine was modeled using data from five clinical studies. An allometric two compartment model with first order absorption and elimination from the central compartment best described pyronaridine pharmacokinetics in pediatric malaria patients. The only significant covariate-parameter relationship in the final model was the effect of age on apparent clearance with the power function. The validity of the final population pharmacokinetic model for pyronaridine in pediatric malaria patients was confirmed by goodness-of-fit plots showing no major bias, bootstrap analysis, Visual Predictive Check, and a condition number.

Table 3.1 A summary of study data, patient demographics and covariates included in the analysis

Characteristics	Phase II	Phase III				All studies
	SP-C-003-05	SP-C-004-06	SP-C-005-06	SP-C-006-06	SP-C-007-07	
Number of subjects [N]	57	40	143	9	83	332
Number of observations						
Total	702	79	272	17	150	1220
Excluded as LOQ [N(%)]	14 (2)	21 (26.6)	75 (27.6)	6 (35.3)	49 (32.7)	165 (13.5)
Excluded as outliers [N(%)]	0 (0)	0 (0)	1 (0.4)	0 (0)	1 (0.7)	2 (0.2)
Included in the analysis [N(%)]	688 (98)	58 (73.4)	196 (72.1)	11 (64.7)	100 (66.6)	1053 (86.3)
Median age (range) (years)	5 (2-14)	11 (5-15)	9 (5-15)	14 (9-15)	5 (0.6-10)	8 (0.6-15)
Median weight (range) (kg)	16.2 (10-36.4)	20.9 (20-46.4)	26.6 (20-56.2)	31.5 (20-46.7)	17 (9-24.3)	22.1 (9-56.2)
Median BMI (range) (kg/m^2)	15 (12.8-17.6)	15.1 (11-20)	16.6 (11.5-26.5)	15.8 (13.6-19.2)	15 (6-23)	19.8 (6-26.5)
Median LBW (range) (kg)	14.4 (8.7-31.7)	22.5 (15.5-36.9)	22.9 (15.6-47.3)	28.3 (18.1-39.9)	14.7 (7.3-22)	19.8 (7.3-47.3)
Median Creatinine Clearance (range) (mL/min)	51.2 (18.5-164.3)	64.1 (36.4-132.5)	66.6 (25.9-219.2)	68.0 (50.6-85.1)	33.8 (12.5-114.6)	54.7 (12.5-219.2)

Table 3.1 -continued

Characteristics	Phase II	Phase III				All studies
	SP-C-003-05	SP-C-004-06	SP-C-005-06	SP-C-006-06	SP-C-007-07	
Baseline Parasite Count (range) (per µL)	6,304 (1,072-174,241)	10,559 (1,201-92,500)	13,088 (1,000-93,923)	8,632 (1,193-51,947)	14,400 (153-188,488)	10,7556 (153-188,488)
Median baseline hemoglobin (range) (g/dL)	102 (74-129)	110 (82-130)	115 (84-208)	113 (93-135)	100 (80-123)	108 (74-208)
Formulation [N(%)]						
Tablet	42 (73.7)	40 (100)	143 (100)	9 (100)	0 (0)	234 (70.5)
Granule	15 (26.3)	0 (0)	0 (0)	0 (0)	83 (100)	98 (29.5)
Gender [N(%)]						
Female	28 (49.1)	19 (47.5)	78 (54.5)	3 (33.3)	45 (54.2)	173 (52.1)
Male	29 (50.9)	21 (52.5)	65 (45.5)	6 (66.7)	38 (45.8)	159 (47.9)
AST>1.5 ULN	36	5	6	0	3	50
ALT>1.5 ULN	5	1	2	0	0	8

Table 3.2 A summary of covariate model development

Step	**Covariate added to Base model**	**MOFV**	**Δ MOFV**
0	Base model	182.296	-
1	Age on CL/F	173.306	9.99
2	Age on CL/F, Formulation on K_a (Full model)	165.222	8.08
Step	**Covariate removed from Full model**	**MOFV**	**Δ MOFV**
1	Age on CL/F	184.501	19.28
	Formulation on K_a	172.306	7.08

Table 3.3 Final population pharmacokinetic and bootstrap results for pyronaridine

Parameter [a]	**Estimate (95%CI)**	**%RSE** [b]	**%CV** [c]	**Bootstrap estimate (95% CI)** [d]
PK Parameters				
CL/F (L/day)	459 (405-513)	5.97		458 (408-521)
V2/F (L)	2,720 (2,360-3,080)	6.73		2,717 (2,360-3,133)
V3/F (L)	2,470 (2,030-2,910)	9.19		2,457 (2,025-2,945)
Q/F (L/day)	700 (553-847)	10.7		719 (571-903)
K_a (day^{-1})	27 (19.2-34.8)	14.8		27 (20.1-36.2)
Age on CL/F	0.295 (0.0598-0.530)	40.7		0.303 (0.063-0.534)
IIV				
IIV-CL/F	0.152 (0.0352-0.269)	39.2	39.0	0.147 (0.059-0.276)
IIV-V2/F	0.920 (0.757-1.08)	9.05	95.9	0.927 (0.756-1.104)
IIV-V3/F	-	-	-	-
IIV-Q/F	-	-	-	-
IIV-K_a	0.681 (0.320-1.04)	27.0	82.5	0.677 (0.362-1.078)
RV (additive error)				
RV	0.219 (0.165-0.273)	12.6		0.220 (0.166-0.274)

[a] CL/F = apparent clearance, V2/F = apparent central volume of distribution, V3/F = apparent peripheral volume of distribution, Q/F = apparent intercompartmental clearance, K_a = first-order absorption rate constant, F = bioavailability.

[b] %RSE = relative standard error computed by (SE/mean)x100%.

[c] %CV= coefficient of variation computed by $\%CV = \sqrt{\exp(\omega^2) - 1} * 100\%$

[d] 95% CI of bootstrap estimate are the 2.5 and 97.5 percentile of the bootstrap estimates.

Table 3.4 Derived parameters obtained from post-hoc Bayes estimates of the final model

Parameter	Estimate (mean ± SD)
$t_{½\alpha}$ (days) [a]	
Age < 2 years	1.41 ± 0.28
Age 2-12 years	1.10 ± 0.47
Age 12-16 years	1.20 ± 0.46
$t_{½\beta}$ (days) [a]	
Age < 2 years	22.13 ± 8.71
Age 2-12 years	11.45 ± 5.35
Age 12-16 years	10.06 ± 3.35
$AUC_{(0-\infty)}$ (mg*day/L) [b]	
Age < 2 years	1.84 ± 0.30
Age 2-12 years	1.33 ± 0.46
Age 12-16 years	1.30 ± 0.36
Predicted pyronaridine day 7 concentration (ng/mL) [c]	
Age < 2 years	38.61 ± 10.55
Age 2-12 years	36.64 ± 13.12
Age 12-16 years	37.76 ± 9.94

[a] $t_{½\alpha}$ and $t_{½\beta}$ are the distribution and elimination half-lives, respectively.

[b] Area under the concentration-time curve from 0 to ∞ was computed using a 3 day dose of PA and microparameters obtained from post-hoc Bayes estimates of the final model.

[c] Predicted pyronaridine day 7 concentrations were computed using a 3 day dose of PA and microparameters obtained from post-hoc Bayes estimates of the final model.

Table 3.5 Weight normalized individual empirical Bayes parameter estimates for pediatric malaria patients in each age range

Parameters	Age < 2 years (Mean ± SD)	Age 2-12 years (Mean ± SD)	Age 12-16 years (Mean ± SD)
CL/F/WT (L/day/kg)	15.51 ± 1.91	20.13 ± 4.60	22.14 ± 4.36
V2/F/WT (L/kg)	359.36 ± 177.67	175.72 ± 166.61	154.92 ± 124.51

Table 3.6 Dosage regimen of current proposed PA granule labeling

Weight range (kg)	Number of Dosage Units	PP dose (mg/kg)
5 - 7 kg	1 (60 mg)	8.6 – 12.0
8 - 14 kg	2 (120 mg)	8.6 – 15.0
15 - 19 kg	3 (180 mg)	9.5 – 12.0

Figure 3.1 Distribution of continuous covariates in pediatric population

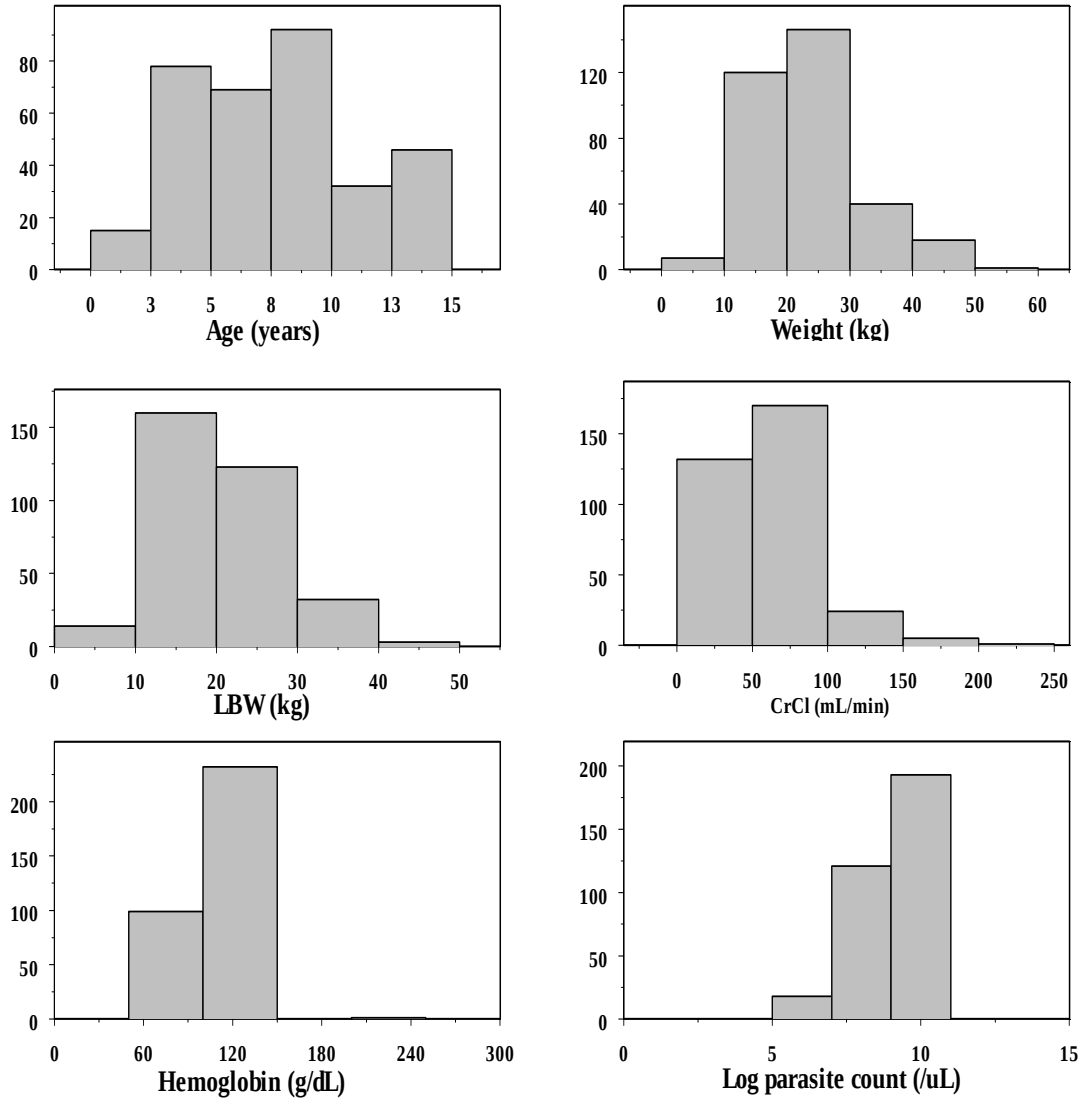

Figure 3.2 Correlation matrix between continuous covariates

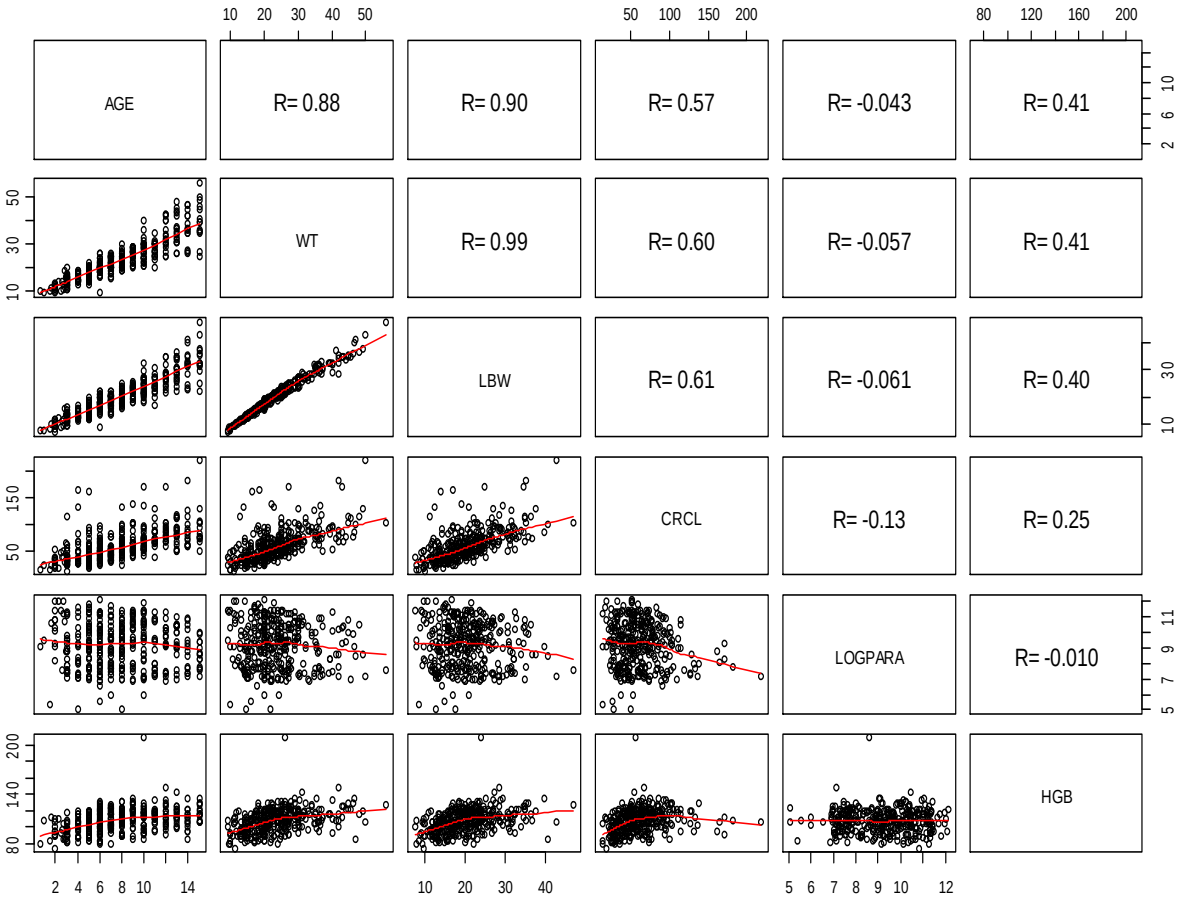

Figure 3.3 Plots of population and individual predicted Ln PYR concentration versus observed Ln PYR concentration for the final model. The solid lines are lines of identity. The broken lines are loess smoothing lines

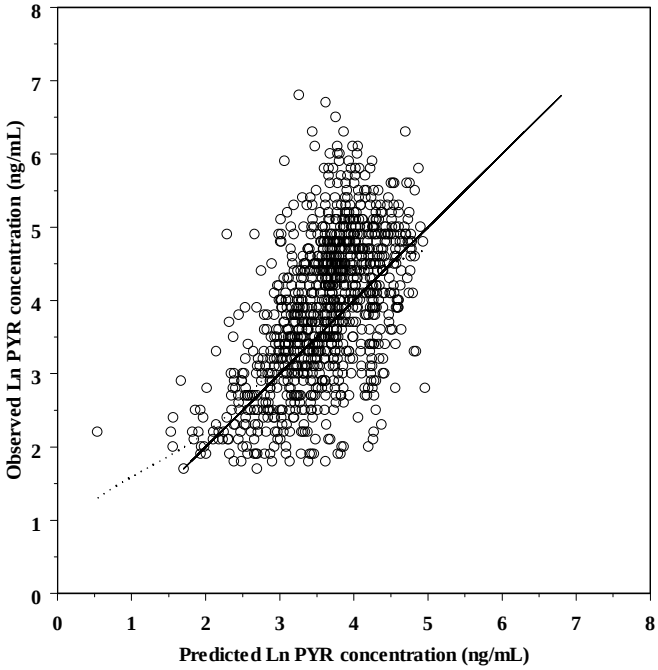

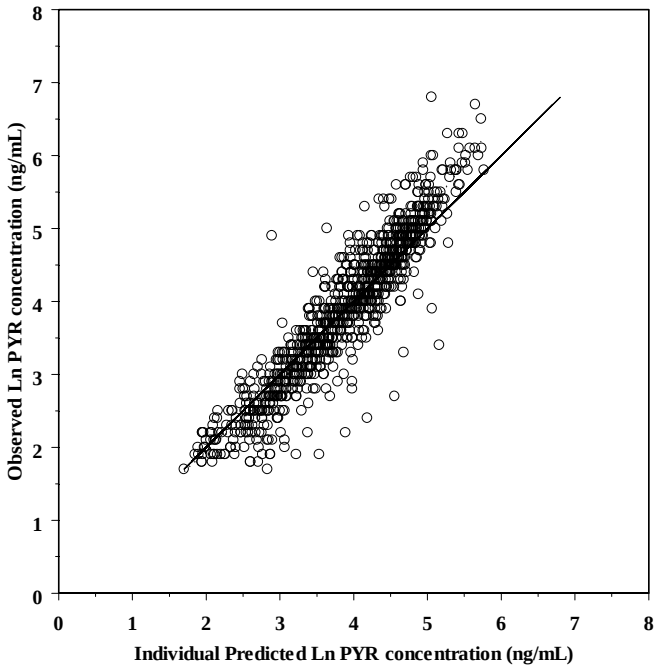

Figure 3.4 Plots of conditional weighted residuals versus population predicted Ln PYR concentration and time after dose of the final model. The broken lines are loess smoothing lines

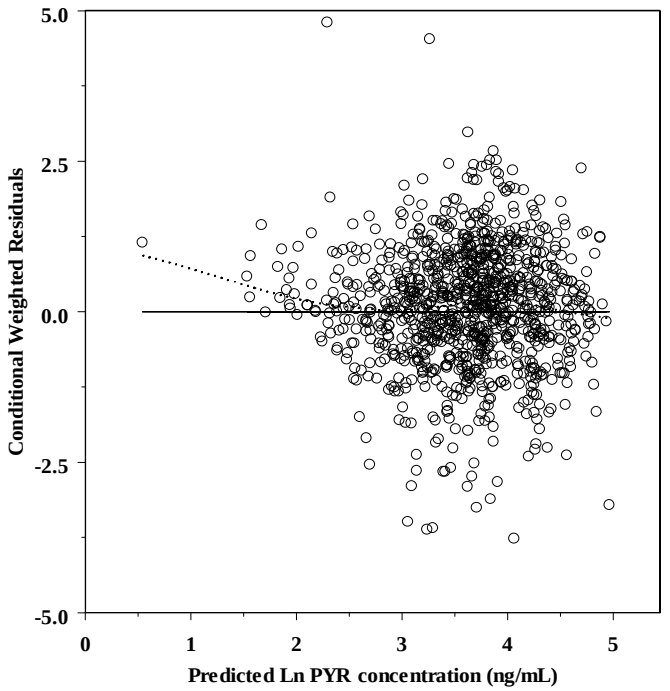

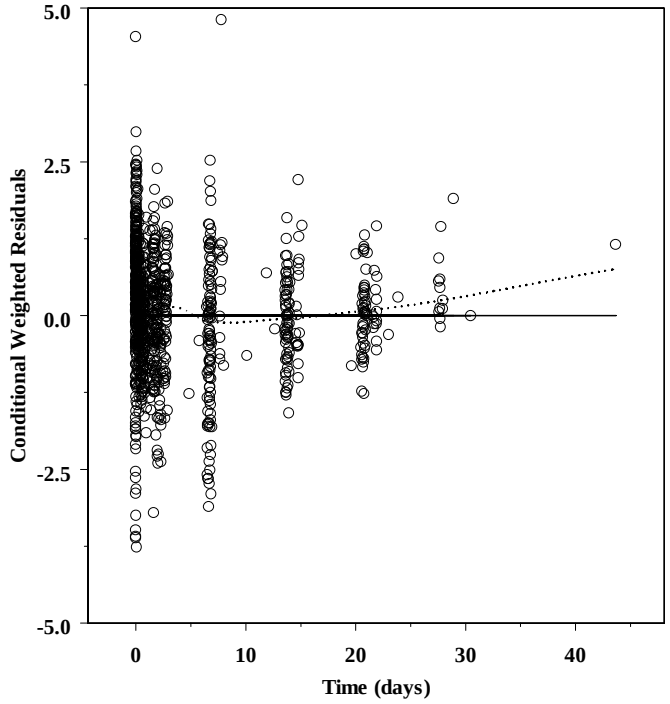

Figure 3.5 Plots of observed (open circles), population predicted (solid lines) and individual predicted (dotted lines) Ln pyronaridine concentrations obtained from intensive sampling versus time form the final model for selected subject

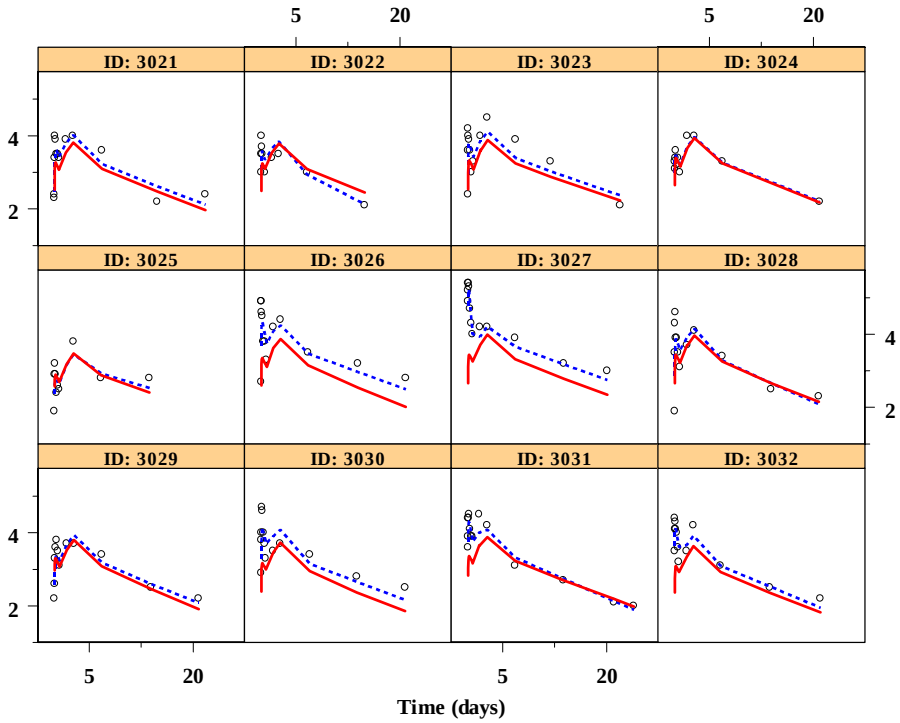

Figure 3.6 Plots of observed (open circles), population predicted (solid lines) and individual predicted (dotted lines) Ln pyronaridine concentrations obtained from sparse sampling versus time form the final model for selected subject

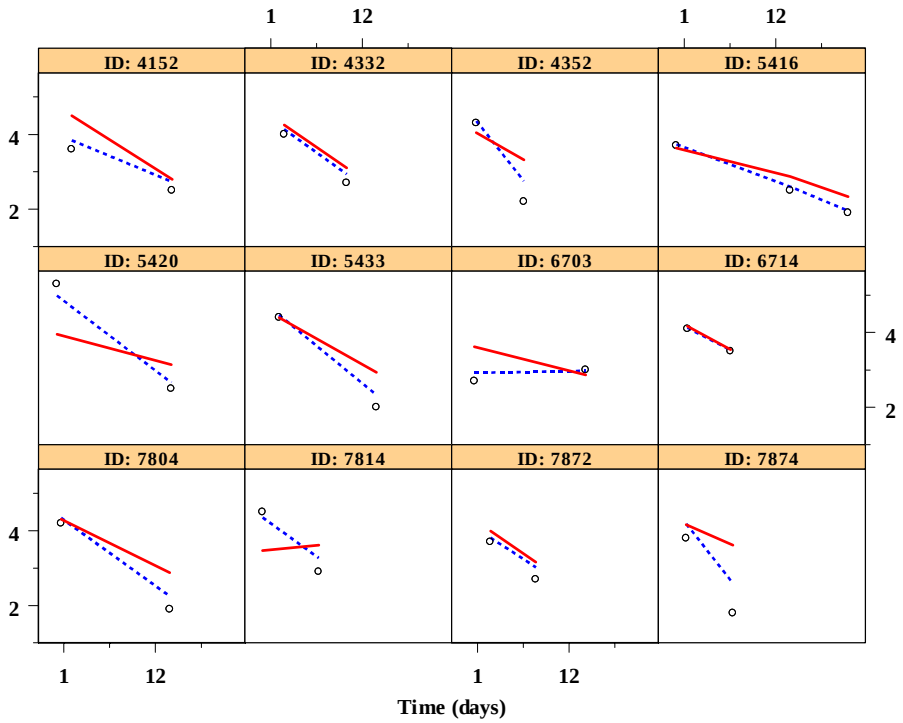

Figure 3.7 Visual Predictive Check of the final model. The open circles represent the observed concentrations, the dotted lines represent the 5th and 95th percentile, and the solid line represents the 50th percentile obtained from the simulations

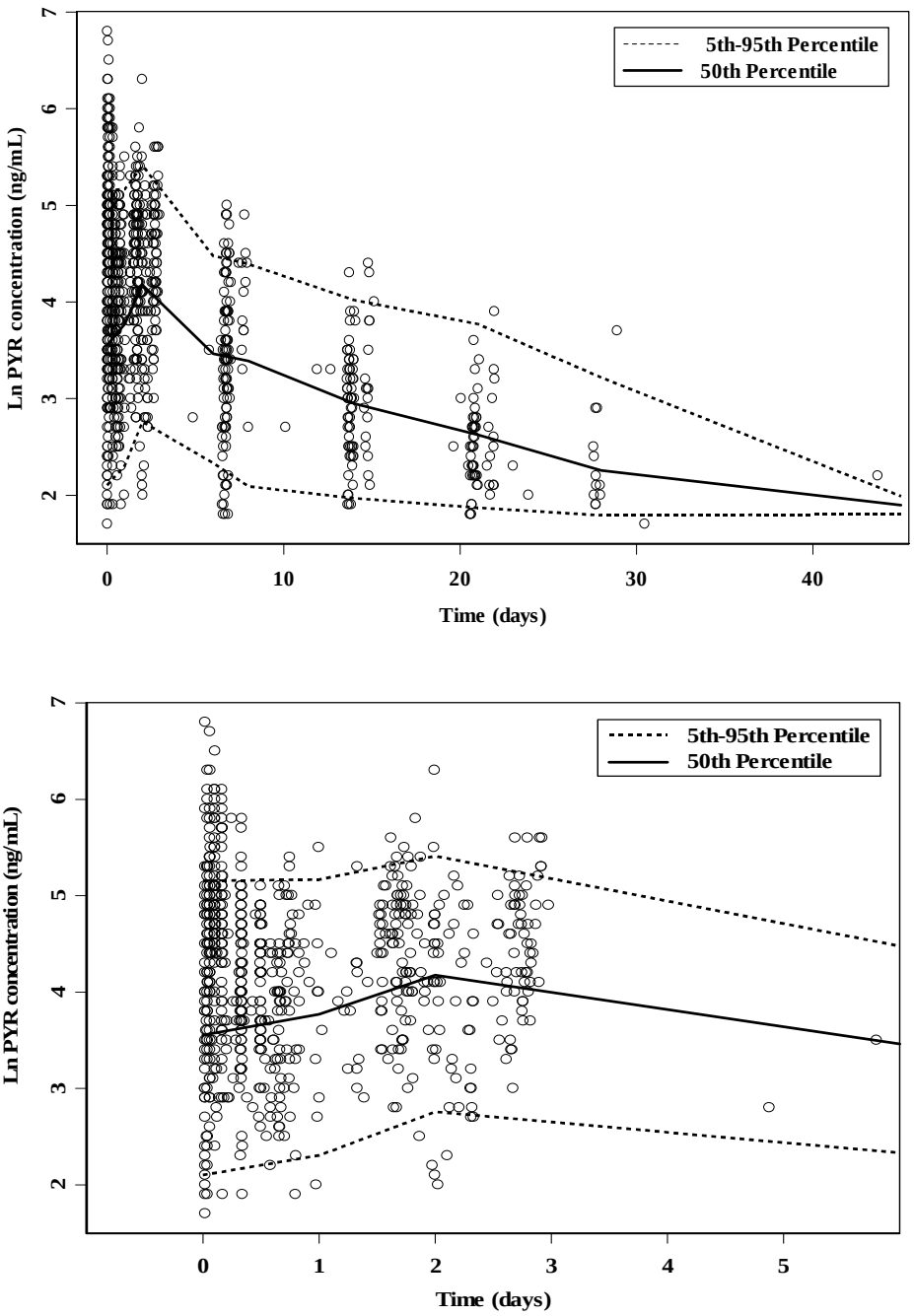

Figure 3.8 Monte Carlo simulations for pediatric malaria patients in each age range. The PP dose of 10 mg/kg and the median weight of 22 kg were used for the simulation

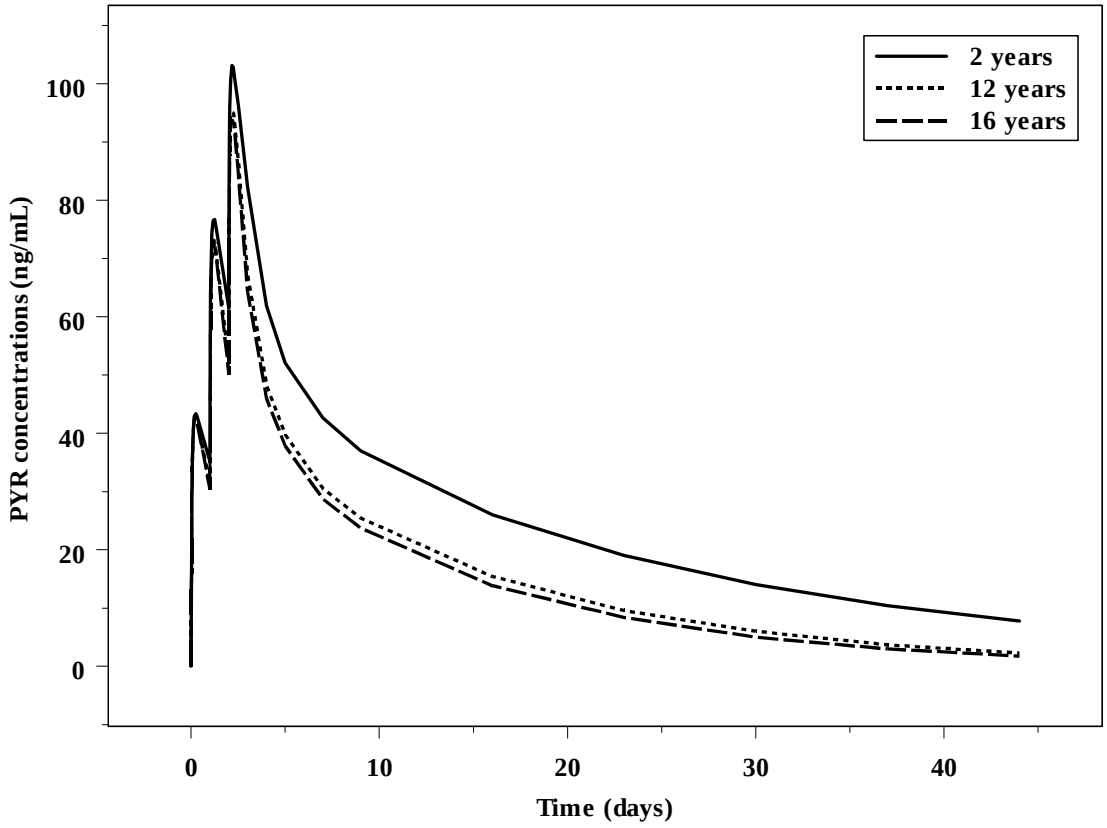

Figure 3.9 Box-plot depicting number of dosage units and Ln(AUC) distribution of pyronaridine based on 3 dosing regimens for pediatric malaria patients; bars represent 25th and 75th percentiles; whiskers represent 10th and 90th percentiles

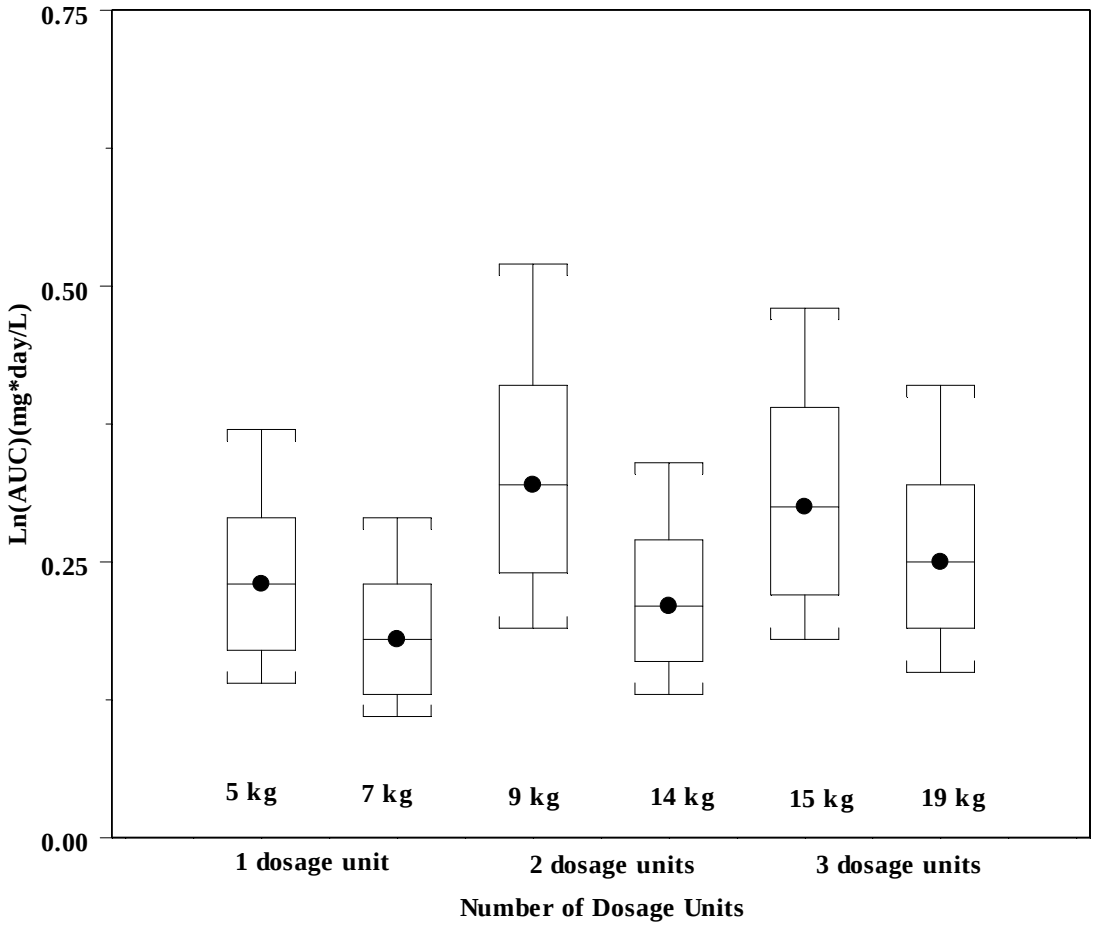

Figure 3.10 A plot of weight normalized empirical Bayes estimates of apparent clearance versus age

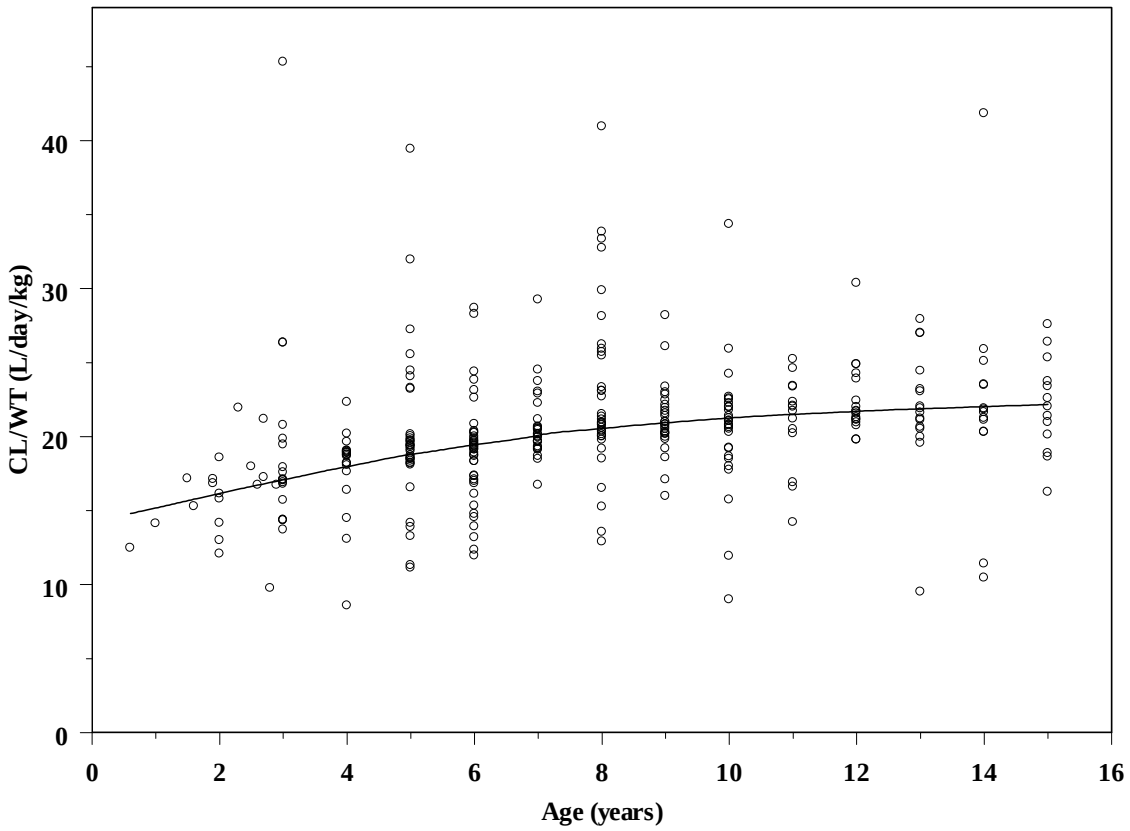

Figure 3.11 A plot of weight normalized empirical Bayes estimates of apparent central volume of distribution versus age

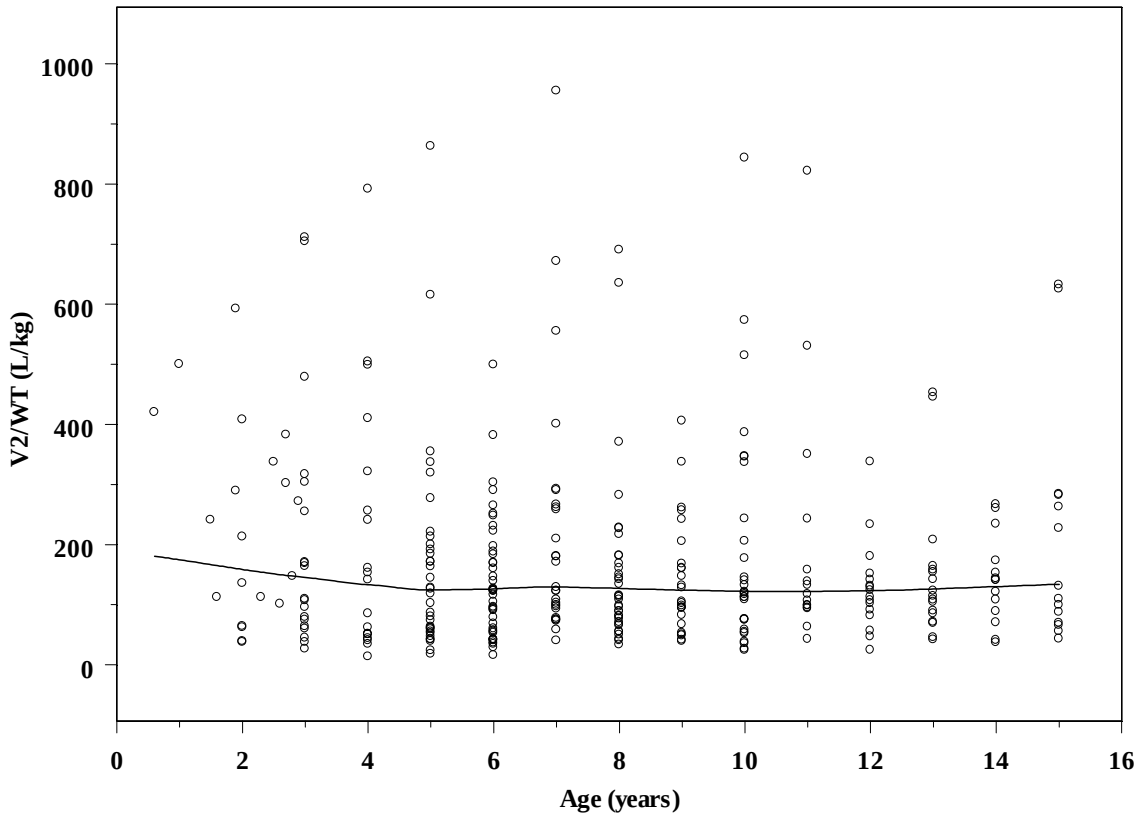

Figure 3.12 Box-plot depicting age versus distribution of pediatric malaria patients receiving different formulations of PA; bars represent 25th and 75th percentiles; whiskers represent 10th and 90th percentiles

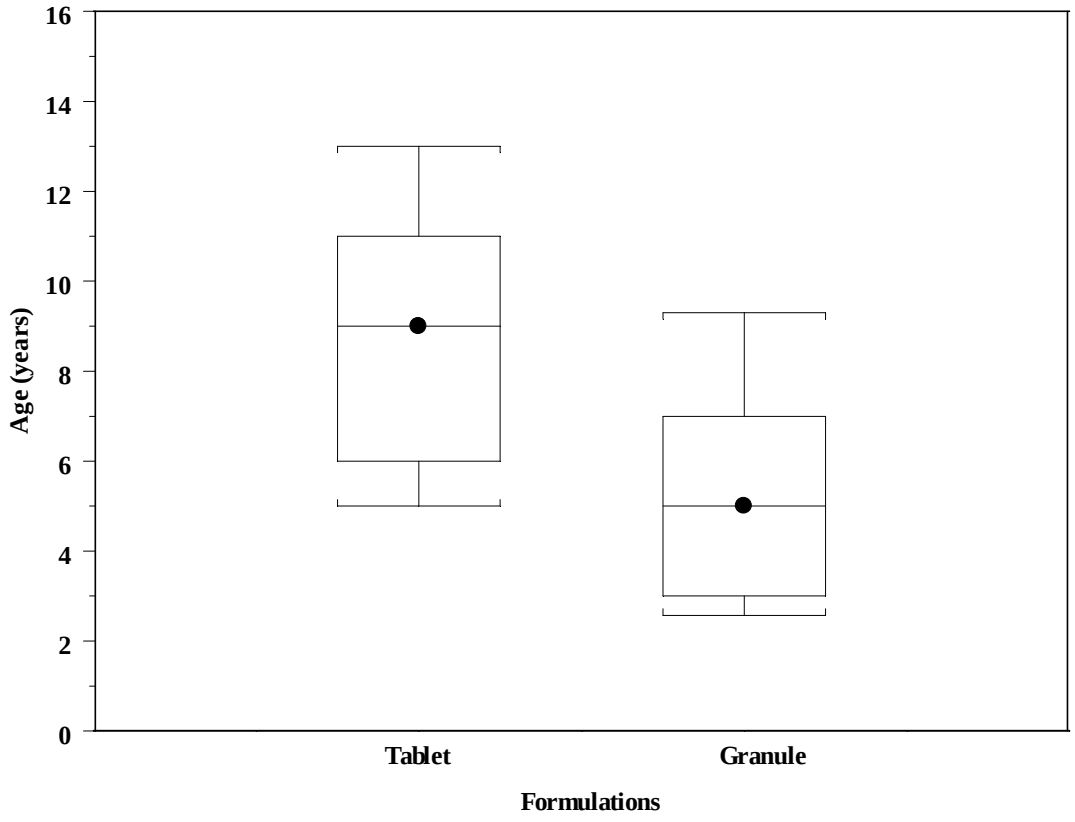

Figure 3.13 A plot between empirical Bayes estimates of absorption rate constant of pyronaridine and formulations

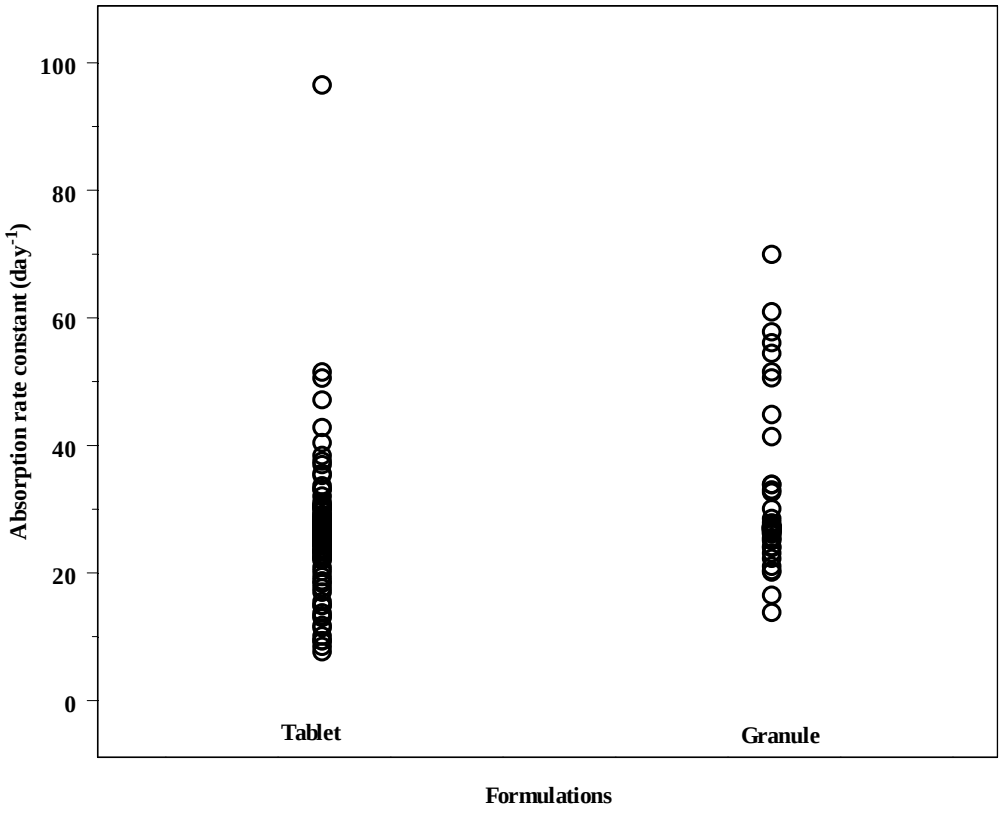

CHAPTER 4

RELATION OF PYRONARIDINE PHARMACOKINETIC PARAMETERS AND TREATMENT OUTCOME

Introduction

Malaria is an infectious disease that causes significant morbidity and mortality in the world population. Although it is a life-threatening disease, malaria deaths can be prevented with appropriate treatment. Currently, artemisinin-based combination therapies (ACTs) are recommended by WHO as a first line treatment for uncomplicated malaria (6). A combination of artemisinins and another antimalarial drug with different modes of action has proven to reduce rate of malaria resistance and increase the rate of successful treatment outcome (7-11). Following a three day course of ACTs, artemisinins can reduce the number of parasites by 10^8 leaving approximately 10^3-10^5 parasites to be removed by the partner drug (79). Therefore, the properties of the partner drug play an important role on the efficacy of ACTs to completely eliminate the residual parasites. The ideal partner drug of artemisinins should have reasonably long half-life, no adverse pharmacological interaction, and no additional toxicity (79).

Pyronaridine-artesunate (PA) 3:1 fixed dose combination, a new ACT developed for the treatment of uncomplicated *P. falciparum* and blood stages of *P. vivax* malaria, has completed nine clinical studies in Phase I, Phase II, and Phase III. Pyronaridine is an antimalarial agent that targets the blood stages of malaria parasites (22). Its mechanism of action is by inhibiting β-haematin formation and interfering with glutathione-dependent heme detoxification (32-34). The pharmacokinetics of pyronaridine was studied and reported in Chapter 2 and Chapter 3. To achieve optimal therapeutic outcome, it is of importance to understand the relationship between pharmacokinetic properties of pyronaridine and the outcome of malaria treatment as well as the thresholds of pharmacokinetic parameters associated with successful treatment outcomes. However,

there are several factors affecting treatment outcome apart from pharmacokinetic properties of the drug, such as a patient's characteristics and severity of the disease. Therefore the objectives of this analysis were: to determine the relationship between time to the occurrence of treatment failure and pyronaridine pharmacokinetics as well as host factors, and to determine cut-off values of pyronaridine pharmacokinetic parameters associated with a successful treatment outcome.

Background

Outcome of malaria treatment

Treatment outcomes in studies of antimalarial drug efficacy can be classified as follows (80):

Early treatment failure is present with the following signs and symptoms:

- Development of danger signs or severe malaria on Day 1, Day 2, or Day 3 in the presence of parasitemia.
- Parasitemia on Day 2 higher than the Day 0 predose count, irrespective of body temperature
- Parasitemia on Day 3 with axillary temperature $\geq 37.5^{\circ}$ C

Late clinical failure is present with the following signs and symptoms:

- Development of danger signs or severe malaria on any day from Day 4 in the presence of parasitemia, without previously meeting any of the criteria of early treatment failure.
- Presence of parasitemia and axillary temperature $\geq 37.5^{\circ}$ C on any day from Day 4, without previously meeting any of the criteria of early treatment failure.
- Presence of parasitemia on any day from Day 7 and axillary temperature $< 37.5^{\circ}$ C, without previously meeting any of the criteria of early treatment failure or late clinical failure.

Late parasitological failure is present with the following signs and symptoms:

- Presence of parasitemia on any day from Day 7 to Day 28 and axillary temperature < 37.5° C, without previously meeting any of the criteria of early treatment failure or late clinical failure.

Adequate clinical and parasitological response (ACPR) is defined as follows:

- Absence of parasitemia on day 28, irrespective of axillary temperature without previously meeting any of the criteria of early treatment failure, late clinical failure or late parasitological failure.

To effectively evaluate the efficacy of treatment, it is necessary to distinguish treatment failure due to recrudescence (recurrence of parasitemia after the treatment with the same infection that cause illness) from that due to re-infection (recurrence of parasitemia after the treatment with the new parasite strains). Polymerase Chain Reaction (PCR) for genotyping of malaria parasites is a commonly used method to differentiate recrudescence from re-infection due to its feasibility, high sensitivity, and high resolution (81). The genotyping was performed prior to initial dosing on Day 0 and in the case of reappearance of parasites.

Receiver Operating Characteristic Curve

In this analysis, Receiver Operating Characteristic (ROC) curve was used to identify the threshold of pharmacokinetic parameters associated with successful treatment outcome. The ROC curve is a tool used to assess accuracy of a diagnostic test. It can also be used to compare two or more diagnostic tests. The principle of ROC curve analysis is summarized as follows (82-89):

For each diagnostic test, there is a cut-off point or criterion value used to discriminate between the two states of health (i.e. disease positive and disease negative). The distributions of these two populations are not perfectly separated. Therefore, some

cases, disease positive will be classified as disease negative and vice versa. The outcomes of any diagnostic test can be categorized into four types as follows:

True positive (Sensitivity): is defined as a probability that a test result will be positive when the disease is present ($Pr(T^+/D^+)$).

True negative (Specificity): is defined as probability that a test result will be negative when the disease is not present ($Pr(T^-/D^-)$).

False positive (1-Specificity): is defined as a probability that a test result will be positive when the disease is not present ($Pr(T^+/D^-)$).

False negative (1-Sensitivity): is defined as a probability that a test result will be negative when the disease is present ($Pr(T^-/D^+)$).

The ROC curve is a plot of sensitivity against (1-specificity) for different cut-off values. The ROC curve for a perfect diagnostic test will pass through the upper left corner (100% sensitivity and 100% specificity). A good diagnostic test would result in the ROC curve close to the upper left corner. An area under the ROC (AUROC) curve is used to quantify the performance of a diagnostic test. AUROC ranges between 0.5 and 1. The closer the AUROC is to 1, the higher the overall accuracy of the test. For any diagnostic test, we test the hypothesis that the AUROC is greater than 0.5, that is, whether using the test is better than random guess. The following arbitrary criteria have been used for interpretation of AUROC values.

Low accuracy: $0.5 < \text{AUROC} \leq 0.7$

Moderate accuracy: $0.7 < \text{AUROC} \leq 0.9$

High accuracy: $0.9 < \text{AUROC} \leq 1$

Several methods are used to obtained optimal threshold values from an ROC curve (90): points on curve closest to the (0, 1); the Youden index; and the minimize cost criterion. The last method is rarely used because it considers cost from several sources such as cost for false diagnosis, cost of discomfort to person caused by treatment, and

cost of further investigation when needed, and these factors are difficult to accurately estimated.

The distance (d) between any points on ROC curve and point (0, 1) can be obtained using the following equation:

$$d = \sqrt{(1 - \text{sensitivity})^2 + (1 - \text{specificity})^2} \quad 4.1$$

The optimal threshold is the point where the distance is minimal.

The Youden index (J) is a method that finds the maximum vertical distance from the line of equality to the point on ROC curve. The aim of this method is to maximize the difference between true positive and false positive. The Youden index (J) can be obtained using the following equation:

$$\text{Youden index (J)} = \text{sensitivity} + \text{specificity} - 1 \quad 4.2$$

In this analysis, the Youden index is used as a criterion to identify the cut-off threshold because it reflects the maximum of the correct classification rate.

Cox Proportional Hazard Model

The Cox proportional hazard model is the method used to explore association between the survival time of patients and several covariates (91). Survival time is the time to the occurrence of a particular event which could be death, relapse, or the development of a disease. In this analysis, survival time refers to the time to the occurrence of recrudescence. These survival times can be characterized by a hazard function (h(t)) which is the probability of an event happening in a short time interval assuming that the subject has survived to the beginning of the interval. The hazard function can be obtained according to the following equation:

$$h\,(t) = \frac{\text{Number of individuals experiencing an event in interval beginning at t}}{(\text{number of individuals surviving at tiem t}) * (\text{interval width})} \quad 4.3$$

The Cox proportional hazard model can be given as follows:

$$h(t) = h_0(t) * \exp\,(\beta_1 X_1 + \beta_2 X_2 + \cdots + \beta_n X_n) \quad 4.4$$

where $h_0(t)$ is the baseline or underlying hazard function (the probability of reaching a particular event when all explanatory variables are zero), βs are the regression coefficients (the proportional changes expected in the hazard, related to the changes in explanatory variables), and X_1, X_2,…X_n are the explanatory variables or covariates.

Materials and methods

Study design and clinical outcome

Clinical outcome from two Phase II clinical studies (SP-C-002-05, SP-C-003-05) and four Phase III clinical studies (SP-C-004-06, SP-C-005-06, SP-C-006-06 and SP-C-007-07) were included in the analysis.

Phase II (SP-C-002-05 and SP-C-003-05)

SP-C-002-05 was conducted to assess safety, tolerability and efficacy of the 3 day regimen of PA in adult patients with acute uncomplicated *P. falciparum* malaria. Patients were randomized to one of 3 treatment groups: Group A: PA 6:2 mg/kg, Group B: PA 9:3 mg/kg, and Group C: PA 12:4 mg/kg. Blood samples for determining pyronaridine concentration were collected immediately before each dose, and at 0.5, 1, 1.5, 2, 2.5, 4, 8, 16, 24 hours and 3, 5, 12, 19 days after the third dose. Parasite counts were examined at screening on Day 0 to confirm inclusion/exclusion criteria and on Days 1, 2, 3, 7, 14, 21,

28, 35, and 42 or on any other day if the patient spontaneously returns. Samples were taken for PCR prior to Day 0 and Day 1 dosing. Additionally, samples for PCR were taken at time of treatment failure to assess status of recrudescence or re-infection.

SP-C-003-05 was aimed to assess safety, tolerability and pharmacokinetics of the 3 day regimen of PA in tablets and granules formulations for the treatment of uncomplicated *P. falciparum* malaria in pediatric patients in Gabon. For PA tablets, patients were sequentially assigned to one of 3 treatment groups similar to those in **SP-C-002-05.** For granule formulations, the PA dose of 9:3 mg/kg was used. Blood samples were collected immediately before each dose and at 0.5, 1, 1.5, 2.5, 4, 8, 12 hours, and at 3, 7, 14 and 21 days after first dose. Parasite counts were examined at screening on Day 0 to confirm inclusion/exclusion criteria and every 8 hours until 72 hours or until a negative result had been recorded. In addition, parasite counts were also examined on Days 3, 7, 14, 21, 28, 35, and 42 or on any other day if the patient spontaneously returns. PCR for genotyping was performed prior to initial dosing on Day 0 and Day 1 as well as at time for any treatment failure to assess status of recrudescence or re-infection.

Phase III (SP-C-004-06, SP-C-005-06, SP-C-006-06, and SP-C-007-07)

SP-C-004-06 and SP-C-005-06 were comparative, randomized studies to assess the efficacy and safety of PA (180:60 mg) with that of mefloquine (250 mg) plus artesunate (100 mg) and with that of artemether-lumefantrine (20:120 mg) (Coartem®), respectively in children and adult patients with uncomplicated *P. falciparum* malaria.

SP-C-006-06 was a comparative, randomized double blind, double dummy study to assess the safety and efficacy of PA (180:60 mg) with that of chloroquine (155 mg) in patients with acute *P. vivax* malaria.

SP-C-007-07 was a comparative, randomized study to assess safety and efficacy of a granule formulation (60:20 mg) (pediatric PYRAMAX®) versus Coartem® crushed

tablets in infants and children with acute uncomplicated *P. falciparum* malaria. For SP-C-004-06, SP-C- 005-06, and SP-C-006-06, PA was given according to body weight: 20 - ≤ 25 kg received one tablet, 26 - < 45 kg received two tablets, ≥ 45 - < 65 kg received three tablets, and ≥ 65 - 90 kg received four tablets. For SP-C-007-07, PA was given as follows: ≥ 5 - < 9 kg received one sachet, 9 - < 17 kg received two sachets, and 17 - < 25 kg received three sachets. For all Phase III studies, one or two blood samples were collected at two different time points (between Day 0 and Day 3, and between Day 4 and Day 42). Parasite counts were examined on Day 0 to confirm inclusion/exclusion criteria and every 8 hours following first dose administration for at least 72 hours or until the parasites have cleared. Moreover, parasite counts were also examined on Days 3, 7, 14, 21, 28, 35, and 42 or on any other day if the patient spontaneously returns. Genotyping studies by PCR to differentiate re-infection from recrudescence were assessed prior to initial dosing on Day 0 and Day 1 as well as in the case of reappearance of parasites as judged by a positive microscopy.

Derivation of secondary pharmacokinetic parameters

Derived secondary pharmacokinetic parameters following a 3 day dose of PA used for statistical analysis were obtained from empirical Bayes estimates of micro-parameters from the final model using the following equations:

1. Area under the concentration-time curve from 0 to ∞ ($AUC_{0-\infty}$)

$$AUC_{0-\infty} = \int_0^{\infty} \frac{k_a FD}{V_2} * \left[\frac{(k_{32}-\alpha)*e^{-\alpha t}}{(k_a-\alpha)(\beta-\alpha)} + \frac{(k_{32}-\beta)*e^{-\beta t}}{(k_a-\beta)(\alpha-\beta)} + \frac{(k_{32}-k_a)*e^{-k_a t}}{(\alpha-k_a)(\beta-k_a)}\right] \quad 4.5$$

2. Predicted pyronaridine concentrations on day 7 and on day 14

$$C = \frac{k_a FD}{V_2} * [\frac{(k_{32}-\alpha)*e^{-\alpha t}}{(k_a-\alpha)(\beta-\alpha)} + \frac{(k_{32}-\beta)*e^{-\beta t}}{(k_a-\beta)(\alpha-\beta)} + \frac{(k_{32}-k_a)*e^{-k_a t}}{(\alpha-k_a)(\beta-k_a)}] \quad 4\text{-}6$$

Statistical analysis

The influences of age, sex, baseline haemoglobin, baseline parasite count, formulation, $AUC_{0-\infty,}$ and predicted pyronaridine concentrations on day 7 and on day 14 on treatment outcome (recrudescence, re-infection, or successful outcome) were evaluated using the Cox proportional hazard model. The effects of $AUC_{0-\infty}$ and predicted pyronaridine concentrations on day 7 and on day 14 were evaluated separately since these determinants are all measures of drug exposures and are highly correlated. Moreover, the cut-off values for $AUC_{0-\infty}$ and predicted pyronaridine concentrations on day 7 and on day 14 associated with successful treatment outcome were identified using a ROC curve. The Youden index was used for selecting the cut-off pyronaridine concentrations on day 7 and on day 14 and $AUC_{0-\infty}$ (90). All statistical analyses were performed using SPSS version 19.0 (IBM, 1989, SPSS, Inc., 2010) and SAS version 9.3 (SAS institute, Cary, NC, USA, 2002-2010) with the significance level of 0.05.

Results

The characteristics and number of patients who had recrudescence, re-infection and successful treatment outcome were summarized in Table 4.1. Of the 642 malaria patients, ninety eight patients (15.26%) experienced treatment failure. Genotyping was performed to differentiate treatment failure due to recrudescence and re-infection. Of the patients who had treatment failure, twenty-eight patients had recrudescence and seventy patients had re-infection. Most of patients who developed re-infection were children (median age 12.3 years), whereas those who had recrudescence were adult patients (median age 21.7 years). The median predicted day 7 concentration, predicted day 14 concentration and predicted $AUC_{0-\infty}$ value were lower in recrudescence group as compared to those in the success group. The median baseline haemoglobin and median baseline parasite count between the recrudescence group and success group were comparable.

Influence of pharmacokinetic parameters and characteristics of patients on the time to the occurrence of treatment failure

The effects of pyronaridine pharmacokinetic parameters and patient's characteristics on the time to the occurrence of recrudescence and re-infection were evaluated using Cox regression analysis. All the covariates were tested for Cox proportional hazard assumption. Since predicted $AUC_{0-\infty}$ and predicted pyronaridine concentrations on day 7 and on day 14 were derived from individual Bayes estimates obtained from the final population pharmacokinetic model, these variables are highly correlated and were tested separately.

Of all the covariates tested, only predicted day 7 concentration was a significant predictor for time to the occurrence of recrudescence (p-value = 0.0455). Predicted $AUC_{0-\infty}$ was marginally significant with the p-value of 0.064, and predicted day 14 concentration was not a significant predictor for the time to the occurrence of recrudescence (p-value = 0.09). The hazard ratio (HR) for predicted day 7 concentration and predicted $AUC_{0-\infty}$ were estimated to be 0.954 (95%CI: 0.911-0.999) and 0.366 (95%CI: 0.126-1.062).

Similarly, predicted day 7 concentration was a significant predictor for time to the occurrence of re-infection after adjusting for the influence of age (p-value=0.026). Predicted $AUC_{0-\infty}$ was marginally significant with the p-value of 0.079. However, predicted day 14 concentration was not a significant predictor (p-value=0.228). The estimated hazard ratios for predicted day 7 concentration and predicted $AUC_{0-\infty}$ were 0.972 (95%CI: 0.948-0.997) and 0.608 (95%CI: 0.348-1.060), respectively.

Optimal values of pharmacokinetic parameters

associated with successful treatment outcome

Since the level of exposure to pyronaridine is used as a determinant of therapeutic response, predicted pyronaridine concentrations on day 7 and on day 14 and predicted $AUC_{0-\infty}$ levels associated with successful treatment outcome were evaluated by means of ROC curves (Figure 4.1-4.3). The cut-off level for predicted $AUC_{0-\infty}$ (area under ROC curve = 0.659, p-value = 0.004, 95%CI: 0.566-0.753) was found to be 1.06 mg*day/L. $AUC_{0-\infty}$ levels below this cut-off were observed in 60.71% (17/28) of subjects with recrudescence and in 34.74% (189/544) of subjects in the success group. The optimal cut-off for predicted pyronaridine concentrations on day 7 (area under ROC curve = 0.645, p-value = 0.01, 95%CI: 0.543-0.746) and on day14 (area under ROC curve = 0.669, p-value = 0.002, 95%CI: 0.590-0.749) were evaluated to be 31.3 ng/mL and 17.6 ng/mL, respectively. About 60.71% (17/28) and 92.86% (26/28) of subjects with recrudescence had predicted pyronaridine concentrations on day 7 and on day 14 below these thresholds. Whereas, 37.13% (202/544) and 60.48% (329/544) of subjects in the success group had predicted pyronaridine concentrations on day 7 and on day 14 below the cut-off values.

Discussion

This study aimed to determine association between pyronaridine pharmacokinetics and its therapeutic response. The area under concentration time curve of pyronaridine is used as a determinant for therapeutic outcome since it reflects both time and amount of drug exposure that is sufficient for parasite killing. White et al. has reported that antimalarial drug concentration on day 7 can be used as a determinant of therapeutic response for a combination therapy with a long half-life antimalarial agent (92). Moreover, an efficacy assessment of the patients is generally assessed on day 7 or day 14 after treatment starts. Therefore, in this analysis, we investigated the effects of

predicted $AUC_{0-\infty}$, and predicted pyronaridine concentrations on day 7 and on day 14 on the time to the occurrence of treatment failure (recrudescence and re-infection) using Cox regression analysis. All of these parameters were analyzed separately since they all were measures of drug exposure and were interrelated (93). Only predicted day 7 concentration was a significant predictor on the time to the occurrence of recrudescence and re-infection. Predicted $AUC_{0-\infty}$ was marginally significant but predicted day 14 concentration was not significant for both time to the occurrence of recrudescence and re-infection. The estimates showed that the mean risk of acquiring recrudescence and re-infection at any point in the follow up period of 42 days decreased by 4.6% and 2.8%, respectively, for each increase of 1 ng/mL in predicted day 7 concentration. These findings support the hypothesis that the higher levels of predicted pyronaridine concentrations on day 7 are associated with the decrease risk of acquiring recrudescence or re-infection. Although we did not find significant effect of predicted $AUC_{0-\infty}$ on time to the occurrence of recrudescence and time to the occurrence of re-infection, there was a trend that the mean risk of acquiring recrudescence and re-infection at any point in the follow up period of 42 days decreased by 63.4% (p-value=0.064) and 39.2% (p-value=0.079), respectively for each increase of 1 mg*days/L in $AUC_{0-\infty}$.

The contribution of host factors (age, gender, baseline hemoglobin, baseline parasite count, and formulation of the drug) on the time to the occurrence of treatment failure was also evaluated. Age was the only host factor that was found to be a statistically significant predictor on time to the occurrence of re-infection. The mean risk of acquiring a re-infection at any point in the follow-up period will increase by 4% for each decrease of 1 year of age. Several studies of different antimalarial treatments have reported the association between increasing age and decreasing risk of treatment failure (94-97). However, this relationship may not hold for very young infants. Higher parasite clearance in infants has been reported. This could be explained by a high prevalence of

fetal hemoglobin, circulating maternal antibodies, and age related immunological changes (98,99).

An association between higher baseline parasitemia and an increased risk of treatment failure has been presented by several studies since patients with higher level of parasitemia might be more likely to harbor a resistant strain (96). In this analysis, we did not find a statistically significant effect of baseline parasite count on the time to the occurrence of treatment failure. This could be explained by the fact that the patients in all clinical studies had mild uncomplicated malaria as characterized by lower levels of parasitemia (1,000-100,000 asexual parasite count/μL of blood).

The low level of hemoglobin (less than 10 g/dL) has been reported to be a predictor of treatment failure (95). Baseline hemoglobin level was not significant in this analysis. This would be expected given that the median baseline hemoglobin levels were comparable in recrudescence, re-infection and success groups. Moreover, the exclusion criteria for clinical studies included in this analysis did not allow patients in severely ill-condition (hemoglobin levels below 8 g/dL) to participate in these studies.

The cut-off values obtained from ROC curves of predicted $AUC_{0-\infty}$, predicted pyronaridine concentration on day 7 and on day 14 were 1.06 mg*day/L, 31.3 ng/mL and 17.6 ng/mL, respectively. The cut-off values of predicted $AUC_{0-\infty}$, and predicted pyronaridine concentration on day 7 had approximately 60% sensitivity and 60% specificity. For pyronaridine concentration on day 14, concentrations below the cut-off value predicted recrudescence with 92.86% sensitivity and 39.52% specificity. The low area under the ROC curve, sensitivity and specificity observed in this study are probably due to the limited number of subjects who had recrudescence. The validity of these thresholds should be confirmed by data that includes a larger number of recrudescence subjects.

Conclusions

In summary, the association between predicted $AUC_{0-\infty}$, predicted pyronaridine concentrations on day 7 and on day 14 and time to the occurrence of treatment failure can be used optimize the outcome of malaria treatment. As the levels of predicted pyronaridine concentrations on day 7 increased, the risks of acquiring re-infection or recrudescence decreased. Although, sensitivity and specificity were relatively low, the cut-off values of predicted pyronaridine concentrations on day 7 associated with successful treatment outcome obtained from ROC curve can be used as guidance to conduct further clinical trials.

Table 4.1 Demographic data of patients with recrudescence, re-infection and successful outcome

Characteristics	Recrudescence Mean (SD)	Re-infection Mean (SD)	Successful outcome Mean (SD)
Number of patients in each clinical studies (N)			
SP-C-002-05	-	-	16
SP-C-003-05	2	12	43
SP-C-004-06	23	18	212
SP-C-005-06	2	23	199
SP-C-006-06	-	-	34
SP-C-007-07	1	17	65
Age (years)	21.7 (11.33)	12.3 (12.44)	18.6 (12.88)
Weight (kg)	42.2 (14.64)	27.7 (14.66)	39.0 (16.68)
Predicted day 7 concentration (ng/mL)	29.7 (7.78)	33.2 (10.76)	34.8 (10.36)
Predicted day 14 concentration (ng/mL)	14.4 (3.24)	18.7 (6.87)	17.8 (6.79)
Predicted $AUC_{0-\infty}$ (mg*day/L)	1.1 (0.21)	1.2 (0.37)	1.23 (0.38)
Elimination half-life (days)	22.46 (7.78)	15.69 (8.69)	18.1 (8.17)
Hemoglobin (g/dL)	119.4 (19.32)	110.0 (13.04)	116.0 (18.75)
Parasite count (/µL)	25930.1 (28416.02)	19389.1 (22937.07)	22741.2 (28928.58)
Gender [N(%)]			
Male	20 (71.43)	43 (61.43)	316 (58.09)
Female	8 (28.57)	27 (38.57)	228 (41.91)
Formulation [N(%)]			
Tablet	26 (92.86)	27 (38.57)	466 (85.66)
Granule	2 (7.14)	43 (61.43)	78 (14.34)

Table 4.2 Cox regression analysis for patients with recrudescence

Predicted day 7 concentration								
Parameter	**DF**	**Parameter Estimate**	**Standard Error**	**Chi-Square**	**Pr > ChiSq**	**Hazard Ratio**	**95% Hazard Ratio Confidence Limits**	
Day 7 conc.	1	-0.04698	0.02349	3.9987	0.0455	0.954	0.911	0.999

Predicted day 14 concentration								
Parameter	**DF**	**Parameter Estimate**	**Standard Error**	**Chi-Square**	**Pr > ChiSq**	**Hazard Ratio**	**95% Hazard Ratio Confidence Limits**	
Day 14 conc.	1	-0.05876	0.03466	2.8743	0.0900	0.943	0.881	1.009

Predicted day $AUC_{0-\infty}$								
Parameter	**DF**	**Parameter Estimate**	**Standard Error**	**Chi-Square**	**Pr > ChiSq**	**Hazard Ratio**	**95% Hazard Ratio Confidence Limits**	
$AUC_{0-\infty}$	1	-1.00428	0.54304	3.4202	0.0644	0.366	0.126	1.062

Table 4.3 Cox regression analysis for patients with re-infection

Predicted day 7 concentration								
Parameter	**DF**	**Parameter Estimate**	**Standard Error**	**Chi-Square**	**Pr > ChiSq**	**Hazard Ratio**	**95% Hazard Ratio Confidence Limits**	
Day7	1	-0.02818	0.01264	4.9711	0.0258	0.972	0.948	0.997

Predicted day 14 concentration								
Parameter	**DF**	**Parameter Estimate**	**Standard Error**	**Chi-Square**	**Pr > ChiSq**	**Hazard Ratio**	**95% Hazard Ratio Confidence Limits**	
Day14	1	-0.02332	0.01935	1.4533	0.2280	0.977	0.941	1.015

Predicted day $AUC_{0-\infty}$								
Parameter	**DF**	**Parameter Estimate**	**Standard Error**	**Chi-Square**	**Pr > ChiSq**	**Hazard Ratio**	**95% Hazard Ratio Confidence Limits**	
AUC	1	-0.49818	0.28399	3.0773	0.0794	0.608	0.348	1.060

Age								
Parameter	**DF**	**Parameter Estimate**	**Standard Error**	**Chi-Square**	**Pr > ChiSq**	**Hazard Ratio**	**95% Hazard Ratio Confidence Limits**	
AGE	1	-0.04096	0.01260	10.5599	0.0012	0.960	0.936	0.984

Table 4.4 Area under ROC curve associated with recrudescence patients for predicted $AUC_{0-\infty,}$ predicted pyronaridine day 7 concentrations, and predicted pyronaridine day 14 concentrations

Test Result Variable(s)	Area Under the ROC Curve	Std. Error[a]	Sig[b]	Asymptotic 95% CI	
				Lower Bound	Upper Bound
$AUC_{0-\infty}$ (mg*day/L)	0.659	0.048	0.004	0.566	0.753
Day7 Concentration (ng/mL)	0.645	0.052	0.010	0.543	0.746
Day 14 Concentration (ng/mL)	0.669	0.041	0.002	0.590	0.749

a. Under the nonparametric assumption

b. Null hypothesis: true area = 0.5

Table 4.5 Cut-off values for predicted $AUC_{0-\infty,}$ predicted pyronaridine concentration on day 7, and predicted pyronaridine concentration on day 14 associated with recrudescence patients

Parameters	Cut-off values
$AUC_{0-\infty}$ (mg*day/L)	1.06
Day7 Concentration (ng/mL)	31.3
Day14 Concentration (ng/mL)	17.6

Figure 4.1 ROC curve for predicted $AUC_{0-\infty}$

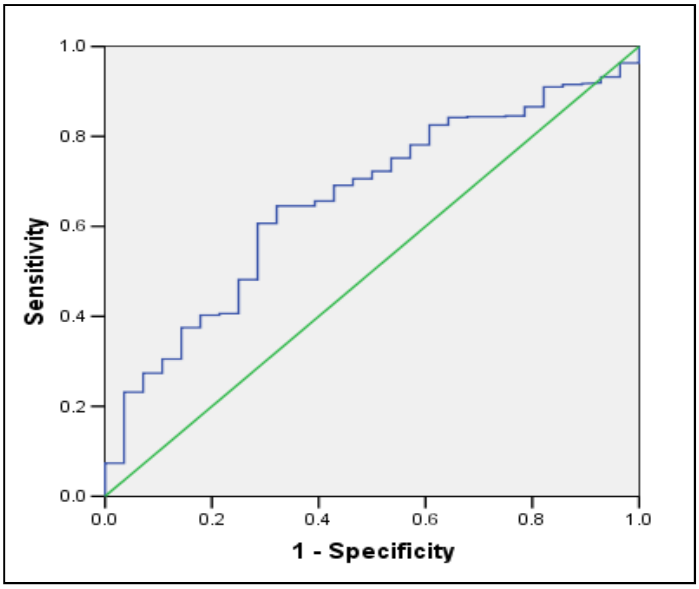

Figure 4.2 ROC curve for predicted pyronaridine day 7 concentrations

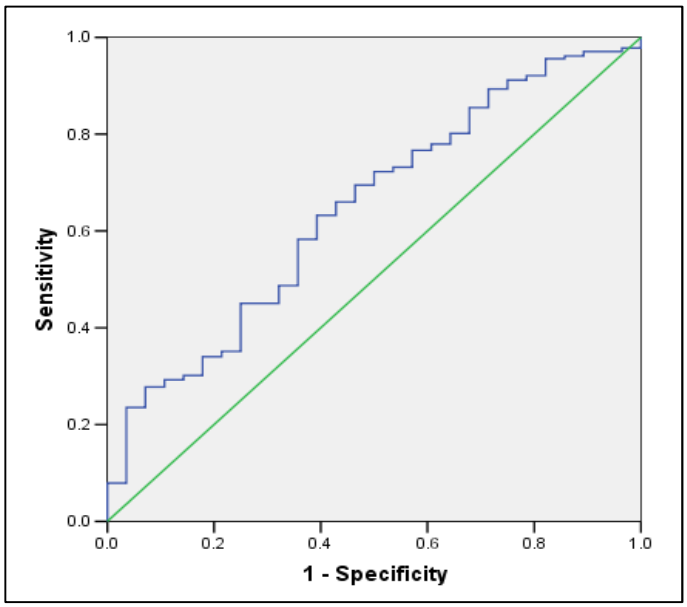

Figure 4.3 ROC curve for predicted pyronaridine day 14 concentrations

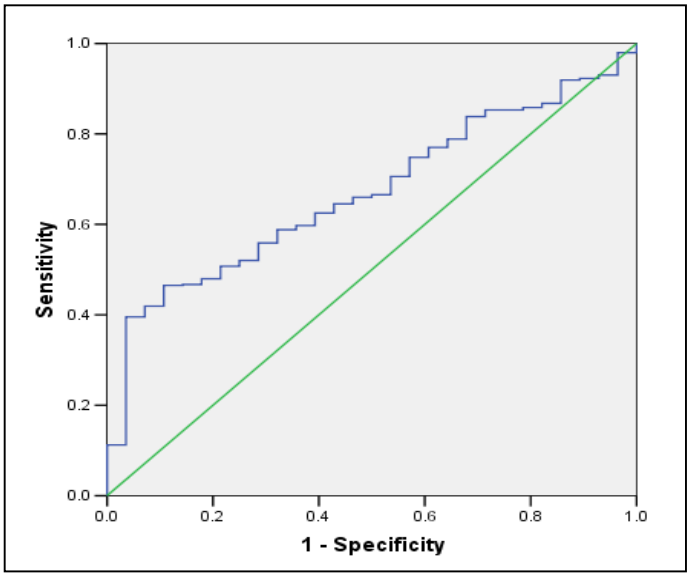

CHAPTER 5

DRUG-DRUG INTERACTION OF PYRONARIDINE WITH PROTEASE INHIBITOR RITONAVIR

Introduction

Malaria and Human Immunodeficiency Virus (HIV) coexist in global distribution. This can result in high rates of HIV and malaria co-infection (100,101). Cuadros has reported a higher risk of being HIV positive in individuals living in areas with high *P. falciparum* parasite rate compared with those living in areas with low *P. falciparum* parasite rate (102). The higher rate of *P. falciparum* infection was also reported among HIV-infected individuals in Southern India (103). Co-administration of antimalarial agents and antiretroviral drugs in HIV and malaria co-infection may lead to a potential drug-drug interaction which may result in severe toxicity or ineffectiveness of therapeutic outcome.

Artemisinin-based combination therapies (ACTs) are currently recommended by the World Health Organization (WHO) as a first line treatment of uncomplicated malaria (6). The rapid action of artemisinin derivatives helps in eliminating the majority of parasitemia leaving the residual parasites to be cleared by longer acting partner drugs. Pyronaridine-Artesunate (PA, Pyramax®) was developed as a fixed dose 3:1 for the treatment of uncomplicated falciparum and vivax malaria. Pyronaridine is mainly eliminated by metabolism via cytochrome P450. The cytochrome P450 isoenzymes responsible for pyronaridine metabolism include CYP1A2, CYP3A4 and CYP2D6. *In vitro* studies have shown inhibitory effect of pyronaridine on CYP2D6 (with an IC_{50} in human liver microsomes of 1.1 µM) and a weak inhibitory effect on CYP3A4 (IC_{50} > 50 µM). Moreover, pyronaridine has been shown to act as both a substrate and inhibitor of P-glycoprotein (P-gp) (38,39). Ritonavir, a booster in antiretroviral drug regimens, is both an inhibitor and substrate of CYP3A4, CYP2D6 and P-gp (64,66,104). It can also

induce expression of CYP3A4, CYP1A2 and UDP-glucuronosyltransferases (UGTs) (64). Based on the overlap for the pathways of metabolism, inhibitory effect, and induction effect of pyronaridine and ritonavir, the objective of this study was to determine whether there was a pharmacokinetic drug-drug interaction between pyronaridine and ritonavir in healthy volunteers.

Materials and Methods

Study design and blood sampling

This study was a phase I, randomized, multiple dose, parallel group study to evaluate any pharmacokinetic drug-drug interaction between fixed dose PA (Pyramax®) and ritonavir (SP-C-010-10). The design for pharmacokinetic analysis and statistics was conducted by Clinical Pharmacokinetic Laboratory, College of Pharmacy, the University of Iowa. Written informed consent was obtained from each subject. This study was approved by the Ethics Committee of both Basel and Swissmedic.

Subjects who met all of the following criteria were included in the study:

- Healthy male or female subjects (non-childbearing potential) age 18 to 55 years with body weight 50-90 kg.
- Medically normal subjects with no significant abnormal findings at the screening examination.
- Subjects can be able to understand and comply with all the study procedures.

Subjects who had one of the following criteria were excluded from the study:

- Known history or evidence of clinically significant disorders, hypersensitivity or allergic to pyronaridine, artesunate or ritonavir.
- Known active Hepatitis A IgM (HAV-IgM), Hepatitis B surface antigen (HBsAG), Hepatitis C antibody (HCV Ab), or seropositive HIV antibody.

- Previous participation in any clinical study with Pyramax or participation in any clinical study in last 2 months.
- Presence or recent history of tobacco abuse (≥ 10 cigarettes/day).
- Known or suspected alcohol abuse.
- Intake of grapefruit or caffeine containing food or beverages within 48 hours before study drug administration.
- Use of over-the-counter medications including vitamins, analgesics, or antacids within 1 week before the study start.
- Use of prescription medications 14 days before the study start or required chronic use of any prescription medication.

All subjects were randomly assigned (1:1) to receive fixed dose PA plus ritonavir (arm A) or fixed dose PA alone (arm B). Dosage regimens and blood sampling were as follows:

Arm A:

Subjects received 100 mg ritonavir soft gelatin capsule every 12 hours on Study Days 1-17 (the evening dose on Day 1 was omitted) and fixed dose PA (3 tablets for weight 45-<65 kg and 4 tablets for weight 65-≤ 90 kg) once daily in the morning for 3 days on Study Days 8-10. Blood samples for plasma ritonavir concentrations were collected on Days 1 and 10 at the following time points 0, 1, 2, 3, 4, 6, 8, 9, 12, 18, and 24 hours post-dose. Blood concentrations for pyronaridine were collected on Day 10 at 0, 0.5, 1, 1.5, 2, 3, 4, 6, 8, 12 and 24 hours and at 2, 3, 5, 12, 19, 26, 33 and 40 days post-dose. In addition, trough concentrations for both ritonavir and pyronaridine were assessed on study Days 8 and 9 in samples drawn prior to the administration of the morning dose.

Arm B:

Subjects received fixed dose PA alone (3 tablets for weight 45-<65 kg and 4 tablets for weight 65-≤ 90 kg) once daily in the morning for 3 days on Study Days 1-3. Blood concentrations for pyronaridine were collected on Day 3 at 0, 0.5, 1, 1.5, 2, 3, 4, 6,

8, 12 and 24 hrs. and at 2, 3, 5, 12, 19, 26, 33 and 40 days post-dose. In addition, trough concentrations were assessed on study Days 1 and 2 in samples drawn prior to the administration of the morning dose.

Genotyping for cytochrome P450 2D6 was performed prior to initial dosing on Day 1 for both arm A and arm B. Study drugs were given with 240 mL of non-carbonated mineral water. Food was not allowed during the 3 hours following study drug administration. Standard light breakfast, lunch, and dinner were served at 3 hours, 5 hours, and 12 hours post morning dose. Liquid consumption was allowed *ad libitum* after lunch but no alcohol, grapefruit, or xanthine-containing food or drinks until last pharmacokinetic sample collection in each treatment arm.

Sample Analysis

Two milliliters of blood pyronaridine samples were collected into tubes containing heparin as the anticoagulant (sodium heparin Vacutainer® tubes). All samples were stored at or below -80°C until analysis. Pyronaridine concentrations were determined by a validated liquid chromatography-mass spectrometric method (LC/MS) as described by Naik et al (61). The coefficient of variations for intra-day and inter-day precision were less than 15%. The lower limit of quantification (LLOQ) for pyronaridine was 5.7 ng/mL.

For ritonavir, 2 mL of blood was collected in pre-chilled tubes containing fluoride oxalate. The plasma was separated and transferred into screw cap cryovials. All samples were stored at or below -80°C until analysis. Plasma ritonavir concentrations were determined by a validated LC/MS developed by Naik and others (105). The coefficient of variations for intra-day and inter-day precision were less than 15%. The lower limit of quantification (LLOQ) for ritonavir was 4 ng/mL.

Pharmacokinetic Analysis

The following pharmacokinetic parameters for pyronaridine and ritonavir were computed for each subject.

- T_{max}: Time of maximum concentration
- C_{max}: Maximum peak observed concentration
- C_{trough}: Observed concentration at trough. For Day 1 ritonavir data, C_{trough} was substituted by C_{12h}, the observed concentration 12 hours after dosing.
- K_{el}: The magnitude of the slope of the linear regression of the log concentration vs. time profile during the terminal phase.
- $T_{½}$: Half-life, computed as ln (2)/K_{el}
- $AUC_{0\text{-}tau}$: Area under the concentration-time curve from hour 0 to the scheduled time of the next dose. For the ritonavir profile on Day 1, $AUC_{0\text{-}12h}$ was calculated as a surrogate for $AUC_{0\text{-}tau}$
- $AUC_{0\text{-}t}$: Area under the concentration-time curve from hour 0 through the last quantifiable concentration time (LQCT).
- $AUC_{0\text{-}\infty}$: Area under the concentration-time curve from 0 to infinity, computed using the linear trapezoidal rule as $AUC_{last} + C_{LQCT} / K_{el}$

For ritonavir, T_{max}, C_{max}, C_{12h}, K_{el}, $T_{1/2}$, and $AUC_{0\text{-}tau}$ were computed for both Day 1 (0 – 24 hours post-dose) and Day 10 (0 – 12 hours post-morning dose) concentration-time profiles. Additionally, an observed ritonavir accumulation factor for each subject in Arm A was computed as the ratio of Day 10 ritonavir $AUC_{0\text{-}12hr}$ to Day 1 ritonavir $AUC_{0\text{-}12hr}$.

To account for different in mg/kg doses administered to each subject and to reduce variability in pharmacokinetic parameters, C_{max}, $AUC_{0\text{-}tau}$, $AUC_{0\text{-}\infty}$ and $AUC_{0\text{-}t}$ estimates were adjusted to common mg/kg doses of 9.72 mg/kg pyronaridine tetraphosphate and 1.4 mg/kg ritonavir as per the following equation for pyronaridine:

$$(\text{Cmax or AUC}) \times \frac{9.72 \text{ mg/kg}}{(\text{administered PYR dose in mg/subject weight in kg})}$$

In all calculations, zero was substituted for concentrations below the quantification limit (BQL) of the assay, unless no other quantifiable concentrations were found thereafter. If no other quantifiable concentrations were found thereafter, the concentrations were not used in the calculations. K_{el} was only considered estimable if the adjusted r^2 value for the regression line was equal to at least 0.85 and if a concentration decline of one half occurred between the first and last points used in the regression. Pharmacokinetic analysis was performed using WinNonlin version 5.0 (Pharsight Corporation). Statistical analysis was performed using SPSS 17.

Drug –Drug Interaction Assessment

The effects of ritonavir on the pharmacokinetics of pyronaridine were assessed using 90% confidence intervals based on two, one-sided t-tests for the geometric mean of the test (drug administered with ritonavir)/reference (drug administered alone) ratio for the parameters C_{max}, $AUC_{0\text{-}t}$, $AUC_{0\text{-}\infty}$, and $AUC_{0\text{-}tau}$.

The effects of pyronaridine on the pharmacokinetics of ritonavir were assessed using 90% confidence intervals based on a paired sample t-test for the geometric mean ratio between the $AUC_{0\text{-}12hr}$, on day 10 (during administration of ritonavir with fixed dose PA) and the $AUC_{0\text{-}\infty}$ on Day 1. The treatment differences of 33% or larger (90% CIs for the ratios were not contained in the interval 0.667-1.50) in the presence and absence of

ritonavir or fixed dose PA were use as criteria to indicate the presence of a drug interaction.

Results

A total of 34 healthy adults were enrolled in this study and equally randomized to arm A and arm B. A summary of subject's demographics in each study arm is presented in Table 5.1. Adjusted pharmacokinetic parameters for pyronaridine for arm A and arm B are presented in Table 5.2. Figures 5.1, 5.2, and 5.3 are comparative plots of $AUC_{0\text{-}t,}$ $AUC_{0\text{-}tau,}$ and C_{max} between the two arms, respectively. The 90% confidence intervals for the ratios of geometric means of C_{max}, $AUC_{0\text{-}t,}$ $AUC_{0\text{-}\infty}$ and $AUC_{0\text{-}tau}$ using parameters adjusted for mg/kg dose are summarized in Table 5.3. The mean half-life of pyronaridine was 14.2 and 13.1 days, for Arm A and Arm B, respectively. The 90% confidence intervals for the ratios of geometric means of most pharmacokinetic parameters were contained in the 0.6667-1.500 range. The only exception was C_{max}, for which the 90% confidence intervals obtained using parameters adjusted for mg/kg dose (point estimate 1.2255 with a 90% CI: 0.9983, 1.5045) was not wholly contained in the acceptance range.

There were three subjects with CYP2D6 poor metabolizer status in Arm A and one subject with CYP2D6 poor metabolizer status in Arm B. The pyronaridine pharmacokinetic parameters are presented for each subject separately by CYP2D6 genotype in Table 5.4-5.5. Plots of $AUC_{0\text{-}t}$, $AUC_{0\text{-}tau}$, and C_{max} by genotype are given in Figures 5.4, 5.5, and 5.6, respectively. Although the number of subjects with poor metabolizer status was small, the CYP2D6 genotype did not appear to have an effect on the pharmacokinetic parameters of pyronaridine.

Five subjects in Arm A had clinically relevant elevation in aminotransferases. Of these, four subjects were discontinued from the study. $AUC_{0\text{-}t}$, $AUC_{0\text{-}tau}$ and C_{max} values trended higher in these subjects as compared to subjects in arm A without clinically relevant elevation of aminotransferases, as demonstrated by the plots in Figures 5.7 ($AUC_{0\text{-}t}$), 5.8 ($AUC_{0\text{-}tau}$), and 5.9 (C_{max}). Figure 5.10-5.11 present forest plots depicting 90% confidence interval of geometric mean for C_{max}, $AUC_{0\text{-}tau}$, $AUC_{0\text{-}t}$, and $AUC_{0\text{-}\infty}$ ratios for pyronaridine and 90% confidence interval of geometric mean for C_{max}/C_{12hr} and $AUC_{0\text{-}12hr}/AUC_{0\text{-}\infty}$ on day 10 relative to day 1 ratios for ritonavir, respectively.

Adjusted pharmacokinetic parameters for ritonavir on Day 1 and on Day 10 are presented in Table 5.6. The 90% confidence intervals for the ratios of geometric means of $AUC_{12hr}/AUC_{0\text{-}\infty}$ and C_{max}/C_{12hr} on day 10 to day 1 using parameters adjusted for mg/kg dose are summarized in Table 5.7.

The mean half-life for ritonavir on Day 1 and on Day 10 was estimated to be 6.46 and 3.96 hours, respectively. Due to the increase in K_{el} estimate of ritonavir from Day 1 to Day 10 in 16 out of 17 subjects, the ratio of Day 10 ritonavir $AUC_{0\text{-}12hr}$/ Day 1 ritonavir $AUC_{0\text{-}12hr}$ computed using the following accumulation factor could not be considered reasonable.

$$\left(\frac{1}{1-e^{-kel*tau}}\right)$$

However, the geometric mean ratio of C_{max}/C_{12hr} on Day 10 to Day 1 is estimated to be 1.9772 (90%CI: 1.6412, 2.3674). The ratio of approximately 2 could be explained by the higher C_{max} (2751 vs. 492 ng/mL) and shorter half-life (3.96 vs. 6.46 hours) of ritonavir in the presence of a fixed dose PA. Moreover, the geometric mean ratio of

$AUC_{0\text{-}12h}$ / $AUC_{0\text{-}\infty}$ on Day 10 to Day 1 was equal to 3.2001 (90% CI: 2.5678, 3.9882) suggesting the presence of a drug interaction in ritonavir pharmacokinetics.

Discussion

The objective of this study was to determine whether there was a significant pharmacokinetic drug interaction between ritonavir and pyronaridine in healthy subjects receiving co-administration of fixed dose PA and ritonavir. The details regarding interaction effects between artesunate and ritonavir can be found elsewhere (67). Based on *in vitro* studies, pyronaridine could be metabolized by CYP2D6, CYP1A2 and CYP3A4. Ritonavir is both an inhibitor and substrate of CYP3A4, CYP2D6, and the drug efflux pump, P-glycoprotein (P-gp) (64-66). Moreover, it is an inducer of CYP1A2 and CYP3A4. Therefore, the potential drug-drug interaction between ritonavir and pyronaridine is of clinical concern.

In this study, there was considerable inter-subject variability in the pharmacokinetics of pyronaridine. Based on the 90% confidence interval for the ratio of geometric means of C_{max} there was an effect, on average, of ritonavir on pyronaridine pharmacokinetics. However, given that the 90% confidence interval was very close to the acceptance range, these findings appeared to lack clinical relevance. Selective increases in concentrations of pyronaridine were observed in some subjects, and in some cases this was accompanied by liver enzyme elevations. The elevations of pyronaridine concentrations could possibly be explained by the inhibitory effect of ritonavir on CYP3A4, CYP2D6 as well as on the efflux transporter, P-gp (65,66,104). There were three subjects with CYP2D6 poor metabolizer status in arm A and one subject with CYP2D6 poor metabolizer status in arm B. Although there was no obvious relationship between pyronaridine C_{max} or AUC and CYP2D6 genotype, this study was not powered to detect such a relationship. Pyronaridine and ritonavir act as both substrates and inhibitors of P-gp (37,39,106). The inhibitory effect of ritonavir on pyronaridine efflux

could result in the higher concentrations of pyronaridine and this effect would be most apparent during the absorption phase. Additionally, the absorption of pyronaridine may vary among subjects due to differences in baseline expression of P-gp (39).

The exposure of ritonavir increased when co-administered with fixed dose PA. This could be explained by two reasons: the decrease in total body clearance (CL) and/or the increase in the extent of absorption (F). *In vitro* studies have shown that pyronaridine is an inhibitor of CYP2D6 and P-gp (37,38) which is involved in metabolism and efflux transport of ritonavir, respectively. This could play a role in the increased ritonavir exposure observed. However, ritonavir half-life on day 10 observed in this study decreased or remained constant as compared to day 1. This suggests that the increase in exposure of ritonavir in the presence of fixed dose PA might be due to pyronaridine inhibition of P-gp mediated ritonavir efflux rather than CYP2D6 inhibition.

Increases in ALT, with or without increases in AST, occurred in five subjects in arm A. A trend toward higher pyronaridine C_{max} and $AUC_{0\text{-}tau}$ was observed in these five subjects. However, these parameters were found to be overlapped between subjects displaying and not displaying liver enzyme elevations. Clinical trials have shown that ritonavir is associated with hepatic enzyme elevations (65). However, ritonavir exposures in this trial were below exposures resulting from the 600 mg twice daily ritonavir regimen used for antiretroviral therapy in many ritonavir clinical trials. Therefore, liver enzyme elevations observed in this study cannot be accounted for by the observed pharmacokinetic parameters from either pyronaridine or ritonavir.

Conclusions

In summary, the pharmacokinetic drug interaction effects between ritonavir and fixed dose PA were evaluated in 34 healthy subjects. Although, there was an effect of ritonavir on pyronaridine pharmacokinetics, the results were not considered clinically

relevant. An increase in ritonavir exposure was observed in the presence of fixed dose PA. This is most likely due to the inhibition of P-gp by pyronaridine.

Table 5.1 A summary of subject demographics

	Arm A (N=17) Mean (range), [N]	Arm B (N=17) Mean (range), [N]
Age (years)	42.3 (19-53)	43.7 (22-55)
Weight (kg)	69.3 (53.3-90.1)	72.4 (60.2-86.7)
BMI (kg/m^2)	23.1 (19.6-27.5)	24.2 (19.9-29.4)
Gender (N)		
Male	9	11
Female	8	6
CYP2D6 classification (N)		
Poor	3	1
Intermediate	8	6
Extensive	6	9

Table 5.2 Pharmacokinetic parameters of pyronaridine in subjects receiving PA and ritonavir (Arm A) or receiving PA alone (Arm B)

	Arm A (N = 17)		**Arm B (N = 16)**	
	Geometric Mean	**%CV**	**Geometric Mean**	**%CV**
K_{el} (1/day)	0.049	50.08	0.053	20.4
Half-life (day)	14.2	50.33	13.1	20.5
T_{max} (day)	0.078	65.46	0.059	25.7
C_{max} (ng/mL)	462	28.52	377.2	42.6
C_{trough} (ng/mL)	119.2	47.49	114.1	36.8
AUC_{0-t} (day*ng/mL)	955	38.02	1059	34.7
$AUC_{0-\infty}$ (day*ng/mL)	1212	24.25	1248	34.4
AUC_{0-tau} (day*ng/mL)	222	36.52	210	36.8

Table 5.3 Geometric mean ratio and 90% confidence intervals for pharmacokinetic parameters of pyronaridine following administration with ritonavir (Arm A) or without ritonavir (Arm B) using parameters adjusted for mg/kg dose

Compute parameter*	**Ratio (Arm A/Arm B)**	**90% Confidence Intervals**
C_{max} (ng/mL)	1.2255	(0.9983, 1.5045)
AUC_{0-t} (day*ng/mL)	0.9020	(0.7277, 1.1181)
$AUC_{0-\infty}$ (day*ng/mL)	0.9717	(0.8132, 1.1610)
AUC_{0-tau} (day*ng/mL)	1.0590	(0.8589, 1.3058)

*N=33 (N=17 Arm A, N=16 Arm B) for C_{max}, and $AUC_{0-tau,}$ N = 32 (N=16 Arm A, N = 16 Arm B) for $AUC_{0-t,}$ N = 31 (N = 15 Arm A, N = 16 Arm B) for $AUC_{0-\infty}$

Table 5.4 Pharmacokinetic parameters of Pyronaridine separated by CYP2D6 genotype for subjects receiving fixed dose PA with ritonavir (Arm A). All the parameters were adjusted to common dose of 9.72 mg/kg

Subject	K_{el} (1/day)	Half-life (day)	T_{max} (day)	C_{max} (ng/mL)	C_{trough} (ng/mL)	AUC_{0-t} (day*ng/mL)	$AUC_{0-\infty}$ (day*ng/mL)	AUC_{0-tau} (day*ng/mL)
Extensive CYP2D6 metabolizer								
20	0.064	10.8	0.333	396.3	72.1	877	1028	198
22	0.063	11.1	0.335	413.9	116.0	1170	1270	241
25	0.106	6.5	0.083	493.0	104.5	684	756	201
30	0.036	19.4	0.083	532.5	259.2	1441	1623	312
31	0.043	16.2	0.042	596.3	121.3	1042	1255	202
32	0.061	11.3	0.063	398.2	182.8	1304	1464	289
Intermediate CYP2D6 metabolizer								
2	0.026	26.6	0.063	386.6	72.3	690	1030	158
4	0.046	14.9	0.042	332.9	80.2	806	986	148
7	0.078	8.9	0.042	522.1	135.7	1528	1644	267
11	0.046	15.2	0.083	395.8	18.1	963	1115	243
15	0.074	9.4	0.083	378.3	89.6	778	890	167
18	NA*	NA	0.065	374.7	52.3	382	NA	110
23	0.066	10.5	0.083	752.4	258.2	1689	1787	447
26	0.044	15.6	0.063	799.4	143.3	1061	1218	272
Poor CYP2D6 metabolizer								
6	0.016	43.9	0.063	306.0	80.2	700	1262	150
10	NA*	NA	0.063	659.9	NA	NA	NA	NA
17	0.036	19.0	0.063	425.2	147.8	1136	1335	255

*****Not applicable; value cannot be estimated

Table 5.5 Pharmacokinetic parameters of Pyronaridine separated by CYP2D6 genotype for subjects receiving fixed dose PA alone (Arm B). All the parameters were adjusted to common dose of 9.72 mg/kg

Subject	K_{el} (1/day)	Half-life (day)	T_{max} (day)	C_{max} (ng/mL)	C_{trough} (ng/mL)	AUC_{0-t} (day*ng/mL)	$AUC_{0-\infty}$ (day*ng/mL)	AUC_{0-tau} (day*ng/mL)
Extensive CYP2D6 metabolizer								
1	0.069	10.1	0.042	359.6	112.2	1104	1208	182
8	0.068	10.2	0.085	511.5	139.8	1373	1561	279
9	0.050	13.9	0.042	296.3	116.3	800	907	216
12	0.065	10.7	0.063	339.4	123.0	844	968	199
13	0.060	11.6	0.063	423.3	99.2	829	983	200
14	0.044	15.9	0.083	446.6	136.4	991	1156	261
19	0.033	21.1	0.063	234.8	88.2	1021	1322	154
28	0.043	16.3	0.063	608.8	154.9	1439	1723	290
34	0.066	10.6	0.042	345.4	104.9	635	738	154
Intermediate CYP2D6 metabolizer								
3	0.053	13.2	0.063	172.5	56.1	675	785	93
5	0.056	12.3	0.042	253.1	100.0	1088	1320	191
21	0.043	16.3	0.063	251.0	60.8	855	1149	148
24	0.053	13.0	0.063	593.9	169.6	1504	1778	281
27	0.060	11.5	0.083	355.0	155.4	1461	1679	251
33	0.050	14.0	0.043	522.5	95.6	1007	1155	218
Poor CYP2D6 metabolizer								
29	0.052	13.3	0.063	805.6	220.6	2305	2654	438

Table 5.6 Pharmacokinetic parameters of ritonavir from Day 1 and Day 10

	Day 1 (N=17)		Day 10 (N = 17)	
	Geometric Mean	**%CV**	**Geometric Mean**	**%CV**
K_{el} (1/hr)	0.107	27.4	0.175	25.0
Half-life (hr)	6.46	27.3	3.96	25.1
T_{max} (hr)	3.46	51.6	2.27	39.5
C_{max} (ng/mL)	492	81.1	2793.3	52.4
C_{12hr} (ng/mL)	147.7	59.3	424	57.7
$AUC_{0\text{-}12\ hr}$ (hr*ng/mL)	3105	73.8	14947	51.8
$AUC_{0\text{-}24\ hr}$ (hr*ng/mL)	4199	65.2		
$AUC_{0\text{-}\infty}$ (hr*ng/mL)	4746	62.4		

Table 5.7 Geometric mean ratio and 90% confidence intervals for pharmacokinetic parameters of ritonavir on day 10 to day 1 following administration of fixed dose PA and ritonavir (Arm A) using parameters adjusted for mg/kg dose

Compute parameter	Ratio (Day10/Day1)	90% Confidence Intervals
C_{max}/ C_{12hr} (ng/mL)	1.9772	(1.6412, 2.3674)
$AUC_{0\text{-}12\ hr}$ /$AUC_{0\text{-}\infty}$ (hr*ng/mL)	3.2001	(2.5678, 3.9882)

Figure 5.1 Comparative pyronaridine AUC_{0-t} (adjusted for mg/kg dose) for Arm A and Arm B

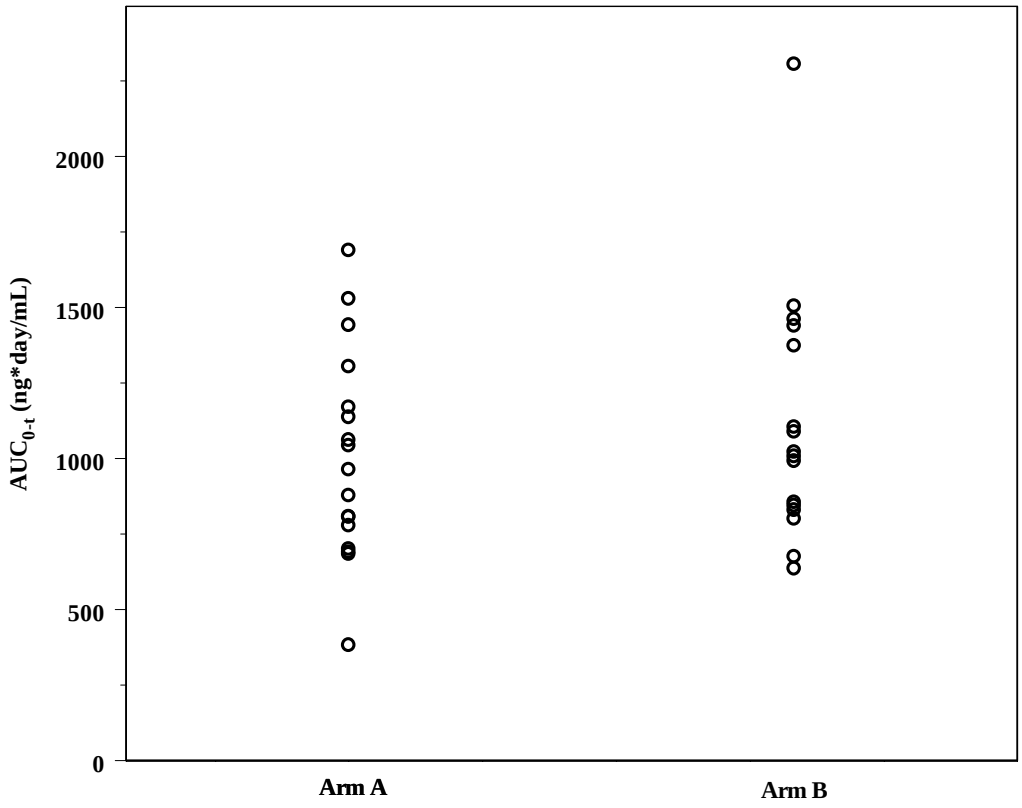

Figure 5.2 Comparative pyronaridine $AUC_{0\text{-}tau}$ (adjusted for mg/kg dose) for Arm A and Arm B

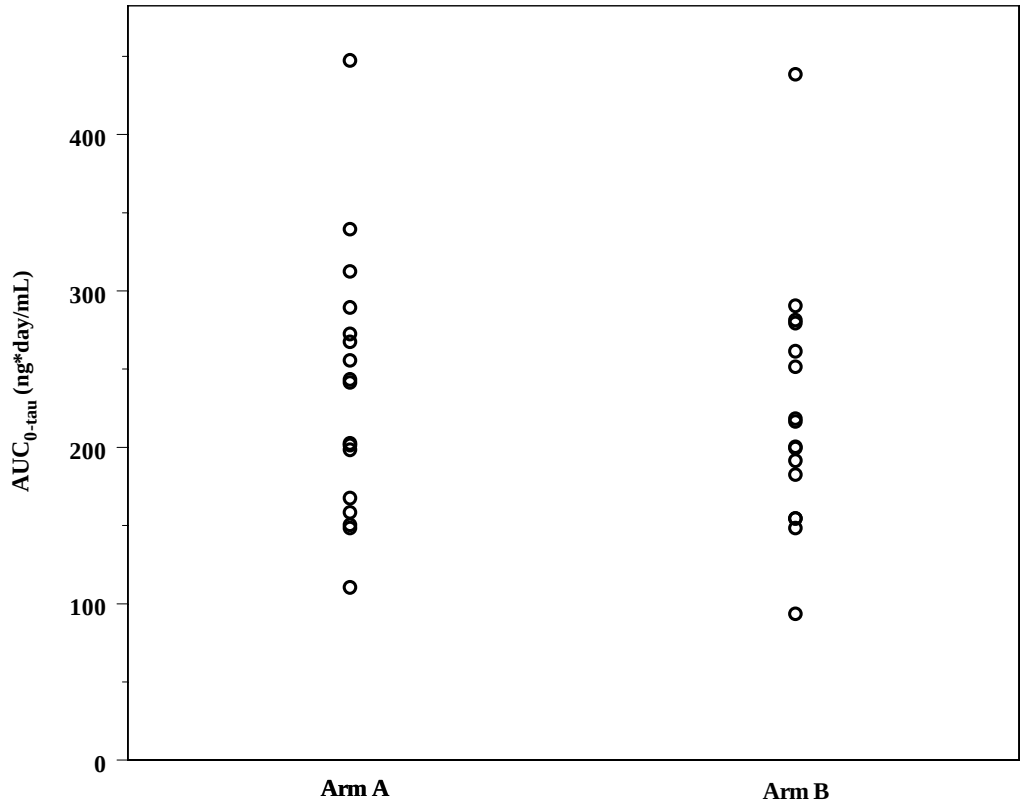

Figure 5.3 Comparative pyronaridine C_{max}(adjusted for mg/kg dose) for Arm A and Arm B

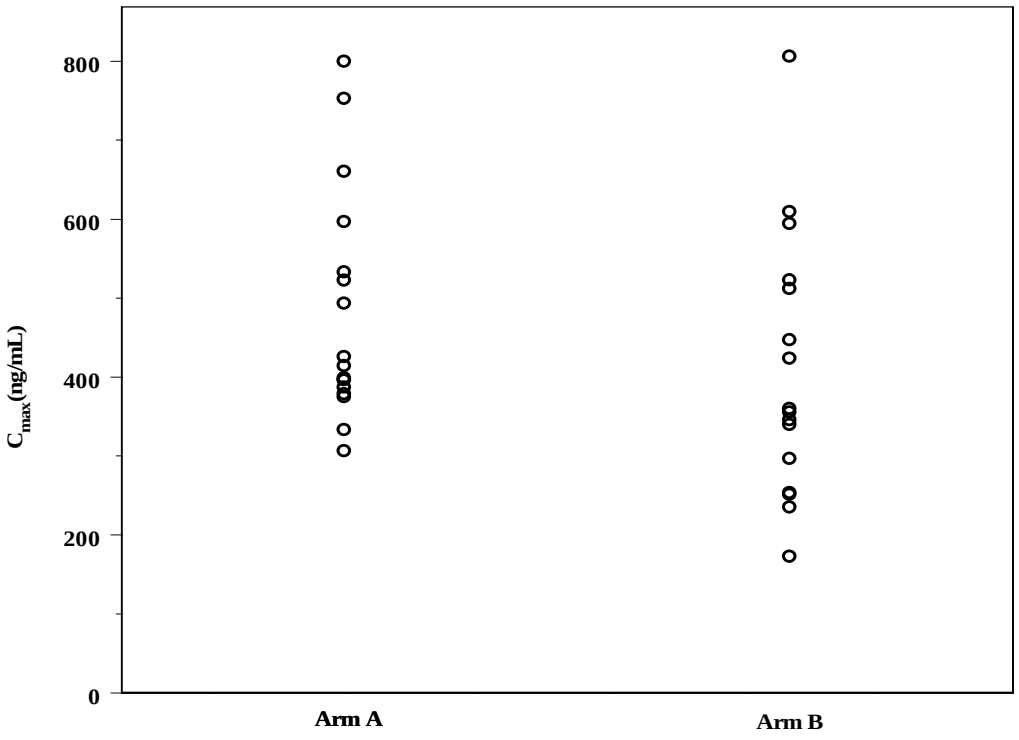

Figure 5.4 Pyronaridine AUC_{0-t} (adjusted for mg/kg dose) by CYP2D6 genotype

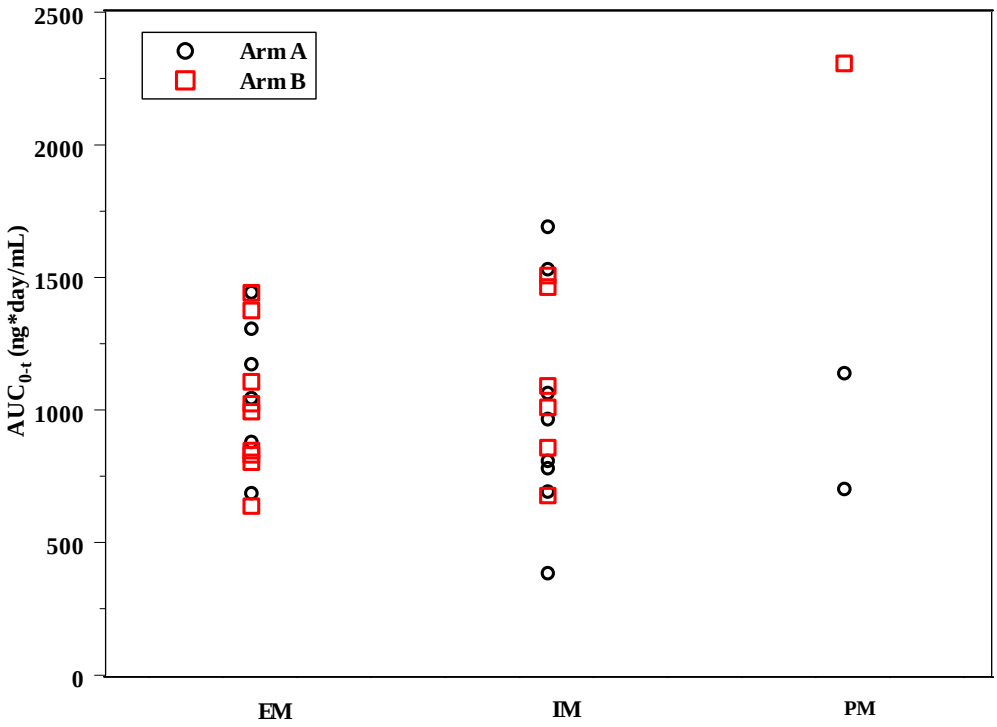

Figure 5.5 Pyronaridine $AUC_{0\text{-}tau}$ (adjusted for mg/kg dose) by CYP2D6 genotype

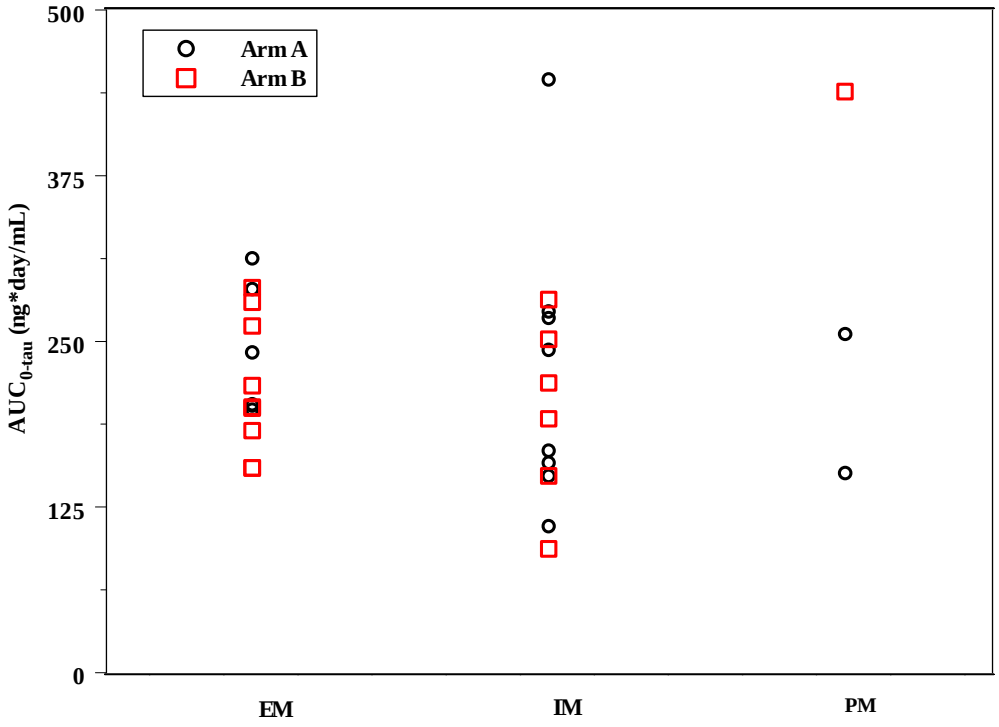

Figure 5.6 Pyronaridine C_{max} (adjusted for mg/kg dose) by CYP2D6 genotype

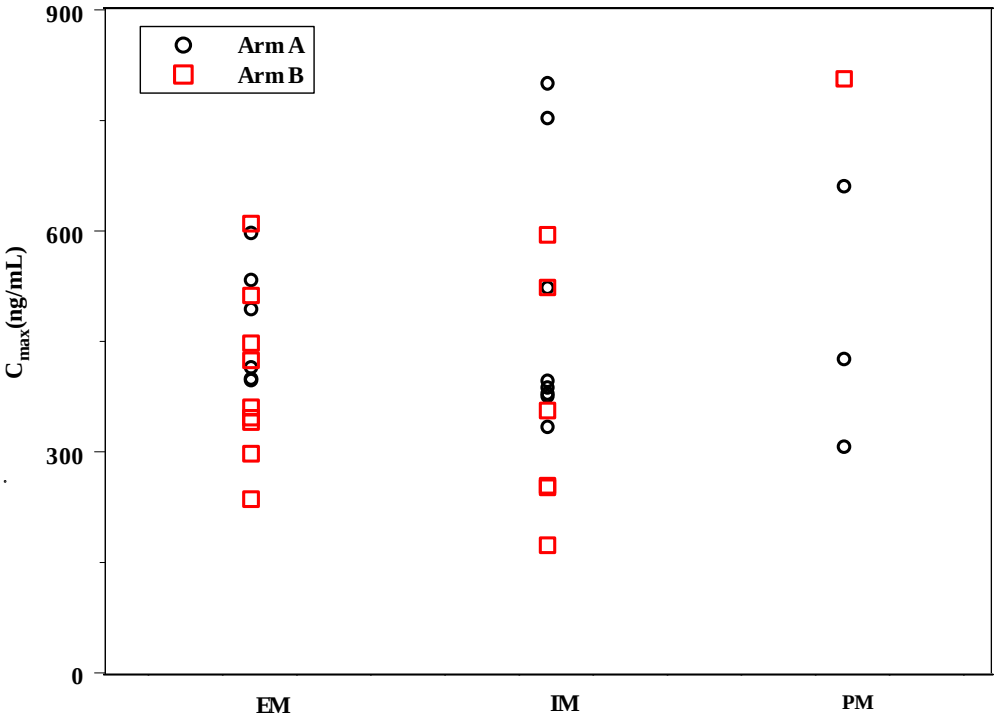

Figure 5.7 Pyronaridine AUC_{0-t} (adjusted for mg/kg dose) for subjects with clinically relevant elevation of liver enzymes and without clinically relevant elevation of liver enzymes

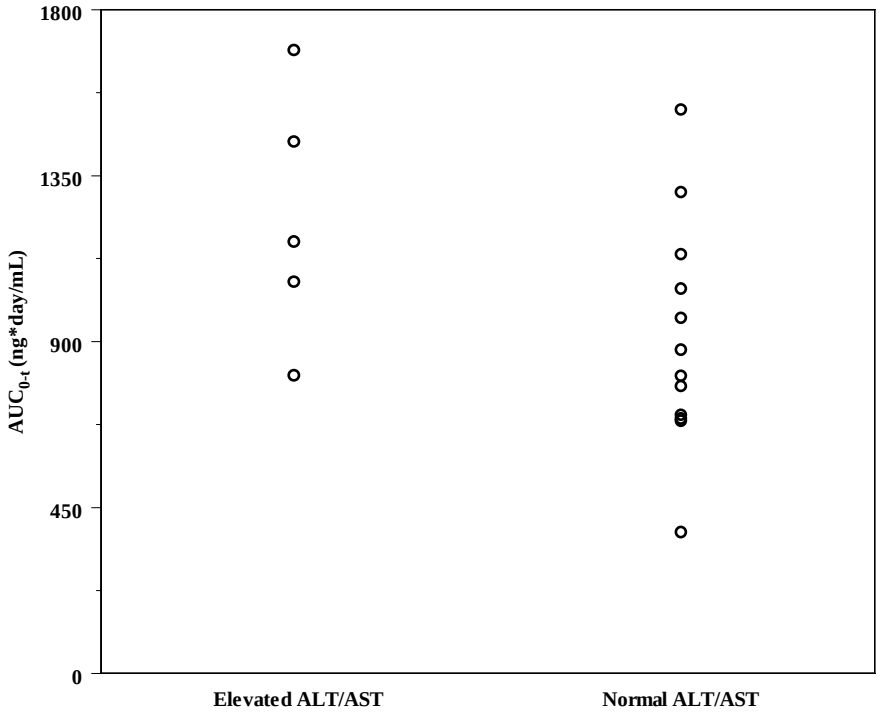

Figure 5.8 Pyronaridine $AUC_{0\text{-}tau}$ (adjusted for mg/kg dose) for subjects with clinically relevant elevation of liver enzymes and without clinically relevant elevation of liver enzymes

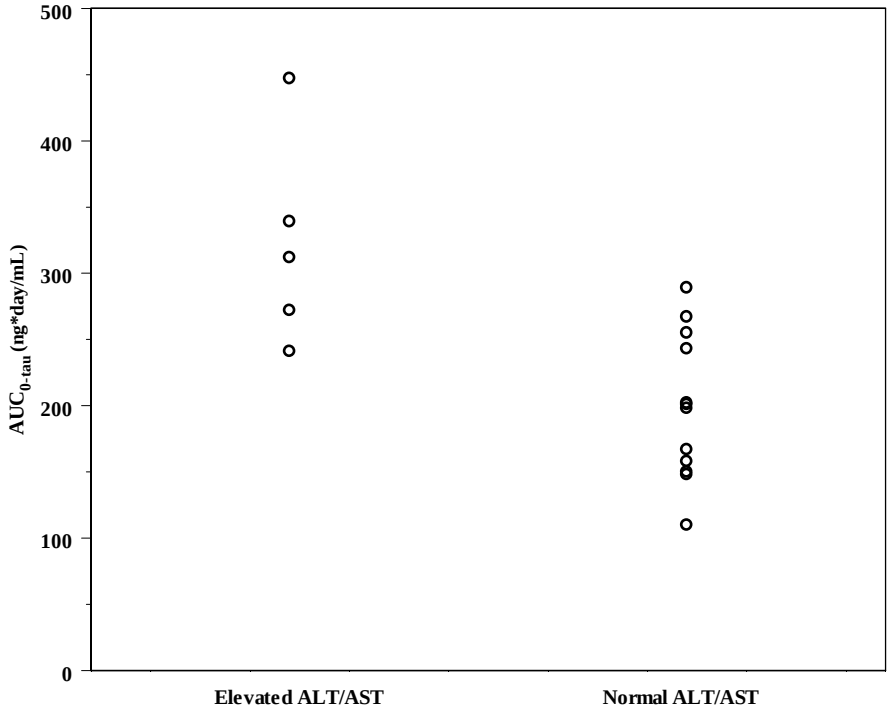

Figure 5.9 Pyronaridine C_{max} (adjusted for mg/kg dose) for subjects with clinically relevant elevation of liver enzymes and without clinically relevant elevation of liver enzymes

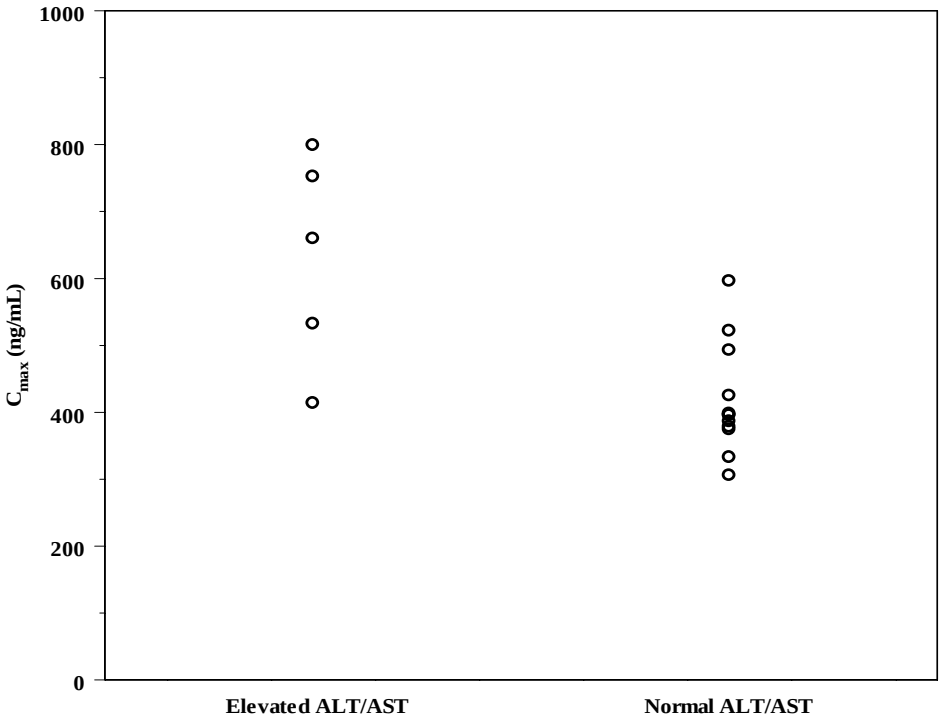

Figure 5.10 A forest plot depicting 90% confidence interval of geometric mean ratios for C_{max}, $AUC_{0\text{-}tau}$, $AUC_{0\text{-}t}$, and $AUC_{0\text{-}\infty}$ for pyronaridine.

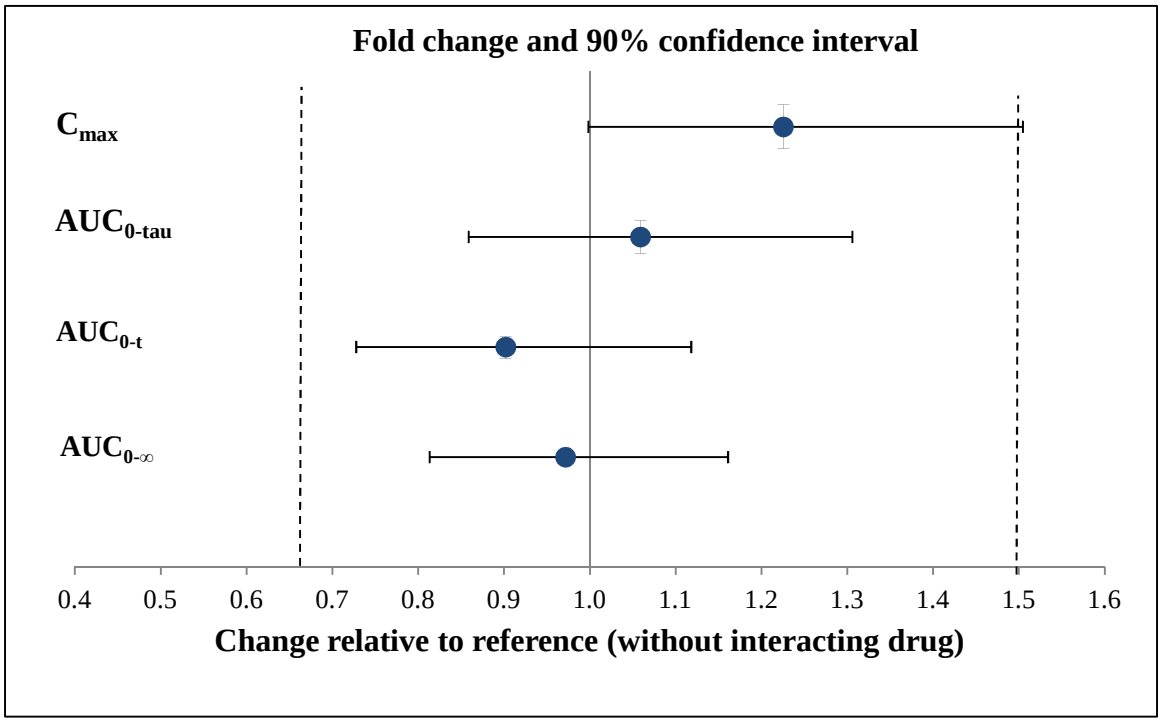

Figure 5.11 A forest plot depicting 90% confidence interval of geometric mean ratios for C_{max}/C_{12hr} and $AUC_{0\text{-}12hr}/AUC_{0\text{-}\infty}$ on day 10 relative to day 1 for ritonavir.

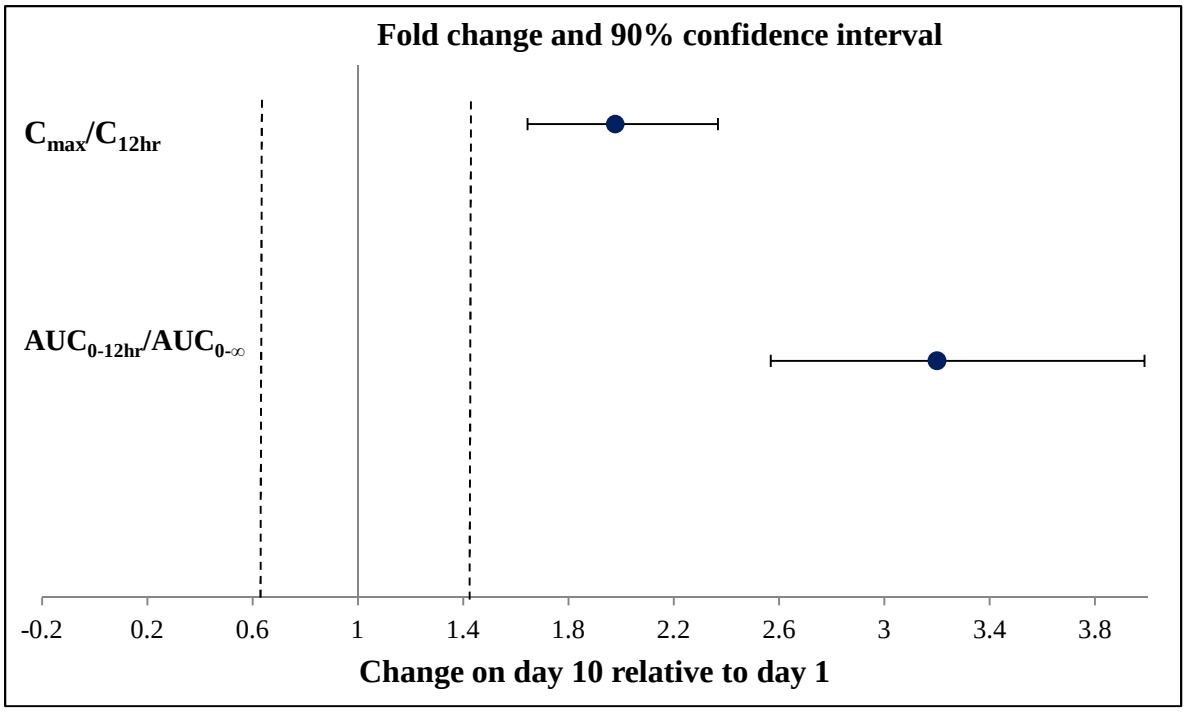

CHAPTER 6

SUMMARY

Pyronaridine is an antimalarial agent that has been used as monotherapy in China since 1980 (31). It has been developed as a fixed dose (3:1) pyronaridine:artesunate for the treatment of uncomplicated falciparum and vivax malaria. Pharmacokinetic properties of pyronaridine have been investigated in rat, rabbit, dog, and rhesus monkey. Most of the studies were published in Chinese. For all animal species, blood pyronaridine concentrations declined in a multiphasic disposition manner suggesting extensive distribution of pyronaridine into tissues (31). Distribution, metabolism and elimination of pyronaridine have been extensively studies in *in vitro* and *in vivo* (107). However, only limited data regarding pharmacokinetics of pyronaridine in human have been reported (108-110). The main objective of this dissertation was to characterize pharmacokinetic properties of pyronaridine in humans by means of population pharmacokinetics. The pharmacodynamics of pyronaridine, as well as potential interaction with a drug (ritonavir) that is an inhibitor/inducer or is metabolized by similar cytochrome P450 isoenzymes were also evaluated.

Population pharmacokinetics of pyronaridine in healthy (166) and malaria infected (310) adults was developed in Chapter 2 using pooled data from 3 Phase I, 1 Phase II, and 3 Phase III clinical studies. Pyronaridine pharmacokinetics were best described by a two-compartment model with first order absorption and elimination from the central compartment. The significant covariates in the final model included malaria infection on apparent clearance (CL/F), apparent central volume of distribution (V2/F), and apparent peripheral volume of distribution (V3/F) and body weight on CL/F and V2/F. Adult malaria patients exhibit 2 times and 14 times higher in CL/F and V2/F as compared to healthy adults. These higher CL/F and V2/F values reflect the mechanism of action of pyronaridine in that it forms a complex with hematin to enhance hematin

induced red blood cell lysis (34). Moreover, the derived elimination half-life of adult malaria patients is much longer than that of healthy adults (25 days vs. 10 days). This result would be expected given the much larger central volume of distribution in adult malaria patients.

In Chapter 3, population pharmacokinetics of pyronaridine in pediatric malaria patients was developed. The model used pooled data from 1 Phase II and 4 Phase III clinical studies. Due to a high correlation between body weight and age, body weight was included as part of the base model *a priori* with an allometric function on clearance (exponent of 0.75) and volume parameters (exponent of 1). A two-compartment model with first order absorption and elimination adequately described the data. The effect of age on CL/F was the only significant covariate-parameter relationship in the final model. The empirical Bayes pharmacokinetic parameter estimates from the final model categorized by 3 age ranges showed that younger children had lower weight normalized clearance and higher weight normalized central volume of distribution as compared to older children. These results could be explained by the low levels of enzymes used to metabolize pyronaridine in younger children and the low levels of protein binding as well as the higher level of extracellular fluid volume of total body water. Overall, the final models developed in Chapter 2 and Chapter 3 are reliable, predictive, stable and can be used for simulation purposes as confirmed by the model evaluation criteria.

Pharmacodynamic properties of pyronaridine were reported in Chapter 4. Pharmacokinetic parameters of pyronaridine and host factors associated with treatment outcome (recrudescence and re-infection) were evaluated by means of Cox proportional regression analysis. Predicted pyronaridine concentration on day 7 was a significant predictor for time to the occurrence of recrudescence and re-infection. An increase in predicted pyronaridine day 7 concentrations resulted in a decrease in the mean risk of acquiring recrudescence and re-infection. Predicted $AUC_{0-\infty}$ was not a significant predictor for time to the occurrence of recrudescence and re-infection. However, there

was a trend toward the decrease in mean risk of acquiring recrudescence and re-infection for an increase in predicted $AUC_{0-\infty}$ values. Moreover, age was also found to be a significant predictor for time to the occurrence of re-infection. A one year decrease in age is associated with 4% increase in the mean risk of acquiring a re-infection.

Receiver Operating Characteristic curve analysis was also performed to identify cut-off values of pharmacokinetic parameters associated with successful treatment outcome. The cut-off values of predicted $AUC_{0-\infty}$, predicted pyronaridine concentration on day 7 and on day 14 identified using Youden's index were estimated to be 1.06 mg*day/L, 31.3 ng/mL and 17.6 ng/mL, respectively. However, due to the limited number of subjects who acquired recrudescence, these cut-off values yielded relatively low sensitivity and specificity. These results should be confirmed by other study with larger number of subjects with recrudescence.

Finally, potential drug-drug interactions between pyronaridine and ritonavir, a protease inhibitor, were assessed and described in Chapter 5. The results showed that pyronaridine C_{max} increased when co-administered with ritonavir. However, these results were not considered clinically significant. An increase in ritonavir exposure was observed when co-administered with fixed dose PA, most likely due to pyronaridine inhibition of P-gp mediated ritonavir efflux.

In summary, this dissertation provides a comprehensive knowledge regarding the pharmacokinetics and pharmacodynamics of pyronaridine in healthy and malaria infected subjects. This information is of importance and can be used to optimize malaria treatment. Additionally, it can be used in guiding future pyronaridine pharmacokinetic/pharmacodynamic studies.

APPENDIX A

NONMEM CONTROL FILE FOR THE FINAL MODEL IN

CHAPTER II

```
Model Desc: 2 CMT FIX Q INFEC ON V2 V3 CL WT ON V2 CL POWER
Project Name: pyronaridine_adult
Project ID: NO PROJECT DESCRIPTION

$PROB RUN# FINAL
$INPUT C ID AMT TIME TAD DV MDV EVID AGE SEX WT HT BMI LBW ALT
AST INFEC RTV BSA IBW SCR SHULL CRCL HCT HGB RBC IFXN GEO COUN
OCC FORM TOUT DAY PARA
$DATA PYRADT3.CSV IGNORE=C
$SUBROUTINES ADVAN4 TRANS4

$PK
  TVCL=(THETA(1)+THETA(8)*INFEC)*((WT/56)**THETA(10))
  CL=TVCL*EXP(ETA(1))
  TVV2=(THETA(2)+THETA(6)*INFEC)*((WT/56)**THETA(9))
  V2=TVV2*EXP(ETA(2))
  TVQ=THETA(3)
  Q=TVQ*EXP(ETA(3))
  TVV3=(THETA(4)+(THETA(7)*INFEC))
  V3=TVV3*EXP(ETA(4))
  TVKA=THETA(5)
  KA=TVKA*EXP(ETA(5))
  S2=V2/1000
  K20=CL/V2
  K23=Q/V2
  K32=Q/V3
  BETA=((K23+K32+K20)-SQRT(((K23+K32+K20)**2)-4*K32*K20))*0.5
  ALPHA=K32*K20/BETA
  TBETA=LOG(2)/BETA
  TALPHA=LOG(2)/ALPHA
  AUC=AMT/CL

$ERROR
  IPRE=0
  IF(F.GT.0) IPRE=LOG(F)
  Y= IPRE+EPS(1)

$EST METHOD=1 PRINT=5 MAX=9999 SIG=2 MSFO=FINAL.MSF NOABORT
```

```
$THETA
  (0, 500) ;[CL]
  (0, 750) ;[V2]
  (0, 1100) ;[Q]
  (0, 5380) ;[V3]
  (0, 16.3) ;[KA]
  (-INF, 9000, INF) ;[INFEC ON V2]
  (-INF, 10600, INF) ;[INFEC ON V3]
  (-INF, 580, INF) ;[INFEC ON CL]
  (-INF, 1.30, INF) ;[WT ON V2 POWER]
  (-INF, 0.875, INF); [WT ON CL POWER]

$OMEGA
  0.125 ;[P] omega(1,1)
  0.4 ;[P] omega(2,2)
  0 FIXED ;[P] omega(3,3)
  0.1 ;[P] omega(4,4)
  0.4 ;[P] omega(5,5)

$SIGMA
  0.2 ;[A] sigma(1,1)

$COV PRINT=E MATRIX=S

$TABLE ID TIME TAD KA CL V2 Q V3 K20 K23 K32 ALPHA BETA TALPHA
TBETA AUC WT INFEC IPRE CWRESI CWRES ONEHEADER NOPRINT
FILE=FINAL.tab
$TABLE ID CL V2 V3 Q KA FIRSTONLY NOAPPEND NOPRINT FILE=FINAL.par
$TABLE ID ETA1 ETA2 ETA3 ETA4 ETA5 FIRSTONLY NOAPPEND NOPRINT
FILE=FINAL.eta.
$TABLE ID CL V2 V3 Q KA ONEHEADER NOPRINT FILE=PATABFINAL
$TABLE ID AGE WT BMI LBW CRCL ONEHEADER NOPRINT
FILE=COTABFINAL
$TABLE ID SEX ALT AST INFEC RTV ONEHEADER NOPRINT
FILE=CATABFINAL
```

APPENDIX B

OUTPUT SUMMARY FOR THE FINAL MODEL IN CHAPTER II

TERMINATION STATUS:
MINIMIZATION SUCCESSFUL
NO. OF FUNCTION EVALUATIONS USED: 533
NO. OF SIG. DIGITS IN FINAL EST.: 2.1

ETABAR IS THE ARITHMETIC MEAN OF THE ETA-ESTIMATES,
AND THE P-VALUE IS GIVEN FOR THE NULL HYPOTHESIS THAT THE TRUE MEAN IS 0.

ETABAR: 8.4309E-03 -1.1156E-02 0.0000E+00 -7.0271E-03 -8.0099E-03
SE: 1.0154E-02 2.3208E-02 0.0000E+00 6.1016E-03 1.2909E-02

P VAL.: 4.0637E-01 6.3073E-01 1.0000E+00 2.4945E-01 5.3494E-01

ETAshrink(%): 3.6701E+01 1.8885E+01 1.0000E+02 5.7292E+01 5.6126E+01
EPSshrink(%): 7.4448E+00

MINIMUM VALUE OF OBJECTIVE FUNCTION: -1469.312
COVARIANCE STEP SUCCESSFUL

	FINAL ESTIMATE	%RSE	95% CONFIDENCE INTERVAL LBOUND	UBOUND	DESCRIPTOR/ VARIABILITY
THETA					
1	501	5.47%	447	555	CL
2	741	11.6%	572	910	V2
3	1.15e+003	2.21%	1.10e+003	1.20e+003	Q
4	5.37e+003	4.04%	4.94e+003	5.80e+003	V3
5	16.3	8.47%	13.6	19.0	KA
6	9.07e+003	5.16%	8.15e+003	9.99e+003	INFEC ON V2
7	1.08e+004	34.4%	3.53e+003	1.81e+004	INFEC ON V3
8	582	16.9%	389	775	INFEC ON CL
9	1.25	17.3%	0.827	1.67	WT ON V2 POWER
10	0.874	16.9%	0.584	1.16	WT ON CL POWER
OMEGA					INTERINDIVIDUAL VARIABILITY
1,1	0.123	14.4%	0.0883	0.158	CV = 35.1%
2,2	0.390	9.67%	0.316	0.464	CV = 62.4%
3,3	0.00	...	...	...	CV = ...
4,4	0.0974	24.5%	0.0506	0.144	CV = 31.2%

5,5	0.413	26.6%	0.197	0.629	CV =	64.3%

SIGMA					RESIDUAL VARIABILITY	
1,1	0.200	1.03%	0.196	0.204	SD =	0.447

*Indicates 95% confidence interval that includes zero
%RSE is percent relative standard error (100% x SE/EST)

Akaike Information Criterion: -1437.31
Schwarz Bayesian Criterion: -1333.86
CONDITION NUMBER = 80.0 (DOES NOT EXCEED 1000)

APPENDIX C
NONMEM CONTROL FILE FOR THE FINAL MODEL IN CHAPTER III

```
Model Desc: BASE 2 CMT FIX Q V3 ALLO AGE ON CL POWER
Project Name: pyronaridine_pediatric
Project ID: NO PROJECT DESCRIPTION

$PROB RUN# FINAL
$INPUT C ID AMT TIME TAD DV MDV EVID AGE SEX WT HT BMI LBW ALT
AST INFEC RTV BSA
IBW SCR SHULL CRCL HCT HGB RBC IFXN GEO COUN OCC FORM TOUT DAY
PARA LOGPARA
$DATA PYRPED.CSV IGNORE=C
$SUBROUTINES ADVAN4 TRANS4

$PK
  TVCL=THETA(1)*((WT/22.1)**0.75)*((AGE/8)**THETA(6))
  CL=TVCL*EXP(ETA(1))
  TVV2=THETA(2)*((WT/22.1)**1.0)
  V2=TVV2*EXP(ETA(2))
  TVQ=THETA(3)*((WT/22.1)**0.75)
  Q=TVQ*EXP(ETA(3))
  TVV3=THETA(4)*((WT/22.1)**1.0)
  V3=TVV3*EXP(ETA(4))
  TVKA=THETA(5)
  KA=TVKA*EXP(ETA(5))
  S2=V2/1000
  K20=CL/V2
  K23=Q/V2
  K32=Q/V3
  BETA=((K23+K32+K20)-SQRT(((K23+K32+K20)**2)-4*K32*K20))*0.5
  ALPHA=K32*K20/BETA
  TBETA=LOG(2)/BETA
  TALPHA=LOG(2)/ALPHA
  AUC=AMT/CL

$ERROR
  IPRE=0
  IF(F.GT.0) IPRE=LOG(F)
  Y= IPRE+EPS(1)

$EST METHOD=1 PRINT=5 MAX=9999 SIG=3 MSFO=FINAL.MSF NOABORT

$THETA
 (0, 480) ;[CL]
 (0, 2700) ;[V2]
```

```
  (0, 700) ;[Q]
  (0, 2500) ;[V3]
  (0, 27) ;[KA]
  (-INF, 0.5, INF) ;[AGE ON CL]

$OMEGA
  0.5 ;[P] omega(1,1)
  1.0 ;[P] omega(2,2)
  0 FIXED ;[P] omega(3,3)
  0 FIXED ;[P] omega(4,4)
  0.7 ;[P] omega(5,5)

$SIGMA
  0.5 ;[A] sigma(1,1)

$COV PRINT=E

$TABLE ID TIME TAD KA CL V2 Q V3 K20 K23 K32 ALPHA BETA TALPHA
TBETA AUC WT AGE IPRE CWRESI CWRES ONEHEADER NOPRINT
FILE=FINAL.tab
$TABLE ID CL V2 V3 Q KA FIRSTONLY NOAPPEND NOPRINT FILE=FINAL.par
$TABLE ID ETA1 ETA2 ETA3 ETA4 ETA5 FIRSTONLY NOAPPEND NOPRINT
FILE=FINAL.eta.
$TABLE ID CL V2 V3 Q KA ONEHEADER NOPRINT FILE=PATABFINAL
$TABLE ID AGE WT LBW CRCL HGB LOGPARA ONEHEADER NOPRINT
FILE=COTABFINAL
$TABLE ID SEX ALT AST FORM ONEHEADER NOPRINT FILE=CATABFINAL
```

APPENDIX D

OUTPUT SUMMARY FOR THE FINAL MODEL IN CHAPTER III

TERMINATION STATUS:
MINIMIZATION SUCCESSFUL
NO. OF FUNCTION EVALUATIONS USED: 256
NO. OF SIG. DIGITS IN FINAL EST.: 3.6

ETABAR IS THE ARITHMETIC MEAN OF THE ETA-ESTIMATES,
AND THE P-VALUE IS GIVEN FOR THE NULL HYPOTHESIS THAT THE TRUE MEAN IS 0.

ETABAR:	2.4188E-03	2.1156E-02	0.0000E+00	0.0000E+00	-1.5061E-02
SE:	1.1280E-02	4.4542E-02	0.0000E+00	0.0000E+00	1.3946E-02
P VAL.:	8.3021E-01	6.3481E-01	1.0000E+00	1.0000E+00	2.8016E-01

ETAshrink(%): 4.7373E+01 1.5534E+01 1.0000E+02 1.0000E+02 6.9251E+01
EPSshrink(%): 1.8714E+01

MINIMUM VALUE OF OBJECTIVE FUNCTION: 172.306
COVARIANCE STEP SUCCESSFUL

	FINAL ESTIMATE	%RSE	95% CONFIDENCE INTERVAL LBOUND	UBOUND	DESCRIPTOR/ VARIABILITY
THETA					
1	459	5.97%	405	513	CL
2	2.72e+003	6.73%	2.36e+003	3.08e+003	V2
3	700	10.7%	553	847	Q
4	2.47e+003	9.19%	2.03e+003	2.91e+003	V3
5	27.0	14.8%	19.2	34.8	KA
6	0.295	40.7%	0.0598	0.530	AGE ON CL
OMEGA					INTERINDIVIDUAL VARIABILITY
1,1	0.152	39.2%	0.0352	0.269	CV = 39.0%
2,2	0.920	9.05%	0.757	1.08	CV = 95.9%
3,3	0.00	...	...	...	CV = ...
4,4	0.00	...	...	...	CV = ...
5,5	0.681	27.0%	0.320	1.04	CV = 82.5%

SIGMA					RESIDUAL VARIABILITY	
1,1	0.219	12.6%	0.165	0.273	SD =	0.468

*Indicates 95% confidence interval that includes zero
%RSE is percent relative standard error (100% x SE/EST)

Akaike Information Criterion: 196.306
Schwarz Bayesian Criterion: 255.819
CONDITION NUMBER = 17.9 (DOES NOT EXCEED 1000)

REFERENCES

1. World Health Organization. World Malaria Report 2011. WHO press 2011. (Accessed June, 2012, at http://www.who.int/malaria/world_malaria_report_2011/en/). 2011.

2. Gallup JL, Sachs JD. The economic burden of malaria. Am J Trop Med Hyg 2001 Jan-Feb;64(1-2 Suppl):85-96.

3. Kappe SH, Vaughan AM, Boddey JA, Cowman AF. That was then but this is now: malaria research in the time of an eradication agenda. Science 2010 May 14;328(5980):862-866.

4. Enayati A, Hemingway J. Malaria management: past, present, and future. Annu Rev Entomol 2010;55:569-591.

5. Walther B, Walther M. What does it take to control malaria? Ann Trop Med Parasitol 2007 Dec;101(8):657-672.

6. World Health Organization. Guidelines for the treatment of malaria. 2nd edition. 2010.

7. Yeung S, Pongtavornpinyo W, Hastings IM, Mills AJ, White NJ. Antimalarial drug resistance, artemisinin-based combination therapy, and the contribution of modeling to elucidating policy choices. Am J Trop Med Hyg 2004 Aug;71(2 Suppl):179-186.

8. Davis TM, Karunajeewa HA, Ilett KF. Artemisinin-based combination therapies for uncomplicated malaria. Med J Aust 2005 Feb 21;182(4):181-185.

9. Nosten F, White NJ. Artemisinin-based combination treatment of falciparum malaria. Am J Trop Med Hyg 2007 Dec;77(6 Suppl):181-192.

10. Baird JK. Effectiveness of antimalarial drugs. N Engl J Med 2005 Apr 14;352(15):1565-1577.

11. Shanks GD. Treatment of falciparum malaria in the age of drug resistance. J Postgrad Med 2006 Oct-Dec;52(4):277-280.

12. Wiesner J, Ortmann R, Jomaa H, Schlitzer M. New antimalarial drugs. Angew Chem Int Ed Engl 2003 Nov 10;42(43):5274-5293.

13. Price RN, Nosten F, Luxemburger C, ter Kuile FO, Paiphun L, Chongsuphajaisiddhi T, et al. Effects of artemisinin derivatives on malaria transmissibility. Lancet 1996 Jun 15;347(9016):1654-1658.

14. White NJ. Antimalarial drug resistance. J Clin Invest 2004 04/15;113(8):1084-1092.

15. Nosten F, Brasseur P. Combination therapy for malaria: the way forward? Drugs 2002;62(9):1315-1329.

16. Makanga M, Krudsood S. The clinical efficacy of artemether/lumefantrine (Coartem). Malar J 2009 Oct 12;8 Suppl 1:S5.

17. Ashley EA, Stepniewska K, Lindegardh N, Annerberg A, Kham A, Brockman A, et al. How much fat is necessary to optimize lumefantrine oral bioavailability? Trop Med Int Health 2007 Feb;12(2):195-200.

18. Toovey S. Mefloquine neurotoxicity: a literature review. Travel Med Infect Dis 2009 Jan;7(1):2-6.

19. Tarning J, Ashley EA, Lindegardh N, Stepniewska K, Phaiphun L, Day NP, et al. Population pharmacokinetics of piperaquine after two different treatment regimens with dihydroartemisinin-piperaquine in patients with Plasmodium falciparum malaria in Thailand. Antimicrob Agents Chemother 2008 Mar;52(3):1052-1061.

20. Hung TY, Davis TM, Ilett KF, Karunajeewa H, Hewitt S, Denis MB, et al. Population pharmacokinetics of piperaquine in adults and children with uncomplicated falciparum or vivax malaria. Br J Clin Pharmacol 2004 Mar;57(3):253-262.

21. Chen C, Zheng X. Development of the new antimalarial drug pyronaridine: a review. Biomed Environ Sci 1992 Jun;5(2):149-160.

22. Chang C, Lin-Hua T, Jantanavivat C. Studies on a new antimalarial compound: pyronaridine. Trans R Soc Trop Med Hyg 1992 Jan-Feb;86(1):7-10.

23. Ringwald P, Bickii J, Basco L. Randomised trial of pyronaridine versus chloroquine for acute uncomplicated falciparum malaria in Africa. Lancet 1996 Jan 6;347(8993):24-28.

24. Looareesuwan S, Kyle DE, Viravan C, Vanijanonta S, Wilairatana P, Wernsdorfer WH. Clinical study of pyronaridine for the treatment of acute uncomplicated falciparum malaria in Thailand. Am J Trop Med Hyg 1996 Feb;54(2):205-209.

25. Ringwald P, Bickii J, Same-Ekobo A, Basco LK. Pyronaridine for treatment of Plasmodium ovale and Plasmodium malariae infections. Antimicrobial Agents and Chemotherapy 1997 October 01;41(10):2317-2319.

26. Tshefu AK, Gaye O, Kayentao K, Thompson R, Bhatt KM, Sesay SS, et al. Efficacy and safety of a fixed-dose oral combination of pyronaridine-artesunate compared with artemether-lumefantrine in children and adults with uncomplicated Plasmodium falciparum malaria: a randomised non-inferiority trial. Lancet 2010 Apr 24;375(9724):1457-1467.

27. Rueangweerayut R, Phyo AP, Uthaisin C, Poravuth Y, Binh TQ, Tinto H, et al. Pyronaridine-artesunate versus mefloquine plus artesunate for malaria. N Engl J Med 2012 Apr 5;366(14):1298-1309.

28. Poravuth Y, Socheat D, Rueangweerayut R, Uthaisin C, Pyae Phyo A, Valecha N, et al. Pyronaridine-artesunate versus chloroquine in patients with acute Plasmodium vivax malaria: a randomized, double-blind, non-inferiority trial. PLoS One 2011 Jan 18;6(1):e14501.

29. Kayentao K, Doumbo O, Penali L, Offianan A, Bhatt K, Kimani J, et al. Pyronaridine-artesunate granules versus artemether-lumefantrine crushed tablets in children with Plasmodium falciparum malaria: a randomized controlled trial. Malaria Journal 2012;11(1):364.

30. Adegoke OA, Babalola CP, Oshitade OS, Famuyiwa AA. Determination of the physicochemical properties of pyronaridine - a new antimalarial drug. Pak J Pharm Sci 2006 Jan;19(1):1-6.

31. Croft S, Duparc S, Arbe-Barnes S, Craft J, Shin C, Fleckenstein L, et al. Review of pyronaridine anti-malarial properties and product characteristics. Malaria Journal 2012;11(1):270.

32. Auparakkitanon S, Noonpakdee W, Ralph RK, Denny WA, Wilairat P. Antimalarial 9-anilinoacridine compounds directed at hematin. Antimicrob Agents Chemother 2003 Dec;47(12):3708-3712.

33. Kumar S, Guha M, Choubey V, Maity P, Bandyopadhyay U. Antimalarial drugs inhibiting hemozoin (beta-hematin) formation: a mechanistic update. Life Sci 2007 Feb 6;80(9):813-828.

34. Auparakkitanon S, Chapoomram S, Kuaha K, Chirachariyavej T, Wilairat P. Targeting of hematin by the antimalarial pyronaridine. Antimicrob Agents Chemother 2006 Jun;50(6):2197-2200.

35. Egan TJ. Haemozoin (malaria pigment): a unique crystalline drug target. TARGETS 2003 6/1;2(3):115-124.

36. Lee J, Son J, Chung S, Lee E, Kim D. In vitro and in vivo metabolism of pyronaridine characterized by low-energy collision-induced dissociation mass spectrometry with electrospray ionization. Journal of Mass Spectrometry 2004;39(9):1036-1043.

37. Qi J, Yang CZ, Wang CY, Wang SB, Yang M, Wang JH. Function and mechanism of pyronaridine: a new inhibitor of P-glycoprotein-mediated multidrug resistance. Acta Pharmacol Sin 2002 Jun;23(6):544-550.

38. Qi J, Wang S, Liu G, Peng H, Wang J, Zhu Z, et al. Pyronaridine, a novel modulator of P-glycoprotein-mediated multidrug resistance in tumor cells in vitro and in vivo. Biochem Biophys Res Commun 2004 7/9;319(4):1124-1131.

39. Crowe A, Ilett KF, Karunajeewa HA, Batty KT, Davis TME. Role of P Glycoprotein in Absorption of Novel Antimalarial Drugs. Antimicrobial Agents and Chemotherapy October 2006 October 2006;50(10):3504-3506.

40. Guidance for Industry. Population pharmacokinetics. United States Food and Drug Administration. 1999. (Accessed June, 2012, at www.fda.gov/downloads/Drugs/../Guidance/UCM072137.pdf).

41. Sparreboom A, Figg WD. Identifying Sources of Interindividual Pharmacokinetic Variability with Population Modeling. Clinical Cancer Research 2006 April 01;12(7):1951-1953.

42. Ette EI, Williams PJ. Population Pharmacokinetics I: Background, Concepts, and Models. The Annals of Pharmacotherapy 2004 October 01;38(10):1702-1706.

43. Aarons L. Population pharmacokinetics: theory and practice. Br J Clin Pharmacol 1991 Dec;32(6):669-670.

44. Ette EI, Williams PJ. Population Pharmacokinetics II: Estimation Methods. The Annals of Pharmacotherapy 2004 November 01;38(11):1907-1915.

45. Sheiner LB, Beal SL. Evaluation of methods for estimating population pharmacokinetics parameters. I. Michaelis-Menten model: routine clinical pharmacokinetic data. J Pharmacokinet Biopharm 1980 Dec;8(6):553-571.

46. Sheiner LB, Beal SL. Evaluation of methods for estimating population pharmacokinetic parameters. II. Biexponential model and experimental pharmacokinetic data. J Pharmacokinet Biopharm 1981 Oct;9(5):635-651.

47. Sheiner LB, Beal SL. Evaluation of methods for estimating population pharmacokinetic parameters. III. Monoexponential model: routine clinical pharmacokinetic data. J Pharmacokinet Biopharm 1983 Jun;11(3):303-319.

48. Bonate P. Nonlinear Mixed Effects Models: Theory. Pharmacokinetic-Pharmacodynamic Modeling and Simulation: Springer US; 2011. p. 233-301.

49. Ette EI, Williams PJ, Kim YH, Lane JR, Liu M, Capparelli EV. Model Appropriateness and Population Pharmacokinetic Modeling. The Journal of Clinical Pharmacology 2003 June 01;43(6):610-623.

50. Centers for Disease Control and Prevention. The malaria parasite life cycle. 2010. (Accessed Dec, 2012, at http://www.cdc.gov/malaria/about/biology/;).

51. Childs GE, Häusler B, Milhous W, Chen C, Wimonwattrawatee T, Pooyindee N, et al. In Vitro Activity of Pyronaridine against Field Isolates and Reference Clones of Plasmodium Falciparum. The American Journal of Tropical Medicine and Hygiene 1988 January 01;38(1):24-29.

52. Dutta GP, Puri SK, Awasthi A, Mishra M, Tripathi R. Pyronaridine: an effective antimalarial against multidrug-resistant malaria. Life Sci 2000 Jul 7;67(7):759-763.

53. Vivas L, Rattray L, Stewart L, Bongard E, Robinson BL, Peters W, et al. Anti-malarial efficacy of pyronaridine and artesunate in combination in vitro and in vivo. Acta Trop 2008 Mar;105(3):222-228.

54. Feng Z, Wu ZF, Wang CY, Jiang NX. Pharmacokinetics of pyronaridine in malaria patients. Zhongguo Yao Li Xue Bao 1987 Nov;8(6):543-546.

55. Beal,S.L., Sheiner, L.B. NONMEM Users Guides - Part V. San Francisco: NONMEM Project Group, University of California at San Francisco. ; 1998.

56. Wang Y. Derivation of various NONMEM estimation methods. Journal of Pharmacokinetics and Pharmacodynamics 2007 -10-01;34(5):575-593.

57. Maitre PO, BÃ¼hrer M, Thomson D, Stanski DR. A three-step approach combining bayesian regression and NONMEM population analysis: Application to midazolam. Journal of Pharmacokinetics and Pharmacodynamics 1991 -08-01;19(4):377-384.

58. Mandema JW, Verotta D, Sheiner LB. Building population pharmacokineticpharmacodynamic models. I. Models for covariate effects. Journal of Pharmacokinetics and Pharmacodynamics 1992 -10-01;20(5):511-528.

59. Brendel K, Comets E, Laffont C, MentrÃ© F. Evaluation of different tests based on observations for external model evaluation of population analyses. Journal of Pharmacokinetics and Pharmacodynamics 2010 -02-01;37(1):49-65.

60. Chen YC, Fleckenstein L. Improved assay method for the determination of pyronaridine in plasma and whole blood by high-performance liquid chromatography for application to clinical pharmacokinetic studies. J Chromatogr B Biomed Sci Appl 2001 Mar 5;752(1):39-46.

61. Naik H, Imming P, Schmidt MS, Murry DJ, Fleckenstein L. Development and validation of a liquid chromatography-mass spectrometry assay for the determination of pyronaridine in human blood for application to clinical pharmacokinetic studies. J Pharm Biomed Anal 2007 Sep 21;45(1):112-119.

62. Guidance for Industry. General Considerations for Pediatric Pharmacokinetic Studies for Drugs and Biological Products, 1998. (Accessed Dec, 2012, at www.fda.gov/downloads/Drugs/.../Guidances/ucm072114.pdf).

63. Bergstrand M, Karlsson MO. Handling data below the limit of quantification in mixed effect models. AAPS J 2009 Jun;11(2):371-380.

64. Foisy MM, Yakiwchuk EM, Hughes CA. Induction effects of ritonavir: implications for drug interactions. Ann Pharmacother 2008 Jul;42(7):1048-1059.

65. Abbott Laboratories. Norvir® (ritonavir) soft gelatin capsules and oral solution prescribing information. North Chicago, IL; 2010.

66. Sankatsing SU, Beijnen JH, Schinkel AH, Lange JM, Prins JM. P glycoprotein in human immunodeficiency virus type 1 infection and therapy. Antimicrob Agents Chemother 2004 Apr;48(4):1073-1081.

67. Morris CA, Lopez-Lazaro L, Jung D, Methaneethorn J, Duparc S, Borghini-Fuhrer I, et al. Drug-drug interaction analysis of pyronaridine/artesunate and ritonavir in healthy volunteers. Am J Trop Med Hyg 2012 Mar;86(3):489-495.

68. Billig E, O'Meara W, Riley E, McKenzie FE. Developmental allometry and paediatric malaria. Malaria Journal 2012;11(1):64.

69. Cock RW, Piana C, Krekels EJ, Danhof M, Allegaert K, Knibbe CJ. The role of population PKâ€“PD modelling in paediatric clinical research. Eur J Clin Pharmacol 2011 05/01;67(1):5-16.

70. Routledge PA. Pharmacokinetics in children. Journal of Antimicrobial Chemotherapy 1994 August 01;34(suppl A):19-24.

71. Bartelink IH, Rademaker CM, Schobben AF, van den Anker JN. Guidelines on paediatric dosing on the basis of developmental physiology and pharmacokinetic considerations. Clin Pharmacokinet 2006;45(11):1077-1097.

72. Stephenson T. How children's responses to drugs differ from adults. Br J Clin Pharmacol 2005 Jun;59(6):670-673.

73. Kearns GL, Abdel-Rahman S, Alander SW, Blowey DL, Leeder JS, Kauffman RE. Developmental Pharmacology — Drug Disposition, Action, and Therapy in Infants and Children. N Engl J Med 2003 09/18; 2012/12;349(12):1157-1167.

74. Anderson B, Allegaert K, Holford NG. Population clinical pharmacology of children: general principles. Eur J Pediatr 2006 11/01;165(11):741-746.

75. Meibohm B, Laer S, Panetta JC, Barrett JS. Population pharmacokinetic studies in pediatrics: issues in design and analysis. AAPS J 2005 Oct 5;7(2):E475-87.

76. Savage VM, Deeds EJ, Fontana W. Sizing Up Allometric Scaling Theory. PLoS Comput Biol 2008 09/12;4(9):e1000171.

77. Mahmood I. Prediction of Drug Clearance in Children: Impact of Allometric Exponents, Body Weight, and Age. Ther Drug Monit 2007;29(3).

78. Benedetti MS, Whomsley R, Canning M. Drug metabolism in the paediatric population and in the elderly. Drug Discov Today 2007 8;12(15–16):599-610.

79. White NJ, Olliaro PL. Strategies for the prevention of antimalarial drug resistance: rationale for combination chemotherapy for malaria. Parasitol Today 1996 Oct;12(10):399-401.

80. Guidelines for the treatment of malaria. World Health Organization, 2006. (Accessed at http://apps.who.int/malaria/docs/TreatmentGuidelines2006.pdf.).

81. Snounou G, Beck HP. The use of PCR genotyping in the assessment of recrudescence or reinfection after antimalarial drug treatment. Parasitol Today 1998 Nov;14(11):462-467.

82. Bewick V, Cheek L, Ball J. Statistics review 13: receiver operating characteristic curves. Crit Care 2004 Dec;8(6):508-512.

83. Choi BCK. Slopes of a Receiver Operating Characteristic Curve and Likelihood Ratios for a Diagnostic Test. American Journal of Epidemiology 1998 December 01;148(11):1127-1132.

84. Florkowski CM. Sensitivity, specificity, receiver-operating characteristic (ROC) curves and likelihood ratios: communicating the performance of diagnostic tests. Clin Biochem Rev 2008 Aug;29 Suppl 1:S83-7.

85. Zweig MH, Campbell G. Receiver-operating characteristic (ROC) plots: a fundamental evaluation tool in clinical medicine. Clinical Chemistry 1993 April 01;39(4):561-577.

86. Gardner IA, Greiner M. Receiver-operating characteristic curves and likelihood ratios: improvements over traditional methods for the evaluation and application of veterinary clinical pathology tests. Vet Clin Pathol 2006 Mar;35(1):8-17.

87. Park SH, Goo JM, Jo CH. Receiver operating characteristic (ROC) curve: practical review for radiologists. Korean J Radiol 2004 Jan-Mar;5(1):11-18.

88. Obuchowski NA. ROC Analysis. American Journal of Roentgenology 2005 February 01;184(2):364-372.

89. Kumar RV, Antony GM. A Review of Methods and Applications of the ROC Curve in Clinical Trials. Drug Information Journal 2010 November 01;44(6):659-671.

90. Kumar R, Indrayan A. Receiver operating characteristic (ROC) curve for medical researchers. Indian Pediatr 2011 Apr;48(4):277-287.

91. Cox, D.R. and Oakes, D. Proportional hazards model. Analysis of Survival Data. 1st ed.: Chapman & Hall; 1996. p. 91.

92. White NJ, Stepniewska K, Barnes K, Price RN, Simpson J. Simplified antimalarial therapeutic monitoring: using the day-7 drug level? Trends Parasitol 2008 4;24(4):159-163.

93. Bell DJ, Nyirongo SK, Mukaka M, Molyneux ME, Winstanley PA, Ward SA. Population pharmacokinetics of sulfadoxine and pyrimethamine in Malawian children with malaria. Clin Pharmacol Ther 2011 Feb;89(2):268-275.

94. ter Kuile FO, Luxemburger C, Nosten F, Thwai KL, Chongsuphajaisiddhi T, White NJ. Predictors of mefloquine treatment failure: a prospective study of 1590 patients with uncomplicated falciparum malaria. Trans R Soc Trop Med Hyg 1995 Nov-Dec;89(6):660-664.

95. Fontanet AL, Walker AM. Predictors of treatment failure in multiple drug-resistant falciparum malaria: results from a 42-day follow-up of 224 patients in eastern Thailand. Am J Trop Med Hyg 1993 Oct;49(4):465-472.

96. Dorsey G, Gasasira AF, Machekano R, Kamya MR, Staedke SG, Hubbard A. The impact of age, temperature, and parasite density on treatment outcomes from antimalarial clinical trials in Kampala, Uganda. Am J Trop Med Hyg 2004 Nov;71(5):531-536.

97. Laufer MK, van Oosterhout JJG, Thesing PC, Dzinjalamala FK, Hsi T, Beraho L, et al. Malaria Treatment Efficacy among People Living with HIV: The Role of Host and Parasite Factors. The American Journal of Tropical Medicine and Hygiene 2007 October 01;77(4):627-632.

98. Riley EM, Wagner GE, Akanmori BD, Koram KA. Do maternally acquired antibodies protect infants from malaria infection? Parasite Immunol 2001;23(2):51-59.

99. Rogerson SJ, Wijesinghe RS, Meshnick SR. Host immunity as a determinant of treatment outcome in Plasmodium falciparum malaria. The Lancet Infectious Diseases 2010 1;10(1):51-59.

100. Hochman S, Kim K. The Impact of HIV and Malaria Coinfection: What Is Known and Suggested Venues for Further Study. Interdiscip Perspect Infect Dis 2009;2009:617954.

101. Hochman S, Kim K. The Impact of HIV Coinfection on Cerebral Malaria Pathogenesis. J Neuroparasitology 2012;3:235547. Epub 2012 Mar 2.

102. Cuadros DF, Branscum AJ, Crowley PH. HIV–malaria co-infection: effects of malaria on the prevalence of HIV in East sub-Saharan Africa. International Journal of Epidemiology 2011 August 01;40(4):931-939.

103. Bharti AR, Saravanan S, Madhavan V, Smith DM, Sharma J, Balakrishnan P, et al. Correlates of HIV and malaria co-infection in Southern India. Malar J 2012 Sep 3;11:306-2875-11-306.

104. Aarnoutse RE, Kleinnijenhuis J, Koopmans PP, Touw DJ, Wieling J, Hekster YA, et al. Effect of low-dose ritonavir (100 mg twice daily) on the activity of cytochrome P450 2D6 in healthy volunteersast]. Clin Pharmacol Ther 2005 print;78(6):664-674.

105. Naik H, Murry DJ, Kirsch LE, Fleckenstein L. Development and validation of a high-performance liquid chromatography–mass spectroscopy assay for determination of artesunate and dihydroartemisinin in human plasma. Journal of Chromatography B 2005 2/25;816(1–2):233-242.

106. Ding R, Tayrouz Y, Riedel KD, Burhenne J, Weiss J, Mikus G, et al. Substantial pharmacokinetic interaction between digoxin and ritonavir in healthy volunteers. Clin Pharmacol Ther 2004 Jul;76(1):73-84.

107. Lee J, Son J, Chung SJ, Lee ES, Kim DH. In vitro and in vivo metabolism of pyronaridine characterized by low-energy collision-induced dissociation mass spectrometry with electrospray ionization. J Mass Spectrom 2004;39:1036-1043.

108. Jayaraman SD, Ismail S, Nair NK, Navaratnam V. Determination of pyronaridine in blood plasma by high-performance liquid chromatography for application in clinical pharmacological studies. J Chromatogr B Biomed Sci Appl 1997;690:253-257.

109. Babalola CP, Scriba GK, Sowunmi A, Alawode OA. Liquid chromatographic determination of pyronaridine in human plasma and oral dosage form. J Chromatogr B Analyt Technol Biomed Life Sci 2003;795:265-272.

110. Ramanathan S, Karupiah S, Nair NK, Olliaro PL, Navaratnam V, Wernsdorfer WH, et al. A new and simple solid-phase extraction method for LC determination of pyronaridine in human plasma. J Chromatogr B Analyt Technol Biomed Life Sci 2005;824:45-50.